AD-A127 219 ANALYSIS OF STEADY TWO-DIMENSIONAL CHEMICALLY REACTING NONEQUILIBRIUM FLO..(U) PURDUE UNIV LAFAYETTE IND THERMAL SCIENCES AND PROPULSION CEN.. 1/2

UNCLASSIFIED R J STILES ET AL. SEP 82 F/G 20/4 NL

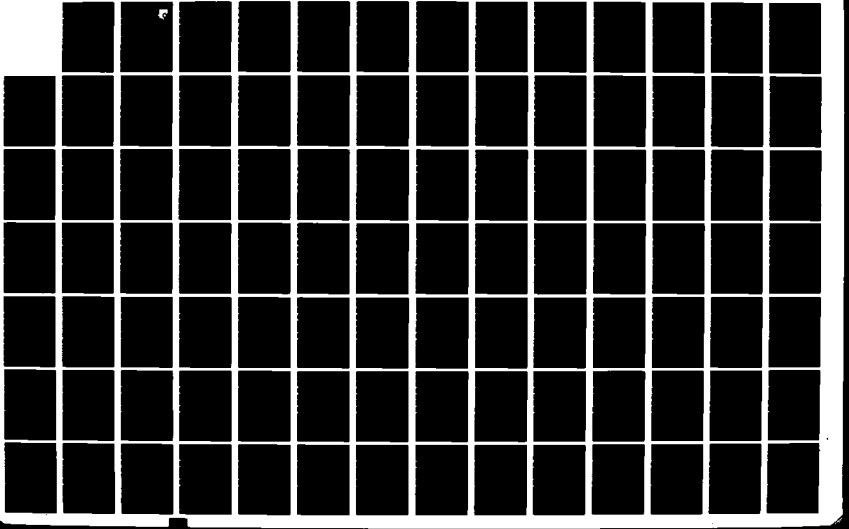

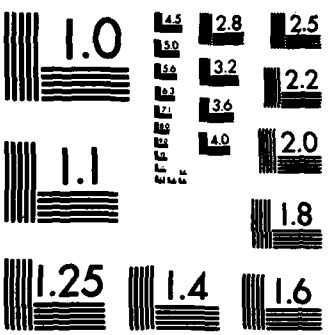

AFWAL-TR-81-2127, Vol I

ANALYSIS OF STEADY, TWO-DIMENSIONAL CHEMICALLY REACTING NONEQUILIBRIUM FLOW BY AN UNSTEADY, ASYMPTOTICALLY CONSISTENT TECHNIQUE

VOLUME I - THEORETICAL DEVELOPMENT

RANDALL J. STILES
JOE D. HOFFMAN

THERMAL SCIENCES AND PROPULSION CENTER
SCHOOL OF MECHANICAL ENGINEERING
PURDUE UNIVERSITY
WEST LAFAYETTE, INDIANA 47907

SEPTEMBER 1982

FINAL REPORT FOR PERIOD SEPTEMBER 1979 - SEPTEMBER 1981

AERO PROPULSION LABORATORY
AIR FORCE WRIGHT AERONAUTICAL LABORATORIES
AIR FORCE SYSTEMS COMMAND
WRIGHT-PATTERSON AIR FORCE BASE, OHIO 45433

NOTICE

When Government drawings, specifications, or other data are used for any purpose other than in connection with a definitely related Government procurement operation, the United States Government thereby incurs no responsibility nor any obligation whatsoever; and the fact that the government may nave formulated, furnished, or in any way supplied the said drawings, specifications, or other data, is not to be regarded by implication or otherwise as in any manner licensing the holder or any other person or corporation, or conveying any rights or permission to manufacture use, or sell any patented invention that may in any way be related thereto.

This report has been reviewed by the Office of Public Affairs (ASD/PA) and is releasable to the National Technical Information Service (NTIS). At NTIS, it will be available to the general public, including foreign nations.

This technical report has been reviewed and is approved for publication.

John R Smith

JOHN R. SMITH, Proj Engr
Analysis & Component Development Grp
Aero Propulsion Laboratory

Frank D Stull

FRANK D. STULL, Chief
Ramjet Technology Branch
Aero Propulsion Laboratory

FOR THE COMMANDER

William G Beecroft

WILLIAM G. BEECROFT, Asst Chief
Ramjet Engine Division
Aero Propulsion Laboratory

"If your address has changed, if you wish to be removed from our mailing list, or if the addressee is no longer employed by your organization please notify AFWAL/PORT, W-PAFB, OH 45433 to help us maintain a current mailing list".

Copies of this report should not be returned unless return is required by security considerations, contractual obligations, or notice on a specific document.

Unclassified

SECURITY CLASSIFICATION OF THIS PAGE (When Data Entered)

REPORT DOCUMENTATION PAGE		READ INSTRUCTIONS BEFORE COMPLETING FORM
1. REPORT NUMBER AFWAL-TR-81-2127, Volume I	2. GOVT ACCESSION NO. AD-A127219	3. RECIPIENT'S CATALOG NUMBER
4. TITLE (and Subtitle) ANALYSIS OF STEADY, TWO-DIMENSIONAL, CHEMICALLY REACTING NONEQUILIBRIUM FLOW BY AN UNSTEADY, ASYMPTOTICALLY CONSISTENT TECHNIQUE, VOLUME I - THEORETICAL DEVELOPMENT		5. TYPE OF REPORT & PERIOD COVERED Final Report for Period Sep 79 - Sep 81
		6. PERFORMING ORG. REPORT NUMBER N/A
7. AUTHOR(s) Randall J. Stiles and Joe D. Hoffman		8. CONTRACT OR GRANT NUMBER(s) F33615-79-C-2065
9. PERFORMING ORGANIZATION NAME AND ADDRESS Thermal Sciences and Propulsion Center School of Mechanical Engineering, Purdue University West Lafayette, Indiana 47907		10. PROGRAM ELEMENT, PROJECT, TASK AREA & WORK UNIT NUMBERS 30121325
11. CONTROLLING OFFICE NAME AND ADDRESS Aero Propulsion Laboratory (AFWAL/PORT) Air Force Wright Aeronautical Laboratories (AFSC) Wright-Patterson AFB, Ohio 45433		12. REPORT DATE September 1982 13. NUMBER OF PAGES 174
14. MONITORING AGENCY NAME & ADDRESS(if different from Controlling Office)		15. SECURITY CLASS. (of this report) UNCLASSIFIED 15a. DECLASSIFICATION/DOWNGRADING SCHEDULE

16. DISTRIBUTION STATEMENT (of this Report)

Approved for public release; distribution unlimited.

17. DISTRIBUTION STATEMENT (of the abstract entered in Block 20, if different from Report)

18. SUPPLEMENTARY NOTES

This report consists of two volumes. Volume II is titled "Computer Program Manual."

19. KEY WORDS (Continue on reverse side if necessary and identify by block number)

Gas Dynamics
Ramjets
Combustion
Nozzles

20. ABSTRACT (Continue on reverse side if necessary and identify by block number)

A method has been developed for solving the equations governing two-dimensional, unsteady, chemically reacting nonequilibrium flow. Subsonic, transonic, and supersonic flow fields can be analyzed using this technique. The steady state solution is obtained as the asymptotic solution to the unsteady equations, with steady flow boundary conditions applied, for large time. Interior mesh points are computed using MacCormack's method. Boundary points are calculated by a reference-plane characteristic scheme. The overall algorithm is inconsistent in time in the treatment of the species continuity equations, but is consistent

DD FORM 1 JAN 73 1473 EDITION OF 1 NOV 65 IS OBSOLETE

Unclassified

SECURITY CLASSIFICATION OF THIS PAGE (When Data Entered)

at the steady state limit. The species continuity equations are integrated by a second-order accurate implicit method. Nonuniform, nonequilibrium conditions may be specified at the nozzle inlet. The chemical kinetics model considers 19 species formed from the elements carbon, hydrogen, oxygen, nitrogen, flourine, and chlorine, and 48 chemical reactions. Unburned hydrocarbons and a sub-global oxidation reaction for these species is also included in the model. A production-type computer program was developed and used to analyze several problems.

PREFACE

This final report was submitted by the Thermal Sciences and Propulsion Center of Purdue University, under Contract No. F33615-79-C-2065. The work was sponsored by the Aero Propulsion Laboratory, Air Force Wright Aeronautical Laboratories, Air Force System Command, Wright-Patterson AFB, Ohio, under Project No. 3012, Task 13, Work Unit 25. John Smith was the Project Engineer for the Air Force. Randall J. Stiles and Joe D. Hoffman performed the technical work for Purdue University.

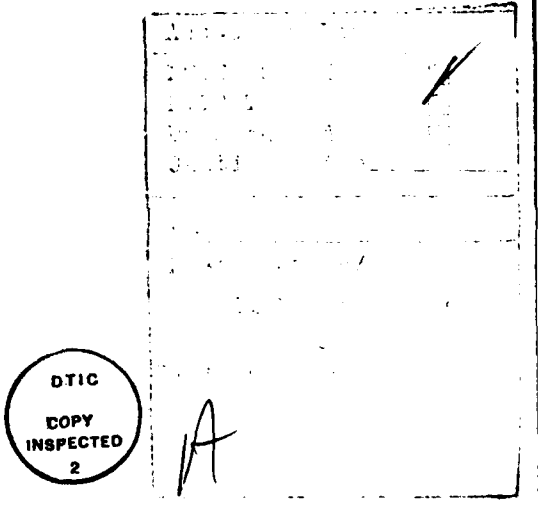

TABLE OF CONTENTS

LIST OF FIGURES

LIST OF TABLES

LIST OF SYMBOLS

English Symbols

a_f	frozen speed of sound
a_{i_j}, b_j, n_j	reaction rate parameters
c	species concentration
C_i	species i mass fraction
C_{pi}	specific heat of species i at constant pressure
f	right-hand side of general ordinary differential equation
f_i	right-hand side of species continuity equation (σ_i/ρ)
g_i	f_i divided by velocity magnitude ($\sigma_i/\rho v$)
h	enthalpy or integration step size
h_i	enthalpy of species i
h_i^o	energy of formation of species i
H_o	total enthalpy
k_{f_j}, k_{r_j}	forward and reverse reaction rate coefficients for reaction j
K_i	change in mass fraction of species i
K_j	function of equilibrium constant for reaction j
$K_{p,j}$	equilibrium constant for reaction j
ℓ_i	multipliers in reference plane characteristic method (Appendix C)
L	Lipshitz constant
L, M, N	finite difference equation indices
m	number of chemical reactions

$\bar{m}_i$	molecular weight of species i
M	Mach number
M_j	third body reaction rate ratio
n	number of chemical species
$\hat{n}$	number of chemical species (Appendix D)
$\bar{N}$	normal to a characteristic curve
N_ζ, N_η, N_τ	components of normal to a characteristic curve
P	pressure
P_o	total pressure
Q	velocity magnitude
R	mixture gas constant
R_i	gas constant of species i
$\bar{R}$	universal gas constant
s	position along streamline
t	time
T	temperature
T_o	reference temperature or total temperature
u,v	velocity components in the x,y coordinate system
$\bar{v}$	defined by equation (A-22)
V	velocity magnitude
$\bar{V}$	velocity vector
$\bar{W}_j$	vectors of Appendix C
x,y,t	physical plane cartesian coordinates
y_c	centerbody coordinate
y_w	wall coordinate

Greek Symbols

α	defined by equation (A-21)
α^*	defined by equation (C-70)
β	defined by equation (A-21)
γ_f	ratio of frozen specific heats
ϵ	term in global continuity equation (ϵ is zero for planar flow and one for axisymmetric flow)
ζ,η,τ	computational plane coordinate system
$\overline{\eta}$	defined by equation (A-23)
θ	inlet flow angle or wall angle
ν'_{ij}	stoichiometric coefficient of reactant i in reaction j
ν''_{ij}	stoichiometric coefficient of product i in reaction j
ρ	density
ρ_i	density of species i
σ_i	species i source function
$\hat{\tau}$	chemical rate characteristic time
χ	defined by equation (D-6)
ψ_i	right hand sides of governing equations in reference plane characteristic method (Appendix C)
ψ_k	energy equation source term

Subscript

c	corrected value
ℓ	intermediate mesh point
L,M	denotes finite difference grid location
n	intermediate mesh point (Appendix D)
p	predicted value
x,y,t	denote partial differentiation with respect to x, y, and t respectively

ζ,η,τ	denote partial differentiation with respect to ζ, η, and τ respectively
*	streamline mesh point

Superscript

N	time level
$\sim$	predicted value

Operators

$d_{\bar{w}_1} f$	directional derivative of the function f in the direction $\bar{w}_1$

SECTION I

INTRODUCTION

1. GENERAL

Performance prediction for a ramjet propulsion system requires a detailed analysis of the flow through each of its major components: the inlet, the combustor, and the exhaust nozzle. The objective of this research was to develop a procedure for calculating the flow field within the converging-diverging nozzle of a high-speed ($M \cong 6$) ramjet propulsion system.

Initial data (at the nozzle inlet) for the nozzle flow field analysis is provided by the results of the combustor analysis. Ramjet combustors are generally axisymmetric in shape with slowly-varying or constant cross-sectional area. Techniques for analysis and performance prediction for a high-speed ramjet combustor are still under development. One technique [Reference (1)] is based on a one-dimensional compound flow analysis of the combustor flow field. The flow is broken into a number of coaxial flow streams and the one-dimensional flow equations are solved within each stream. The static pressure is matched radially across each of the streams resulting in a uniform static pressure distribution across the combustor exit. The fuel injection processes, fuel droplet dynamics, atomization, mixing, vaporization, and combustion kinetics are all included in the flow model.

The final result of the combustor analysis is a complete set of known flow properties and chemical species concentrations at the nozzle entrance where the converging geometry begins to introduce two-dimensional flow effects. The flow at the combustor exit will not necessarily be in chemical equilibrium. At high speeds, the stagnation temperature within the flow will be large and the effects of finite-rate chemical kinetics become important. Also residence times within the combustor may not be sufficient for the flow to reach chemical equilibrium. The technique developed in the subject research will accept a nonuniform, nonequilibrium, distribution of initial conditions at the nozzle inlet.

The analysis within the nozzle can be divided into two parts: the analysis of the subsonic and transonic flow fields in the axisymmetric nozzle entrance and throat regions, and the analysis of the supersonic flow field in the nozzle divergence. The effects of finite-rate kinetics must be included in both parts of the analysis. If the nozzle divergence is axisymmetric, Reference (2) can be used for analysis of the supersonic flow field. If the divergence is not axisymmetric, due to integration with the airframe, then a three-dimensional analysis is required. A highly accurate, three-dimensional, method-of-characteristics scheme for supersonic flow, including finite-rate chemical kinetics effects, has been developed by Cline and Hoffman (3). The subject research has been concerned with the analysis of the subsonic and transonic flow regions. Both axisymmetric and planar nozzle geometries are considered and the nozzle may have a centerbody. Though the present discussion focuses on ramjet propulsion, the

technique which is described is applicable to any subsonic-transonic flow field analysis where the effects of finite-rate chemical kinetics must be considered. The computer program which evolved from this work is an extension of that developed by Cline (4).

2. LITERATURE REVIEW

The literature surveyed for this research can be divided into three groups: 1) one-, two-, and three-dimensional, steady, chemically reacting nonequilibrium flow, 2) two-dimensional, unsteady, nonreacting flow, and 3) unsteady, chemically reacting, nonequilibrium flow. Each of these groups is considered in turn in the following discussion.

Steady, Chemically Reacting, Nonequilibrium Flows

There is a very large amount of literature concerning this topic. Most of the literature deals with one- and two-dimensional flows. For the one-dimensional case, the solutions can be categorized as analytical, semiempirical, and numerical. Analytical solutions are possible only for the very simplest nonequilibrium processes and often approximations such as linearization and the assumption of a high Mach number are introduced. Reference (5) provides examples of analytical solutions. Perhaps the most often used semiempirical method is the "sudden freezing" approximation (5) where equilibrium flow is assumed upstream of an empirically chosen "freezing point," and frozen flow is assumed downstream of that point. Accurate numerical solutions are also available and have been computed by a number of investigators. Examples include the work by Emanual and Vincenti (6 , 7), Sarli (8), Lordi

et al. (9), and Frey et al. (10). Reference (10) is widely used by the propulsion industry.

Two-dimensional, steady, supersonic flows with chemical nonequilibrium have been computed by Widawsky (11), Zupnik et al. (12), Craig (13), Bartlma (14), and Kliegel et al. (2). Reference (2) considers the elements C, H, O, N, F, and Cl, 19 gaseous species containing those elements, and 48 chemical reactions that may occur between those species. A method-of-characteristics procedure is used. The supersonic initial-data line required to start the characteristic calculations can be input or it can be calculated by a transonic analysis within the program. The characteristic equations governing the fluid dynamic variables are integrated by a second-order (modified Euler) explicit method. The species continuity equations are integrated using a first-order, implicit method. It is significant to note that the authors of Reference (2) state that even small interpolation errors in species concentrations cause severe stability and accuracy problems in the numerical integration of the species continuity equations. This fact will be discussed more fully in Section III.

Cline and Hoffman (3) extended an isentropic flow three-dimensional method-of-characteristics scheme, developed by Ransom et al. (15), to include the effects of finite-rate chemical kinetics. Their analysis uses the same chemical kinetics model as used in Reference (2). Initial-value plane data can be obtained from the results of an analysis using Reference (2), but in that case, no account is made for two-dimensional effects upstream of the throat. The subject research provides a two-dimensional, nonequilibrium initial-value

plane for use in the analysis of Reference (3). Cline and Hoffman (3) note the importance of using correct initial data. They found that incorrect data may result in thermal compressions and shocks due to the rapid change in chemical composition just off the initial-value surface. As in Reference (2), the fluid dynamic equations are integrated using a second-order explicit method, but the species continuity equations are integrated using a second-order, implicit scheme. This particular scheme was chosen after an extensive review of various explicit and implicit methods for integrating the species continuity equations.

Unsteady, Nonreacting Flow

The time-dependent technique for the solution of steady-state converging-diverging nozzle flows has been used by a number of investigators [References (4) and (16) to (23)]. References (16) to (22) provide generally good results for typical problems but the techniques yield relatively long computational times. Cline (23) attributes this to "inefficient numerical schemes and poor treatment of the boundaries resulting in the requirement for excessively fine computational meshes." Cline (4, 23) uses MacCormack's method for interior points with the governing equations of motion in nonconservation form. Implicit artificial viscosity is present within this method so explicit artificial viscosity is added only for flows with shock waves. The boundary points are computed using a reference-plane characteristic scheme. Solutions to representative, inviscid, nozzle problems are obtained in approximately one minute using a CDC 6600 computer.

Unsteady, Chemically Reacting, Nonequilibrium Flow

Vamos and Anderson (24) have used a time-dependent scheme to compute the one-dimensional, nonequilibrium flow of reacting gas mixtures. They cite several advantages of their approach as compared to steady, one-dimensional analyses:

1) the use of relatively few grid points with relatively large spatial increments through the nozzle, including the near equilibrium subsonic portion of the nozzle.
2) the straightforward manner in which completely nonequilibrium, subsonic, supersonic flow can be treated. In particular, the usual singularity in the throat region associated with steady flow analyses is not present in the unsteady approach.

MacCormack's method (which is explicit) was used in this work for all the governing equations (including the species continuity equations). Very long computation times were reported ($\sim$1 hour on a CDC 6400) but the results were quite good. No general computer programs have been developed to treat multidimensional, reacting flows by an unsteady approach.

3. REMARKS ON COMPUTATIONAL TIME

Stability, accuracy, and computational time are generally the most important factors used in determining the merit of a particular numerical method. In the subject research, computational time has been especially important for several reasons. First, the flow field to be modeled in the nozzle entrance and throat regions is a two-dimensional, subsonic and transonic flow. For steady subsonic flow,

the governing partial differential equations are elliptic while, for steady supersonic flow, those equations are hyperbolic. In the transonic flow regime, the equations change from elliptic to hyperbolic (i.e., they are mixed). Techniques for solving mixed flow problems are not well developed, but hyperbolic problems have been studied and solved for many years. The mathematical difficulties associated with a mixed flow problem can be avoided by solving the unsteady flow equations which are hyperbolic in both subsonic and supersonic regions. Then the steady flow solution can be obtained as the asymptotic solution to the unsteady equations, with steady flow boundary conditions applied, for large time. The disadvantage of this approach is that another independent variable is introduced into the analysis and the unsteady solution may have to be advanced through many time steps to achieve the steady state. If the allowable time step is small, and/or the time to compute each solution plane is large, then long computational times can result. The time step size is determined from stability considerations for the given equations and numerical methods used. Introducing finite-rate chemical kinetics into the analysis significantly increases the time required to compute each solution plane. This is because the number of equations in the mathematical model increases by the number of chemical species considered, and the calculations required to compute the species source function and to integrate the species continuity equations are very time consuming.

The nature of the species continuity equations must also be considered in a discussion of computational time. For flows near

equilibrium, the species continuity equations are "stiff," and as a result, they are difficult to solve numerically (see Appendix D). Standard explicit integration techniques, when applied to stiff differential equations, are unstable except for very small step sizes. This problem occurred in the work of Vamos and Anderson (24). The use of implicit methods, however, removes the stability problems and allows more reasonable time steps. In addition to obtaining a solution to the subject problem, a significant objective of this research has been to achieve the solution in reasonable computational times.

SECTION II

MODELING THE PROBLEM

1. PHYSICAL MODEL

In Section I it was noted that the initial data for the nozzle flow field analysis is provided by the results of the combustor analysis. Within the combustor, the fuel injection processes, fuel droplet dynamics, atomization, mixing, vaporization, and combustion kinetics may all be considered. However, by the time the flow has reached the combustor exit, it is assumed in this analysis that it is a mixture of thermally perfect gases with no condensed phases. The distribution of fluid dynamic properties and the species concentrations may or may not be uniform across the exit. Also, the flow may be in chemical nonequilibrium at the combustor exit. The flow within the nozzle is treated as continuous, inviscid, and adiabatic. Body forces are neglected. No provisions have been made for diffusion or turbulence modeling within the flow. Finally, only chemical nonequilibrium is treated in this analysis; the flow is assumed to be everywhere in instantaneous translational, rotational, and vibrational equilibrium.

2. MATHEMATICAL MODEL

The equations which correspond to the physical model described above are given in Reference (25) and are discussed in Appendix A.

These equations are the global continuity equation, the momentum equation, the energy equation, the species continuity equations, and the thermal and caloric equations of state. In vector form, they are:

$$\frac{\partial \rho}{\partial t} + \nabla \cdot (\rho \bar{V}) = 0 \tag{1}$$

$$\rho \frac{D\bar{V}}{Dt} + \nabla P = 0 \tag{2}$$

$$\frac{D(h + V^2/2)}{Dt} - \frac{1}{\rho} \frac{\partial P}{\partial t} = 0 \tag{3}$$

$$\frac{\partial \rho_i}{\partial t} + \nabla \cdot (\rho_i \bar{V}) = \sigma_i \qquad (i=1,\ldots,n) \tag{4}$$

$$P = \rho T \sum_{i=1}^{n} C_i R_i \tag{5}$$

$$h = \sum_{i=1}^{n} C_i h_i \quad \text{where } h_i = \int_{T_o}^{T} C_{pi}\, dT + h_i^{o} \tag{6}$$

where ρ is the fluid density, $\bar{V}$ is the velocity, P is the pressure, h is the system enthalpy, T is the temperature, ρ_i are the species densities, C_i are the species mass fractions, σ_i are the species source functions, h_i are the species enthalpies, R_i are the species gas constants, C_{pi} are the species specific heats at constant pressure, and h_i^{o} are the species energies of formation.

In Appendix A, equations (3) and (4) are manipulated to forms which are more convenient for analysis and the entire set of governing equations is written for two-dimensional axisymmetric or planar flow.

The resulting equations are:

$$\rho_t + u\rho_x + v\rho_y + \rho u_x + \rho v_y + \varepsilon(\rho v/y) = 0 \qquad (7)$$

$$u_t + uu_x + vu_y + P_x/\rho = 0 \qquad (8)$$

$$v_t + uv_x + vv_y + P_y/\rho = 0 \qquad (9)$$

$$P_t + uP_x + vP_y - a_f^2(\rho_t + u\rho_x + v\rho_y) = \psi_k \qquad (10)$$

$$C_{it} + uC_{ix} + vC_{iy} = \frac{\sigma_i}{\rho} \qquad (i=1,\ldots,n) \qquad (11)$$

where

$$\psi_k = \sum_{i=1}^{n} [\gamma_f R_i T - (\gamma_f - 1)h_i]\sigma_i$$

The subscripts in these equations denote partial differentiation and ε in equation (7) is zero for planar flow and one for axisymmetric flow. The terms a_f and γ_f are the frozen speed of sound and the ratio of frozen specific heats respectively. Note that the species continuity equations (11) are coupled to equations (7) to (10) by the energy equation source term ψ_k.

Since the interior points in this analysis are to be treated by a fixed grid technique, it is convenient to transform the physical (x,y,t) plane to a rectangular (ζ,η,τ) plane in which the differencing is performed. The following coordinate transformation is used (see Figure 1):

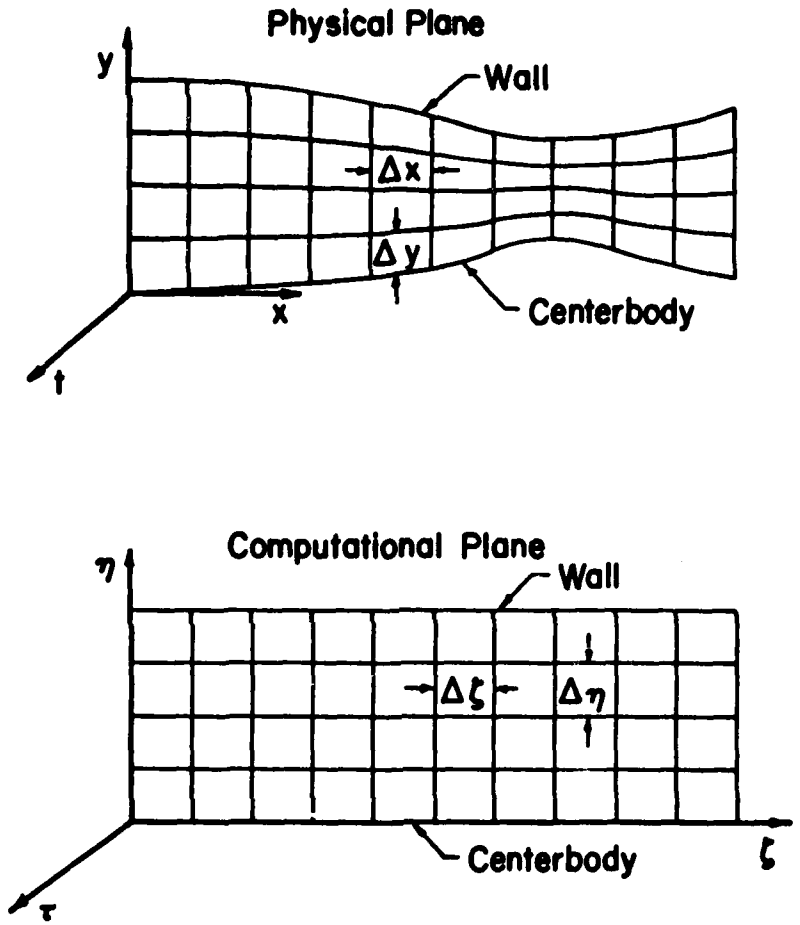

Figure 1. Physical and computational planes.

$$\tau = t$$

$$\zeta = x \tag{12}$$

$$\eta = \frac{y - y_c(x)}{y_w(x) - y_c(x)}$$

where $y_c(x)$ and $y_w(x)$ represent the nozzle centerbody and wall coordinates, respectively, as functions of x. Applying this transformation to equations (7) to (11) yields the forms of the continuity, momentum, energy, and species continuity equations which are used in this analysis.

$$\rho_\tau + u\rho_\zeta + \bar{v}\rho_\eta + \rho u_\zeta + \rho\alpha u_\eta + \rho\beta v_\eta + \varepsilon\rho v/\bar{\eta} = 0 \tag{13}$$

$$u_\tau + uu_\zeta + \bar{v}u_\eta + P_\zeta/\rho + \alpha P_\eta/\rho = 0 \tag{14}$$

$$v_\tau + uv_\zeta + \bar{v}v_\eta + \beta P_\eta/\rho = 0 \tag{15}$$

$$P_\tau + uP_\zeta + \bar{v}P_\eta - a_f^2(\rho_\tau + u\rho_\zeta + \bar{v}\rho_\eta) = \psi_k \tag{16}$$

$$C_{i\tau} + uC_{i\zeta} + \bar{v}C_{i\eta} = \sigma_i/\rho \qquad (i=1,\ldots,n) \tag{17}$$

where

$$\alpha \equiv \frac{\partial\eta}{\partial x} = -\beta\frac{\partial y_c}{\partial x} - \eta\beta\left(\frac{\partial y_w}{\partial x} - \frac{\partial y_c}{\partial x}\right)$$

$$\beta \equiv \frac{\partial\eta}{\partial y} = \frac{1}{y_w - y_c}$$

$$\bar{v} \equiv \alpha u + \beta v$$

$$\bar{\eta} \equiv y_c + \eta/\beta$$

Note that equation (17) may be written as

$$\frac{DC_i}{D\tau} = \frac{\sigma_i}{\rho} \qquad (i=1,\ldots,n) \tag{18}$$

where $DC_i/D\tau$ is the change in C_i following a particle path in the computational plane.

3. CHEMICAL KINETICS

The species source function appears in the forcing terms of both the energy equation (16) and the species continuity equations (18). Before the species source function can be computed, a reaction mechanism must be specified. The reaction mechanism used in this research is the same as that used in Reference (3) with the addition of the *hydrocarbon reaction discussed in Appendix B.* Unburned hydrocarbons may be present in the gas mixture at the combustor exit and therefore, provision for these species must be made in the chemical kinetics model. Edelman, et al. (26) and Edelman and Harsha (27) have developed a kinetics model for use in combustor analyses which includes a "sub-global" partial oxidation step:

$$C_nH_m + \frac{n}{2} O_2 \rightarrow \frac{m}{2} H_2 + nCO \tag{19}$$

Note that this reaction proceeds in the forward direction only. The reaction rate coefficient for equation (19) is determined empirically and is given by (Ref. 27):

$$a_j = 6.0 \times 10^{14} \; p^{0.3} \; c^{\frac{1}{2}}_{C_nH_m} \, c_{O_2} \tag{20}$$

where P has units of atmospheres and c represents species concentrations in g-moles/cc. For a nonequilibrium, chemically reacting flow of a system of thermally perfect gases composed of the six elements carbon, hydrogen, oxygen, nitrogen, flourine, and chlorine, Gold and Weekly (28) have shown that 19 species and 48 chemical reactions should be considered. Tables B-I and B-II of Appendix B show these species and reactions. Experience with this and other reaction mechanisms has indicated that there may be cases when not all of the reactions corresponding to a given set of chemical species should be included in the analysis. The number of reactions in the reaction mechanism is a significant parameter affecting execution time. Therefore, no more reactions than are necessary should be included in the reaction mechanism.

A general reaction equation which is used to represent any reaction mechanism is

$$\sum_{i=1}^{n} \nu'_{ij} X_i \underset{k_{rj}}{\overset{k_{fj}}{\rightleftarrows}} \sum_{i=1}^{n} \nu''_{ij} X_i \qquad (j=1,\ldots,m) \tag{21}$$

where ν'_{ij} and ν''_{ij} are the stoichiometric coefficients of the reactants and products respectively, X_i denotes the ith chemical species, and k_{fj} and k_{rj} are the forward and reverse reaction rate coefficients, respectively, for the jth reaction of the m reactions in the reaction mechanism.

Reaction rate coefficients are not readily predicted at the present time and therefore, they are generally found experimentally. The form for the reverse reaction rate coefficient which is used in this analysis is

$$k_{rj} = a_{ij} T^{-n_j} \exp(-b_j/\bar{R}T) \tag{22}$$

where a_{ij}, n_j, and b_j are empirical coefficients, $\bar{R}$ is the universal gas constant, and T is the local gas temperature.

Expressions for the species source function for both dissociation-recombination reactions and binary exchange reactions are developed in Appendix B. For dissociation-recombination reactions, the species source function is:

$$\sigma_{i_{D-R}} = \bar{m}_i \rho^2 \sum_{j=1}^{m} (\nu''_{ij} - \nu'_{ij}) \left[K_j \prod_{i=1}^{n} (C_i)^{\nu'_{ij}} - \rho \prod_{i=1}^{n} (C_i)^{\nu''_{ij}} \right] \frac{M_j k_{rj}}{\prod_{i=1}^{n} (\bar{m}_i)^{\nu''_{ij}}} \tag{23}$$

where

$$K_{j_{D-R}} = \frac{K_{p,j}}{\bar{R}T} \frac{\prod_{i=1}^{n} (\bar{m}_i)^{\nu''_{ij}}}{\prod_{i=1}^{n} (\bar{m}_i)^{\nu'_{ij}}}$$

For binary exchange reactions the species source function is:

$$\sigma_{i_{B-E}} = \bar{m}_i \rho^2 \sum_{j=1}^{m} (\nu''_{ij} - \nu'_{ij}) \left[K_j \prod_{i=1}^{n} (C_i)^{\nu'_{ij}} - \prod_{i=1}^{n} (C_i)^{\nu''_{ij}} \right] \frac{k_{rj}}{\prod_{i=1}^{n} (\bar{m}_i)^{\nu''_{ij}}} \tag{24}$$

where

$$K_{j_{B-E}} = K_{P,j} \frac{\prod_{i=1}^{n} (\bar{m}_i)^{\nu''_{ij}}}{\prod_{i=1}^{n} (\bar{m}_i)^{\nu'_{ij}}}$$

In equations (23) and (24), $K_{P,j}$ is the equilibrium constant based on partial pressures, M_j is the third body reaction rate ratio, C_i are the species mass fractions, and $\bar{m}_i$ are the species molecular weights.

The effect of different third bodies on dissociation-recombination reactions is accounted for through the use of third body reaction rate ratios M_j as in equation (23). Appendix B contains a discussion of these ratios.

Note that the difficulties in making accurate measurements for the determination of reactions rate coefficients, the necessity of extrapolating experimental data from one situation to another, and the uncertainty as to the reaction mechanism, are all significant factors limiting the accuracy of the analysis presented in this research. However, experience with one-dimensional analyses of reacting flows indicates that the chemical kinetics model used here is adequate for performance prediction.

SECTION III

THE UNSTEADY AND INCONSISTENT SCHEMES

1. GENERAL

The governing equations presented in Section II can be thought of as being composed of two groups: 1) the equations governing the fluid dynamic variables (i.e., the global continuity, momentum, and energy equations), and 2) the species continuity equations. For convenience, the first group will hereafter be called the fluid dynamic equations. Two approaches to the solution of the complete set of governing equations have been considered and are discussed below. The first approach is called the "unsteady scheme" and, though it has not been implemented, it is helpful in understanding the second approach. The second approach is called the "inconsistent scheme" and it has been used successfully in the overall numerical algorithm of this research.

2. THE UNSTEADY SCHEME

Consider an initial-data surface for the subject problem at time level N. Figure 2 illustrates the unsteady scheme at an arbitrary grid point within the computational mesh. The fluid dynamic variables u^N, v^N, P^N, and ρ^N and the species mass fractions C_i^N are known at all mesh points. The superscripts denote the time level. In the unsteady scheme, the solutions of the fluid dynamic equations are advanced one

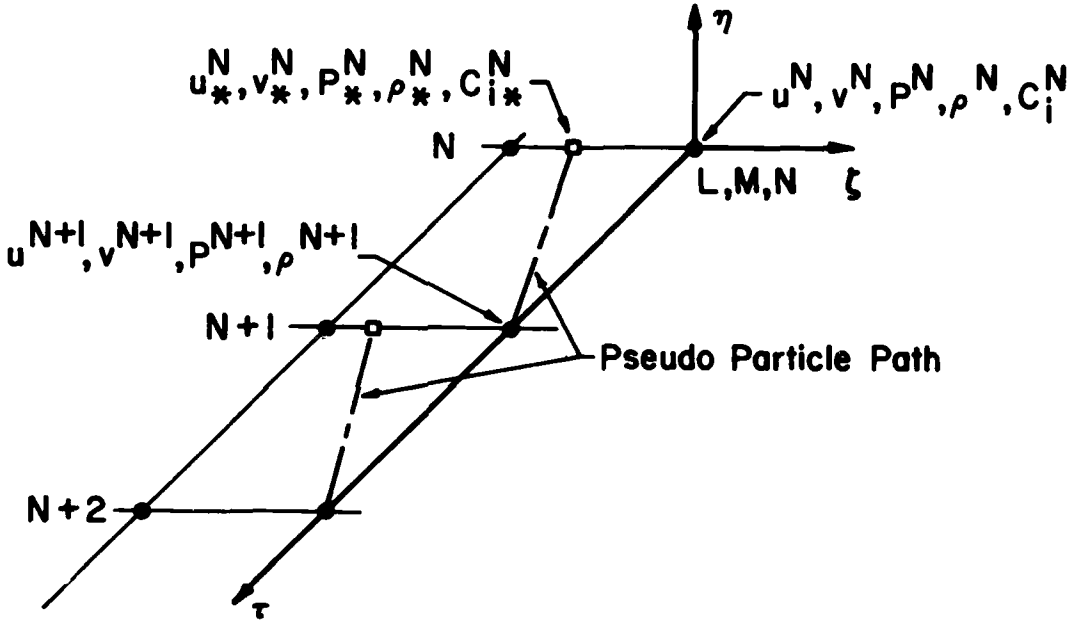

Figure 2. The unsteady scheme.

time step by the methods of Reference (38) to give u^{N+1}, v^{N+1}, p^{N+1}, and ρ^{N+1}. The C_i^N are held constant during this step. In words, the species continuity equations given by equation (18) require that the total change in mass fraction along a particle path, for each of the chemical species, is equal to σ_i/ρ. Therefore, using the solution for u^{N+1} and v^{N+1} and the time step size, the particle path is traced back from the grid point at time N+1 to its origin in the initial data surface (time level N). Then, by interpolation in the two-dimensional initial-value surface, values of u_*^N, v_*^N, P_*^N, ρ_*^N, and C_{i*}^N at the origin are determined. The subscript * indicates values at the particle path origin which will generally not be at a computational mesh point. Given u_*^N, v_*^N, T_*^N, ρ_*^N, C_{i*}^N, u^{N+1}, v^{N+1}, T^{N+1}, and ρ^{N+1}, it is possible to integrate the species continuity equations forward along the particle path and to compute C_i^{N+1}. When the steady state is achieved, the same particle path and * values will be computed for each additional time step and therefore, the solution will not change with time. There are a variety of unit processes which might be implemented with this approach. For example, one might predict the solution for u^{N+1}, v^{N+1}, p^{N+1}, and ρ^{N+1}, generate the particle path and interpolate in the initial-data plane, integrate the species continuity equations forward to give C_{ip}^{N+1}, and then repeat these same steps in a corrector procedure.

The unsteady approach suffers several serious drawbacks. Time consuming interpolation for 4+n variables in the two-dimensional initial-data surface is required. Also, as noted in Reference (2), interpolation for species concentrations is likely to produce numerical

difficulty. Values of the forcing term ψ_k in the energy equation for high temperature, near equilibrium conditions are found to be very sensitive to variations in the species mass fractions. Therefore, any interpolation error in the values of C_i could produce dramatic errors in ψ_k. Recall that ψ_k couples the fluid dynamic equations and the species continuity equations. The unsteady approach is useful because it is conceptually straightforward and provides a clear picture of convergence at the steady state. Also, it provides a basis from which the inconsistent approach can be understood.

3. THE INCONSISTENT SCHEME

Consider the ordinary differential equation

$$\frac{dy}{dt} = f(y,t) \tag{25}$$

The finite difference form of this differential equation is "consistent" if the finite difference equation approaches the differential equation as $\Delta t \to 0$. The overall algorithm used in this analysis is inconsistent because of the treatment of the species continuity equations. Specifically, in the inconsistent approach, the solutions for the fluid dynamic variables are advanced one time step from an initial data surface in the same manner as for the unsteady approach while the species mass fractions are held constant. Then, the flow at time level N+1 is assumed to be steady and as many as four streamlines are traced through the flow field with origins at selected locations along the nozzle inlet. The species continuity equations are then integrated along these streamlines from the nozzle inlet to the exit. This

process of advancing the fluid dynamic variables and then integrating the species continuity equations along streamlines is repeated until convergence at the steady state is achieved. This approach is inconsistent because the finite difference form of the species continuity equations does not approach equation (18) as $\Delta t \to 0$ ($\partial C_i/\partial t$ is neglected).

Figure 3 is helpful in understanding the inconsistent approach and its relationship to the unsteady approach. Note that it corresponds to the special case of $\bar{v}$ equal to zero and a streamline passing through computational mesh points. Advancing the fluid dynamic variables one time step gives values of u^{N+1}, v^{N+1}, P^{N+1}, and ρ^{N+1} at point C in Figure 3. It would be possible to trace a particle path back to point A, corresponding to L-1 in the computational mesh, where values of u, v, P, ρ, and C_i could be determined by interpolation (between values at L-1, M, N and those at L-1, M, N-1). Then, just as in the unsteady approach, the species continuity equations could be integrated forward; in this case, from point A to point C. The proper time step for integration of the species continuity equations would be found from the velocities at A and C and the distance between those two points. This time step would, in general, not be equal to the time increment between N and N+1. In the inconsistent scheme, the species continuity equations are integrated between points B and C with the time step determined by the velocities at B and C and the distance between those two points. If the values of u, v, P, ρ, and C_i are the same at points A and B, then the inconsistent approach gives the same result as the unsteady scheme. Also, in the limit of

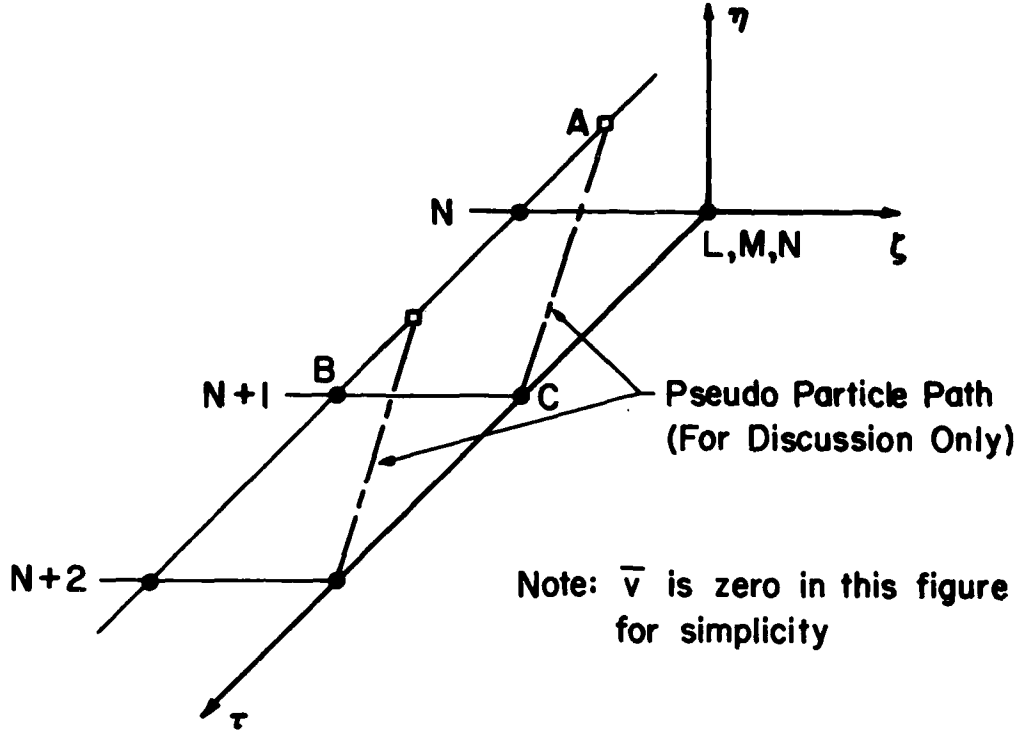

Figure 3. The inconsistent scheme.

steady state, the values of the fluid dynamic variables and species concentrations do not change between points A and B.

The benefit of using the inconsistent scheme is that integration of the species continuity equations always proceeds from the computed values at B to yield new values of the species mass fractions at point C. Interpolation for the species mass fractions is not required.

SECTION IV

SOLUTION OF THE FLUID DYNAMIC EQUATIONS

1. GENERAL

In Section III, the fluid dynamic equations were defined as those equations which govern the fluid dynamic variables u, v, P, and ρ. These equations are the global continuity equation, the component momentum equations, and the energy equation. Recall from Section III that in the inconsistent scheme, the solutions to the fluid dynamic equations are advanced one time step while the distributions of the species mass fractions throughout the nozzle are held constant. This section describes specifically how the solutions to the fluid dynamic equations are determined.

The mesh points in the computational plane may be categorized into four groups: interior, inlet, wall, and exit points (see Figure 4). The inlet, wall, and exit points are known collectively as boundary points. In the following discussion, the numerical treatment used for each type of mesh point is presented.

2. INTERIOR POINTS

Interior mesh points are computed using MacCormack's method (Ref. 29); an explicit, second-order accurate, two-step finite difference scheme. The fluid dynamic equations are employed in non-conservation form. Moretti (30) showed that using the conservation

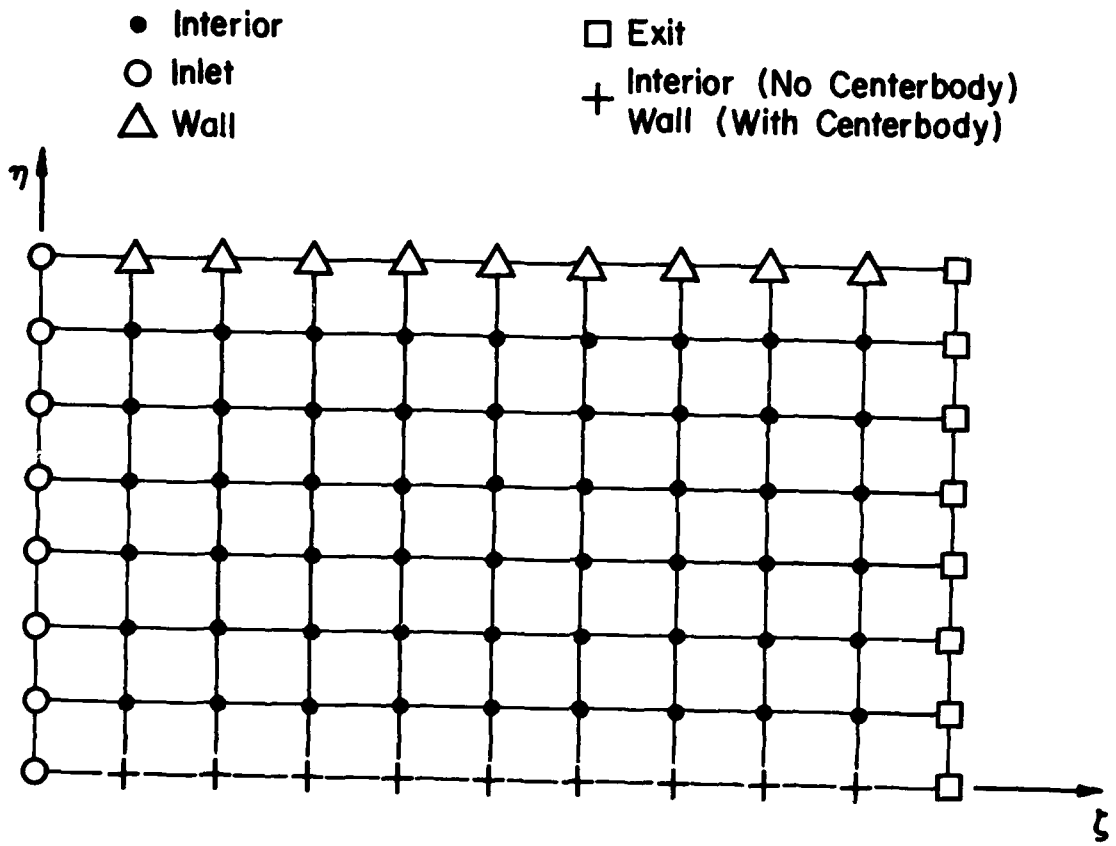

Figure 4. Classification of computational mesh points.

form decreased computational efficiency. Backward differences are used on the first step and forward differences are used on the second step.

As an example, consider the partial differential equation

$$u_t = -uu_x \qquad \text{where } u = u(x,t) \tag{26}$$

Application of MacCormack's method yields the following finite difference equations:

$$\text{Step 1:} \quad \tilde{u}_i^{n+1} = u_i^n - \frac{\Delta t}{\Delta x} u_i^n (u_i^n - u_{i-1}^n) \tag{27}$$

$$\text{Step 2:} \quad u_i^{n+1} = [u_i^n - \frac{\Delta t}{\Delta x} \tilde{u}_i^{n+1} (\tilde{u}_{i+1}^{n+1} - \tilde{u}_i^{n+1}) + \tilde{u}_i^{n+1}]/2$$

or

$$u_i^{n+1} = u_i^n - \frac{\Delta t}{2\Delta x} [\tilde{u}_i^{n+1} (\tilde{u}_{i+1}^{n+1} - \tilde{u}_i^{n+1}) + u_i^n (u_i^n - u_{i-1}^n)] \tag{28}$$

where i denotes mesh points along x, n denotes the time step, and the tilde denotes values calculated by the first step. Similarly, application of MacCormack's method to equation (7) for planar flow yields

$$\tilde{\rho}_{L,M}^{N+1} = \rho_{L,M}^N - \Delta t[u_{L,M}^N (\frac{\rho_{L,M}^N - \rho_{L-1,M}^N}{\Delta x}) + v_{L,M}^N (\frac{\rho_{L,M}^N - \rho_{L,M-1}^N}{\Delta y})$$

$$+ \rho_{L,M}^N (\frac{u_{L,M}^N - u_{L-1,M}^N}{\Delta x}) + \rho_{L,M}^N (\frac{v_{L,M}^N - v_{L,M-1}^N}{\Delta y})] \tag{29}$$

$$\rho_{L,M}^{N+1} = \frac{1}{2}\Big[\rho_{L,M}^N - \Delta t[\tilde{u}_{L,M}^{N+1} (\frac{\tilde{\rho}_{L+1,M}^{N+1} - \tilde{\rho}_{L,M}^{N+1}}{\Delta x}) + \tilde{v}_{L,M}^{N+1} (\frac{\tilde{\rho}_{L,M+1}^{N+1} - \tilde{\rho}_{L,M}^{N+1}}{\Delta y})$$

$$+ \tilde{\rho}_{L,M}^{N+1} (\frac{\tilde{u}_{L+1,M}^{N+1} - \tilde{u}_{L,M}^{N+1}}{\Delta x} + \tilde{\rho}_{L,M}^{N+1} (\frac{\tilde{v}_{L,M+1}^{N+1} - \tilde{v}_{L,M}^{N+1}}{\Delta y})] + \tilde{\rho}_{L,M}^{N+1}\Big] \tag{30}$$

where L and M denote axial and radial mesh points, respectively, N denotes the time step, and the tilde denotes values calculated by the first step.

When the nozzle does not have a centerbody, the centerline points are treated as interior points and solutions at these points are computed by requiring symmetry about the centerline. The velocity component v and derivatives of u, P, and ρ with respect to η are all set to zero. The derivative of v with respect to η is evaluated by a one-sided, second-order accurate formula.

3. BOUNDARY POINTS

All boundary points in the present research are computed using a second-order accurate reference-plane characteristic scheme. A reference-plane scheme is used rather than a *bi*characteristic scheme because the increased complexity and computational time of the bicharacteristic scheme is not warranted in view of the accuracy limitations associated with the chemical kinetics model. In reference-plane characteristic schemes, derivatives with respect to one of the independent variables are approximated and treated as forcing terms, thus reducing the number of independent variables in the problem by one. For example, in the constant η reference-plane scheme, all derivatives with respect to η are approximated (by MacCormack's method) and are placed on the right-hand side of the equal sign in equations (13) to (16). Characteristic relations are then derived for the resulting equations. A constant η reference-plane method is used for inlet and exit points while a constant ζ reference-plane method is used for the wall points.

The characteristic relations for these reference-plane methods are derived in Appendix C. Figures 5 and 6 summarize the results of that Appendix.

Cline (4, 23) computes exit points by linear extrapolation from the first and second adjacent interior points. In the subject problem, the computational mesh extends only a short distance into the supersonic flow field (just far enough so that an accurate initial-data surface for a steady flow, method-of-characteristics scheme can be computed). The constant η reference-plane scheme is used at the exit because it has been found to be more accurate than extrapolation in the "just supersonic" conditions at the exit.

In the following paragraphs, the boundary conditions and unit processes for inlet, wall, and exit points are described in turn.

Inlet Points

Figure 5 illustrates the characteristic relations which apply for subsonic flow at the nozzle inlet. Note that in this case, only one characteristic curve is contained within the flow field. The compatibility and characteristic equations which apply to the subsonic inlet case are (see Appendix C)

$$dP - \rho a_f du = (\psi_4 + a_f{}^2\psi_1 - \rho a_f \psi_2)d\tau \qquad (31)$$

$$\text{along } d\zeta = (u - a_f)d\tau$$

where

$$\psi_1 = -\bar{v}\rho_\eta - \rho\alpha u_\eta - \rho\beta v_\eta - \varepsilon\rho\bar{v}/\bar{\eta} \qquad (32)$$

$$\psi_2 = -\bar{v}u_\eta - \alpha P_\eta/\rho \qquad (33)$$

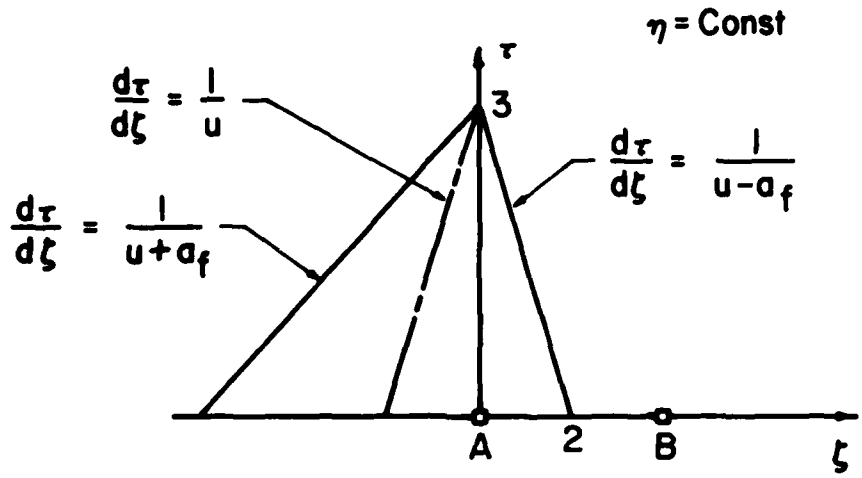

$$dv = \psi_3 \, d\tau$$

$$dP - a_f^2 \, d\rho = \psi_4 \, d\tau$$

$$dC_i = \psi_5 \, d\tau$$

} along $d\zeta = u d\tau$

$$dP + \rho a_f du = (\psi_4 + a_f^2 \psi_1 + \rho a_f \psi_2) d\tau \qquad \text{along} \quad d\zeta = (u + a_f) d\tau$$

$$dP - \rho a_f du = (\psi_4 + a_f^2 \psi_1 - \rho a_f \psi_2) d\tau \qquad \text{along} \quad d\zeta = (u - a_f) d\tau$$

compatibility equations — characteristic curves

Figure 5. Constant η reference-plane characteristic relations.

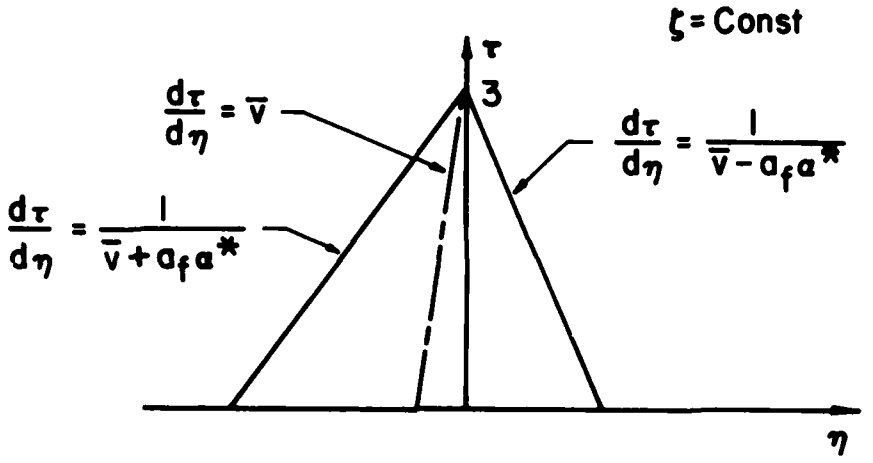

$$\beta du - \alpha dv = (\beta\psi_2 - \alpha\psi_3)d\tau$$

$$dP - a_f^2 d\rho = \psi_f d\tau$$

$$dC_i = \psi_5 d\tau$$

along $d\eta = \bar{v}d\tau$

$$dP + \frac{\rho\alpha a_f}{\alpha^*} du + \frac{\rho\beta a_f}{\alpha^*} dv = (\psi_4 + a_f^2\psi_1 + \frac{\rho\alpha a_f}{\alpha^*}\psi_2 + \frac{\rho\beta a_f\psi_3}{\alpha^*})d\tau$$

along $d\eta = (\bar{v} + a_f\alpha^*)d\tau$

$$dP - \frac{\rho\alpha a_f}{\alpha^*} du + \frac{\rho\beta a_f}{\alpha^*} dv = (\psi_4 + a_f^2\psi_1 - \frac{\rho\alpha a_f\psi_2}{\alpha^*} - \frac{\rho\beta a_f\psi_3}{\alpha^*})d\tau$$

along $d\eta = (\bar{v} - a_f\alpha^*)d\tau$

compatibility equations — characteristic curves

Figure 6. Constant ζ reference-plane characteristic relations.

$$\psi_4 = -\bar{v}P_\eta + a_f^2\bar{v}\rho_\eta + \psi_k \qquad (34)$$

Since there are 4+n unknowns at the inlet (u, v, P, ρ, and C_i, i=1,...,n) and only one compatibility equation, 3+n additional conditions must be specified.

The "correct" specification of steady flow inlet boundary conditions is a difficult problem; a generally preferred choice is not known at the present time. Of the several different sets of inlet boundary conditions which have been tested during this research, specification of θ, H_o, P_o, and C_i appears to give the best results. Here, θ is the inlet flow angle, H_o is the total enthalpy ($h + V^2/2$), P_o is the total pressure based on frozen composition at the combustor exit, and C_i are the species mass fractions. The specification of total conditions at the inlet places an upper limit on the energy of the flow and still allows flexibility in the solution for the static properties at the inlet. The inlet flow angle is determined by experiment or from the following procedure:

1. Determine representative values of the ratio of frozen specific heats γ_f and the gas constant at the combustor exit.
2. Generate a "long inlet" geometry by adding six to ten mesh points upstream of the nozzle inlet, simulating a constant-area duct.
3. Using the program of the subject research for isentropic constant specific heat ratio flow, compute the solution to the long inlet problem described in the preceding two steps. Inlet boundary conditions for the long inlet problem are:

a uniform distribution of zero flow angle, and total pressure P_o and total temperature T_o based on combustor exit conditions.

4. The flow angles at the nozzle inlet for the converged long inlet problem can be used as the inlet flow angles for the reacting flow problem.

Note that the arbitrary specification of zero flow angle at the nozzle inlet has been found to produce unreasonable velocity profiles at the nozzle inlet for some nozzle geometries.

Examination of equation (3) shows that for steady flow, the total enthalpy ($h + V^2/2$) is constant along streamlines. Therefore, the distribution of total enthalpy at the inlet is required to match that at the combustor exit.

A uniform distribution of static pressure at the combustor exit is one of the results expected from the combustor analysis. The specification of θ, H_o, C_i, and uniform static pressure was one of the inlet boundary condition sets tested during this research. For the cases tested, the velocity distributions at the inlet were unreasonable with very low (or negative) velocities at the inlet wall point. The use of total pressure, determined from conditions at the combustor exit and based on stagnation with frozen composition, has proved effective in computing the inlet points.

The species mass fractions C_i are specified at the inlet. Their values are determined by the relaxation of the species continuity equations between combustor exit conditions and the static conditions at the inlet. This relaxation process is described in detail in Section V and Appendix E.

For the case of supersonic flow at the inlet, values of velocity, pressure, density, and the species mass fractions are all specified since downstream conditions do not propogate upstream in a supersonic flow.

The unit process at the inlet for subsonic flow is based on a two-step, predictor-corrector method. The compatibility equation (31) and the specified inlet boundary conditions are used together in an iterative procedure to compute values of the fluid dynamic variables at the solution point. The iterative procedure is described first.

Recall that θ, H_o, P_o, and C_i are all known at the solution point (point 3 in Figure 5). To begin the iterative procedure, the static temperature T_3 is assumed. Then the following sequence of calculations is performed to calculate the values of the fluid dynamic variables:

1. Given the values of static temperature and the species mass fractions at the solution point, compute the gas constant R_3, the enthalpy h_3, the frozen specific heat at constant pressure Cp_3, and the ratio of frozen specific heats γ_{f3}.
2. Using the definition of total enthalpy and its specified value at the inlet, compute the velocity magnitude at the solution point

$$Q_3 = [2(Ho_3 - h_3)]^{\frac{1}{2}} \qquad (35)$$

   Then compute the frozen speed of sound a_{f_3} and the Mach number at the solution point.
3. Use the relation between total and static pressure at the solution point to compute P_3:

$$P_3 = Po_3/[1 + \frac{(\gamma_f-1)}{2} M_3^2]^{\gamma_{f3}/(\gamma_{f3}-1)} \qquad (36)$$

Now, use P_3, R_3 and T_3 in the thermal equation of state to compute ρ_3.

4. Compute u_3 and v_3 from the velocity magnitude at the solution point Q_3, and the given flow angle.
5. Use the compatibility equation as a check on the results of the preceeding steps [i.e., compute P_3 using the compatibility equation (31) and compare with P_3 computed in step 3 above].
6. Iterate on T_3 using the secant method until P_3 computed in steps 3 and 5 agree to within a specified tolerance.

This iterative procedure is used as part of each predictor and corrector step in the overall unit process at the inlet. The predictor-corrector steps are described next.

In order to use the compatibility equation, as described in step 5 of the iterative procedure, the characteristic curve must be constructed and the compatibility equation must be written in finite difference form. This is done by replacing the differentials in equation (31) with differences along the characteristic curve. In the predictor step, all coefficients and derivatives are evaluated in the initial-value plane. Given the time step and the estimate for $(u - a_f)$, the intersection of the characteristic curve with the initial-value line (in the constant η plane) is determined using the finite difference form of the characteristic curve equation. This intersection is point 2 in Figure 5. All coefficients in equations (31) to (34) are

evaluated at the intersection point by linear interpolation between points A and B in Figure 5. In the predictor step, the derivatives with respect to η (in the ψ terms) are evaluated using backward differences in the initial-value plane. When all coefficients and derivatives are evaluated in equations (31) to (34), the iterative procedure is accomplished and the predictor step is complete. This is done for all inlet points before the corrector step is started.

In the corrector step, the characteristic curve must be constructed again. Now, the coefficient $(u - a_f)$ is an average of the values at the solution point (from the predictor step) and values at point 2. Also, all coefficients in equation (31) are computed as the averages of values at the solution and intersection points. Values at point 2 are again determined by linear interpolation. Derivatives with respect to η in the ψ terms are evaluated by forward differences at the solution point and are averaged with the backward difference approximations in the initial-value plane. When all coefficients and derivatives in equations (31) to (34) have been determined by the averaging process described above, the iterative procedure is accomplished and the overall unit process at the inlet is complete.

Wall and Centerbody Points

The wall and centerbody mesh points are computed using the constant ζ reference-plane scheme described in Appendix C. For this scheme, all derivatives with respect to ζ in equations (13) to (16) are placed on the right-hand side of the equal sign and treated as forcing functions. The characteristic and compatibility equations

are summarized in Figure 6.

The wall slope is specified at each mesh point along the wall (or centerbody) for the given flow geometry. This slope provides the single boundary condition necessary for the solution of the fluid dynamic equations at the wall (centerbody) mesh points. For example, consider a wall point. From Figure 6, the appropriate characteristic and compatibility equations are

$$\beta du - \alpha dv = (\beta\psi_2 - \alpha\psi_3)d\tau \qquad (37)$$

$$\text{along } d\eta = \bar{v}d\tau$$

$$dP - a_f^2 d\rho = \psi_4 d\tau \qquad (38)$$

$$dP + \frac{\rho\alpha a_f}{\alpha^*} du + \frac{\rho\beta a_f}{\alpha^*} dv = (\psi_4 + a_f^2\psi_1 + \frac{\rho\alpha a_f}{\alpha^*} \psi_2 + \frac{\rho\beta a_f\psi_3}{\alpha^*})d\tau \qquad (39)$$

$$\text{along } d\eta = (\bar{v} + a_f\alpha^*)$$

$$v = u \tan\theta \qquad (40)$$

These four equations in the four fluid dynamic variables are written in finite difference form and are solved in a predictor-corrector procedure like that for the inlet points. Specifically, equation (40) is substituted into equation (37), which is then solved for u_3 at the solution point. Then v_3 is obtained from equation (40) and P_3 is computed using equation (39). Finally, equation (38) is solved for ρ_3.

Exit Points

Exit points are computed for both subsonic and supersonic flow by the constant η reference-plane procedure (see Figure 7). For subsonic flow, the exit pressure is given and is equal to the ambient pressure.

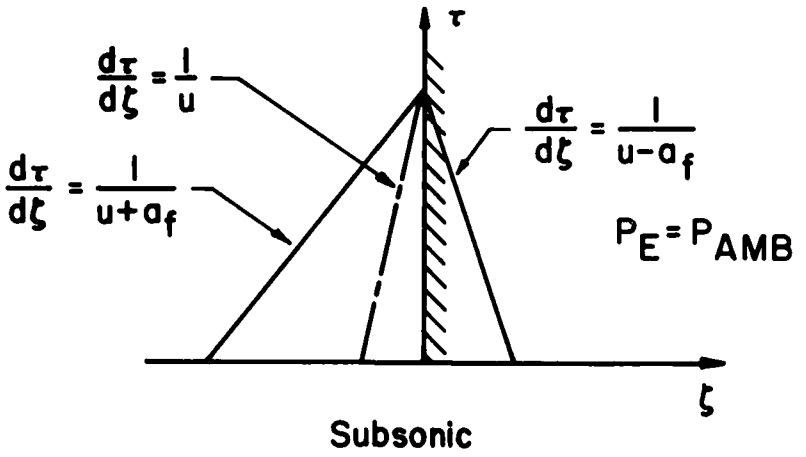

Subsonic

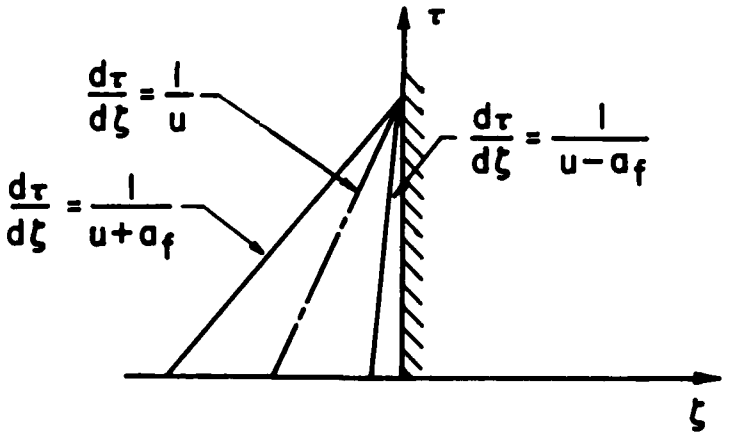

Supersonic

Figure 7. Subsonic and supersonic exit points.

The characteristic relations in this case are

$$dv = \psi_3 d\tau \qquad (41)$$

$$\text{along } d\zeta = u d\tau$$

$$dP - a_f^2 d\rho = \psi_4 d\tau \qquad (42)$$

$$dP + \rho a_f du = (\psi_4 + a_f^2 \psi_1 + \rho a_f \psi_2) d\tau \qquad (43)$$

$$\text{along } d\zeta = (u + a_f) d\tau$$

Equation (41) is solved for v_3, equation (42) is solved for ρ_3, and equation (43) is solved for u_3.

For supersonic flow at the exit, all characteristic curves are within the flow field and so, another compatibility equation is added to equations (41) to (43) above.

$$dP - \rho a_f du = (\psi_4 + a_f^2 \psi_1 - \rho a_f \psi_2) d\tau \qquad (44)$$

$$\text{along } d\zeta = (u - a_f) d\tau$$

Equations (41) to (44) are four equations in the four fluid dynamic variables. Equation (41) is solved for v_3 and equations (42) to (44) are solved iteratively for u_3, P_3, and ρ_3.

For both subsonic and supersonic flow, a predictor-corrector procedure, analogous to that for the inlet mesh points, is employed. Coefficients and derivatives in the characteristic relations are evaluated in the initial-value plane for the predictor step. Derivatives in the ψ terms are approximated by backward differences. In the corrector step, coefficients and derivatives are evaluated in the

solution plane and averaged with results from the predictor step. Derivatives in the ψ terms at the solution point are approximated by forward differences.

SECTION V

SOLUTION OF THE SPECIES CONTINUITY EQUATIONS

1. GENERAL

Recall from Section III that in the inconsistent scheme, the solutions to the fluid dynamic equations are advanced one time step while the distributions of the species mass fractions throughout the nozzle are held constant. Section IV provides the details of this part of the overall numerical algorithm. Then, the new flow field is assumed to be steady and the species continuity equations are integrated along as many as four streamlines from the nozzle inlet to the exit. This section describes specifically how the integration of the species continuity equations is accomplished.

It is well known that integration of the species continuity equations for flows near chemical equilibrium requires special care because the equations become quite "stiff" (Refs. 3, 5, and 31). The concept of a stiff differential equation and a physical explanation for the stiffness of the species continuity equations are provided in Appendix D. Many numerical techniques have been proposed for the solution of the species continuity equations in near equilibrium flows (Refs. 32 and 33). Cline and Hoffman (3) analyzed and tested a number of proposed schemes in their analysis of three-dimensional, steady, non-equilibrium flow. They concluded that explicit schemes and

predictor-corrector methods are stable only for very small step sizes. Also, only some of the implicit methods they tested gave adequate results. A method proposed by Lomax and Bailey (34) was chosen as the preferred method and it is this scheme which has been used in the subject research. The method is second-order accurate, implicit, and is based on a Taylor series expansion of the species continuity equations.

2. SECOND-ORDER, IMPLICIT, TAYLOR EXPANSION

The second-order, implicit Taylor expansion method, as applied to the species continuity equations, is derived in Appendix D. The resulting finite difference equation is

$$C_{i\ell+1} = C_{i\ell} + \frac{h}{2V_\ell}\left[f_{i\ell}\left(3 - \frac{V_{\ell+1}}{V_\ell}\right) + \frac{\partial f_{i\ell}}{\partial \rho}\left(\rho_{\ell+1}-\rho_\ell\right) + \frac{\partial f_{i\ell}}{\partial T}\left(T_{\ell+1}-T_\ell\right) + \sum_{j=1}^{n} \frac{\partial f_{i\ell}}{\partial C_j}\left(C_{j\ell+1} - C_{j\ell}\right)\right] \quad (i=1,\ldots,n) \tag{45}$$

where $h = s_{\ell+1} - s_\ell$, s is the position along the streamline, $f_i = \sigma_i/\rho$, V is the velocity magnitude, and the subscripts ℓ and $\ell+1$ denote points along the streamline. The partial derivatives in equation (45) are determined analytically. When expanded, equation (45) becomes a system of n simultaneous, linear, algebraic equations in the n unknowns $k_i = C_{i\ell+1} - C_{i\ell}$. This system of equations is solved using Gauss elimination with scaling and partial pivoting.

For flows which are not near chemical equilibrium, a modified Euler method is available for integration of the species continuity

equations. The adequacy of this explicit integration method must be determined on a trial-and-error basis.

3. STREAMLINE TRACING

The species continuity equations are integrated along streamlines in the inconsistent scheme. Since streamlines will not pass through computational mesh points in general (except along the wall and centerbody/centerline), it is necessary to trace streamlines through the flow field before the species continuity equations are integrated. The computer program developed during the subject research allows the user to trace as many as four streamlines through the flow field. The two streamlines along the wall and centerbody/centerline must be used and one or two more can be used with origins at arbitrary mesh points along the nozzle inlet. The use of more than four streamlines in the overall algorithm would lead to prohibitively long computational times.

Figure 8 illustrates the streamline tracing procedure. A predictor-corrector method is used. Starting at the point (1,M,N) at the nozzle inlet, the values of u and v at this point are used to project a streamline to the intersection with the line of mesh points at L=2. Then, values of $(u_{*2}, v_{*2})_p$ at the intersection point are found by linear interpolation between known values at the adjacent mesh points at L=2. In the corrector step, the values of $(u_{*2}, v_{*2})_p$ are averaged with u and v at (1,M,N) and the streamline is again projected to the intersection at L=2. Linear interpolation is used to find $(u_{*2}, v_{*2})_c$. This predictor-corrector method is applied at each L station until the streamline has been traced to the nozzle exit.

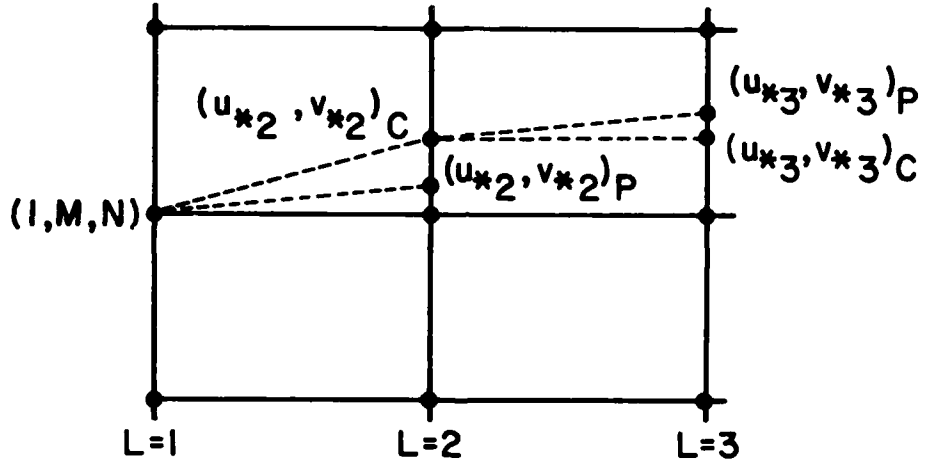

Figure 8. Streamline tracing.

4. ERROR CONTROL

The implicit scheme described previously has been found to be stable for even large step sizes in both Cline and Hoffman's work (3) and in the subject research. However, the method is subject to truncation error, and thus consideration must be given to step size control.

In the derivation of equation (45), third- and higher-order terms have been neglected. The objective of the error control scheme is to estimate the third-order term and (by adjusting the step size) to insure that the ratio of this term to the computed term [the right-hand side of equation (45)] is less than a specified tolerance. An expression for this ratio is derived in Appendix D and is restated here:

$$\text{RATIO}_i = \left| \frac{K_{i\ell+1} - 2K_{i\ell} + K_{i\ell-1}}{6K_{i\ell}} \right| \qquad (i=1,\ldots,n) \qquad (46)$$

Note that RATIO has distinct values for each of the chemical species in the gas mixture at each step in the integration. Also, RATIO can be computed only after three integration steps have been taken.

The error control scheme is implemented by placing intermediate points between grid points along the streamlines (see Figure 9). An estimate is made of the number of intermediate points (NINT) required between L_* and $L+1_*$. Values of temperature, density, and velocity at L_* and $L+1_*$ are determined by linear interpolation between known values at adjacent mesh points at each L station. The values of these same variables at the intermediate points are determined by linear

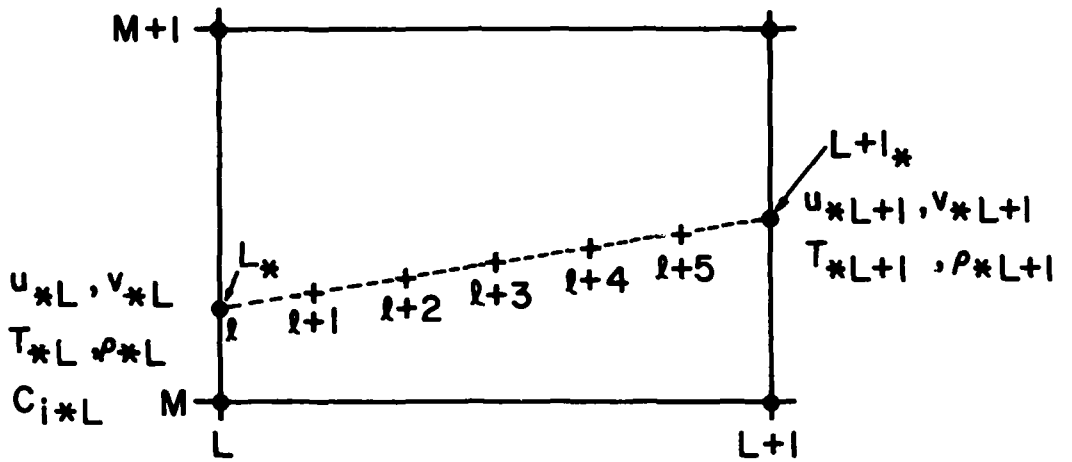

Figure 9. Intermediate points.

interpolation between the corresponding values at L_* and $L+1_*$. Then, the species continuity equations are integrated through the intermediate points from L_* to $L+1_*$ and RATIO is computed for each of the chemical species. If, after the last intermediate integration step, the maximum value of RATIO is less than a user specified tolerance, then the integration proceeds. If the required tolerance is not achieved, then the number of intermediate points is doubled and the integration procedure is restarted from L_*. Also, if the maximum value of RATIO is two orders of magnitude less than the specified tolerance, then the number of intermediate points is halved before the integration from $L+1_*$ to $L+2_*$ proceeds.

Numerical experiments have been performed to illustrate the use of the error control scheme. Details are provided in Appendix D and the results are summarized here.

1. Most of the computational time required to solve the subject problem is related to integration of the species continuity equations. Therefore, the total execution time is nearly directly proportional to the number of intermediate points (NINT).
2. Failure to use intermediate points will, in general, yield poor results for species mass fractions C_i and the energy source term ψ_k.
3. Integrating from equilibrium conditions with very small gradients in temperature and density and a small value of the specified tolerance on RATIO can yield very large numbers of intermediate points.

4. For equilibrium initial conditions, NINT is not particularly sensitive to the sign or magnitude of temperature, density, or velocity gradients between L_* and $L+1_*$ as long as the conditions in conclusion (3) do not occur.
5. For nonequilibrium initial conditions, NINT is sensitive to gradients in temperature and velocity while it is only mildly sensitive to the density gradient between L_* and $L+1_*$. If the property gradients between these points do not match the corresponding gradients between $L-1_*$ and L_*, more intermediate points are likely to be required to achieve a specified tolerance.
6. Conclusions 1 to 5 appear to be valid for the several chemistry systems investigated in this research.

Because of conclusion 3, an upper limit of 20 intermediate points is used in the computer program for the subject problem. Experience indicates that a relatively large tolerance (5 to 10%) should be used until the solution is near convergence and then the tolerance can be reduced to the desired level. Also, the user has the option of specifying the number of intermediate points thereby overriding the error control scheme.

5. RELAXATION AT THE INLET

The choice of inlet boundary conditions was described in Section IV. Recall that the flow angle θ, the total enthalpy H_0, the total pressure based on combustor exit conditions and frozen composition P_0, and the species mass fractions C_i are all specified at each inlet mesh

point. The use of total conditions as inlet boundary conditions establishes the energy level of the flow and allows some flexibility in the distribution of static properties across the inlet. As a result, the distributions of the static properties across the inlet will not necessarily match those across the combustor exit. Discontinuities in static properties between the combustor exit and the nozzle inlet create the need for a relaxation of the species mass fractions between these two points. A detailed description of the relaxation process is provided in Appendix E. Here, the justification for the relaxation and the relaxation process are summarized.

Consider a particle (a small mass of the reactive mixture of gases) at the combustor exit. Also, note that in functional form (see Appendix A)

$$\sigma_i = \sigma_i(\rho,T,C_i) \qquad (i=1,\ldots,n) \tag{47}$$

$$\psi_k = \psi_k(T,\sigma_i,C_i) = \psi_k(\rho,T,C_i) \quad (i=1,\ldots,n) \tag{48}$$

Since all the static properties and the species mass fractions are known at the location of the particle, the species source functions σ_i and the energy source term ψ_k can be computed at this point. In a real flow, there can be no discontinuities in the streamwise distributions of the static properties and species mass fractions at the junction between the combustor exit and the nozzle inlet. Therefore, from equations (47) and (48), the distributions of σ_i and ψ_k along the flow direction must also be continuous at this junction. The discontinuities in the static properties described in the preceding

paragraph are a consequence of the problem model; that is, an attempt to link a two-dimensional nozzle analysis to a quasi-one-dimensional combustor analysis. Since the discontinuities do not represent reality, their effect should be manifest at the inlet before the species continuity equations are integrated through the flow field. This is accomplished by allowing the species mass fractions at the combustor exit to adjust to the static conditions at the nozzle inlet. The species continuity equations are relaxed between conditions at the combustor exit and those at the inlet for a period of time that minimizes the change in ψ_k between these two points. In effect, a short distance is spliced into the junction between the combustor exit and the nozzle inlet so that the discontinuities in static properties produced by the mathematical model can be replaced with linear gradients. The distance is chosen so that the chemical nature of the flow at the combustor exit (as represented by the energy source term ψ_k) is preserved at the nozzle inlet to the extent possible. Figure 10 illustrates the effect of relaxation time on ψ_k for an H-F propellant system. The initial conditions are near equilibrium and curves for several different temperature gradients are shown. Figure 11 shows relaxation curves for the same propellant system and gradients but with nonequilibrium initial data. Several important conclusions regarding ψ_k relaxation curves from Appendix E are restated here:

1. All curves of ψ_k versus relaxation time approach zero as relaxation time increases. This is because the chemical systems move toward an equilibrium condition (where the

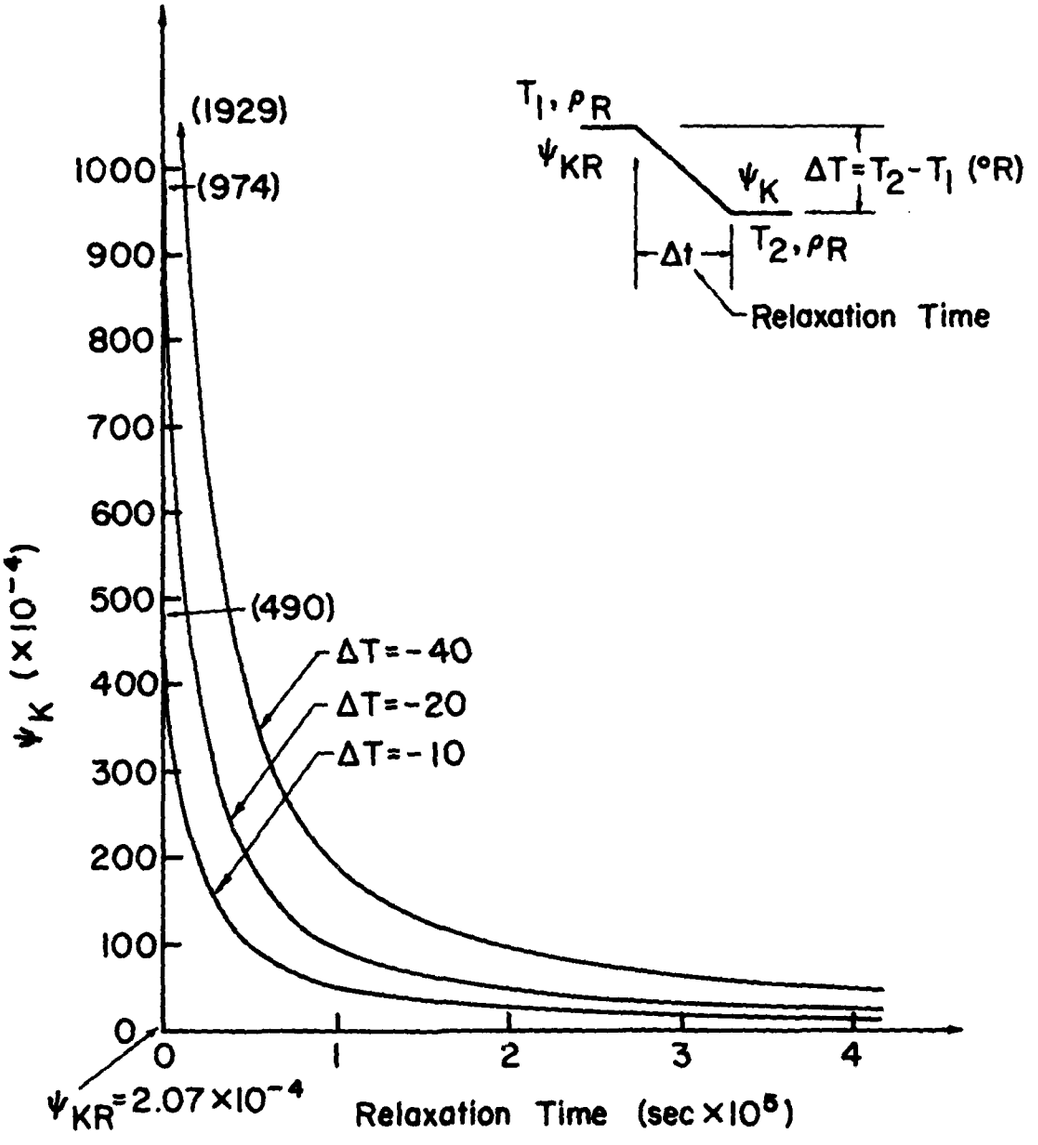

Figure 10. ψ_K versus relaxation time - equilibrium initial conditions (H-F system).

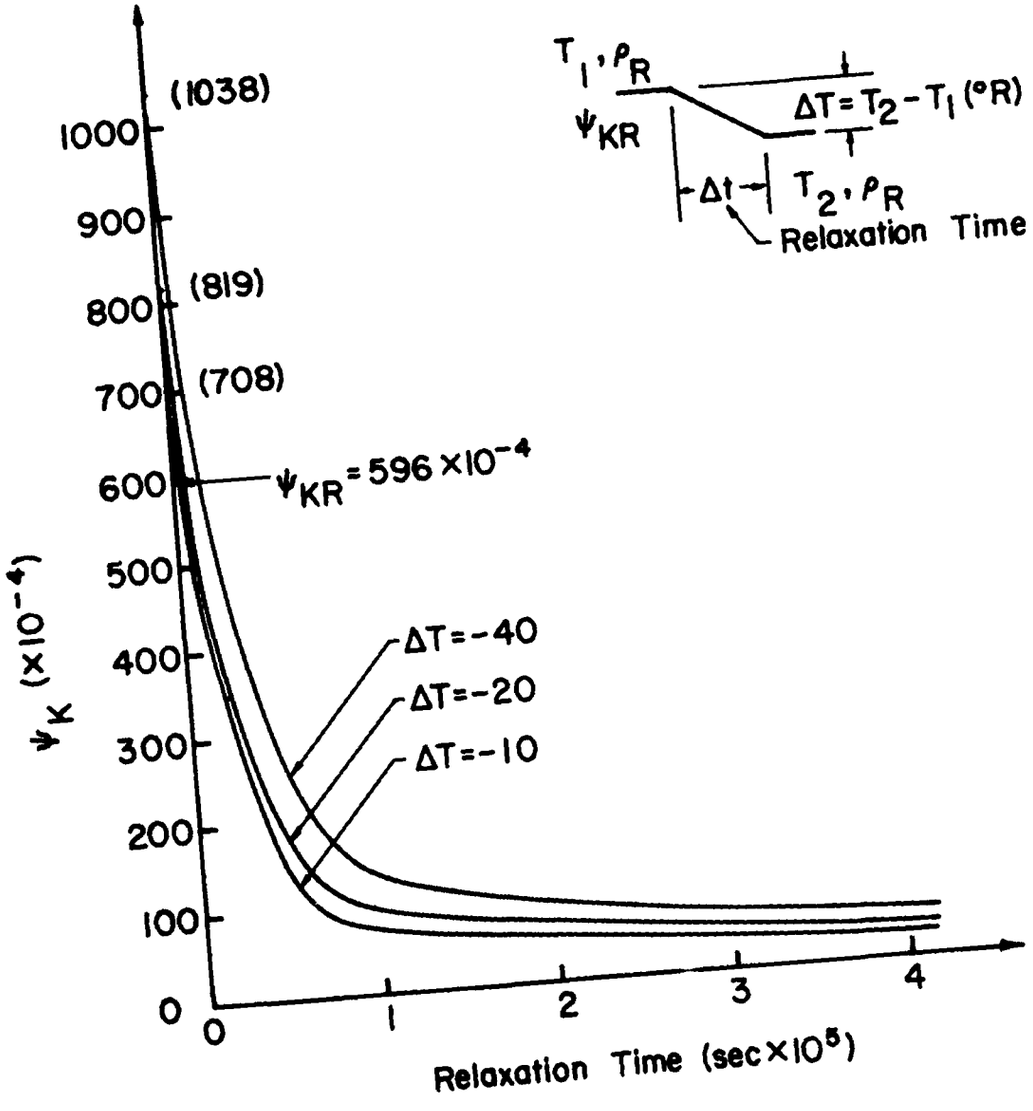

Figure 11. Ψ_K versus relaxation time - nonequilibrium initial conditions (H-F system).

species source functions go to zero) with increasing relaxation time.

2. At high temperatures and near equilibrium conditions, ψ_k is quite sensitive to variations in temperature and density. For example, a 20°R temperature perturbation, with no relaxation, can change the computed value of ψ_k by several orders of magnitude (see Figure 10).
3. For the chemistry systems and static property gradients studied in this research, relatively small changes in composition occur during the relaxation from combustor exit to nozzle inlet conditions. Typically, species mass fractions change by less than two percent.

Failure to relax the species mass fractions at the inlet leads to numerical difficulties for two primary reasons. First, without relaxation, the data set (ρ,T,C_i, i=1,...,n) at the inlet is inconsistent. As noted above, the energy source term ψ_k (and species source function) can then differ by several orders of magnitude from its value at the combustor exit. This causes a "hard start" condition in integration of the species continuity equations away from the inlet. Second, if the species continuity equations are not relaxed before the inlet, they will relax within the computed flow field. This can produce distributions of ψ_k within the flow with dramatic oscillations near the inlet; this ψ_k distribution, in turn, distorts the flow field.

The proper relaxation time is determined as part of the overall numerical algorithm. The scheme is illustrated in Figure 12 which

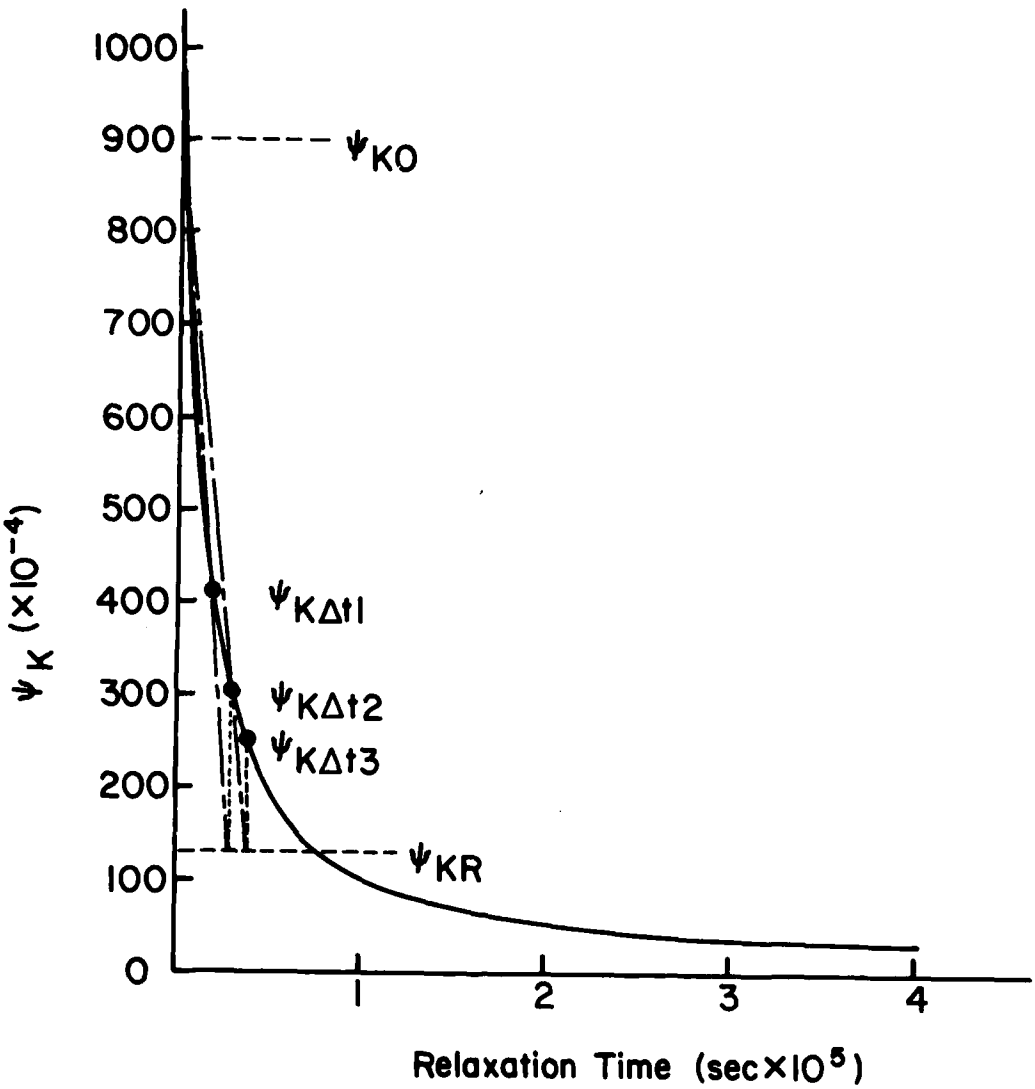

Figure 12. Calculation of relaxation time.

shows a typical ψ_k versus relaxation time curve. In that figure, ψ_{kR} is computed for the conditions at the combustor exit, ψ_{k0} is computed for the species mass fractions at the combustor exit and density and temperature at the nozzle inlet with zero relaxation time, and $\psi_{k\Delta t}$ is computed for the same conditions as ψ_{k0} but with a relaxation time Δt. The values of ψ_{kR} corresponding to each inlet mesh point are computed as part of the initialization procedure for the overall algorithm. They are only computed once and then are stored. Consider time level N in the solution of the subject problem. ψ_{k0} is computed at each streamline origin for the static conditions prevailing at the inlet. There is a minimum relaxation time and if $|\psi_{k0}| < |\psi_{kR}|$, then the minimum relaxation time is used. This is because ψ_k is known to approach zero with increasing relaxation time. Otherwise, the species continuity equations are relaxed through time Δt_1 (see Figure 12) which is the relaxation time computed for a given streamline during previous time steps. Then the species continuity equations are integrated along the given streamline to the nozzle exit. Next, a check is made:

$$\frac{|\psi_{k\Delta t} - \psi_{kR}|}{|\psi_{k0} - \psi_{kR}|} \overset{?}{<} .05 \tag{49}$$

If the check is satisfied, then Δt_1 is not changed and it is saved for use during the next time step in the overall algorithm. However, if the check is not satisfied, then a straight line is extended from ψ_{k0} through $\psi_{k\Delta t_1}$ to intersect ψ_{kR}. The relaxation time Δt_2 corresponding to that intersection is used during the next time step. The same

procedure continues for subsequent time steps as shown in Figure 12 until the check is satisfied.

SECTION VI

OVERALL NUMERICAL ALGORITHM

1. GENERAL

The overall numerical algorithm consists of the repetitive and alternate application of the procedures described in Sections IV and V; the solutions to the fluid dynamic equations are advanced one time step for a given distribution of the species mass fractions throughout the nozzle, and then the flow field is assumed to be steady while the species continuity equations are integrated along as many as four streamlines from the nozzle inlet to the exit. Note that for some problems, the fluid dynamic equations may be advanced more than one time step before the species continuity equations are integrated. If this is possible, the total computational time may be reduced significantly (see Section VII). As discussed in Section III, this overall scheme is inconsistent in time in the treatment of the species continuity equations, but it becomes consistent at the steady state limit. Also, it is necessary to relax the species mass fractions between the specified static conditions at the combustor exit and those at the nozzle inlet before integrating the species continuity equations through the flow. Discontinuities in static properties at the junction between the combustor exit and the nozzle inlet occur because of the choice of inlet boundary conditions for the problem model. An error

control scheme, which limits the size of the truncation error in the integration of the species continuity equations, is available. Convergence is achieved when the computed values of the fluid dynamic variables and the species mass fractions no longer change with time.

Two sets of mesh points are used in the overall algorithm, as illustrated in Figure 13. During the first part of the algorithm, the solutions for u, v, P, and ρ are advanced one time step at all computational mesh points in a predictor-corrector procedure (see Section IV). Then, the flow is assumed to be steady, and streamlines are traced through the flow field to locate the streamline mesh points. The values of static properties at the streamline mesh points which are required for integration of the species continuity equations are determined by interpolation between adjacent computational mesh points at each L station. In addition to computing the distributions of the species mass fractions along streamlines when the species continuity equations are integrated, the energy equation source term ψ_k, the ratio of frozen specific heats γ_f, the gas constant R, and the total enthalpy H_0 are also computed and stored for each streamline mesh point. The variables γ_f, R, and ψ_k are all needed for the solution of the fluid dynamic equations. The total enthalpy distribution is used as a check on the validity and accuracy of the converged solution. The values of these variables at the computational mesh points are determined by linear interpolation between adjacent streamline mesh points at each L station.

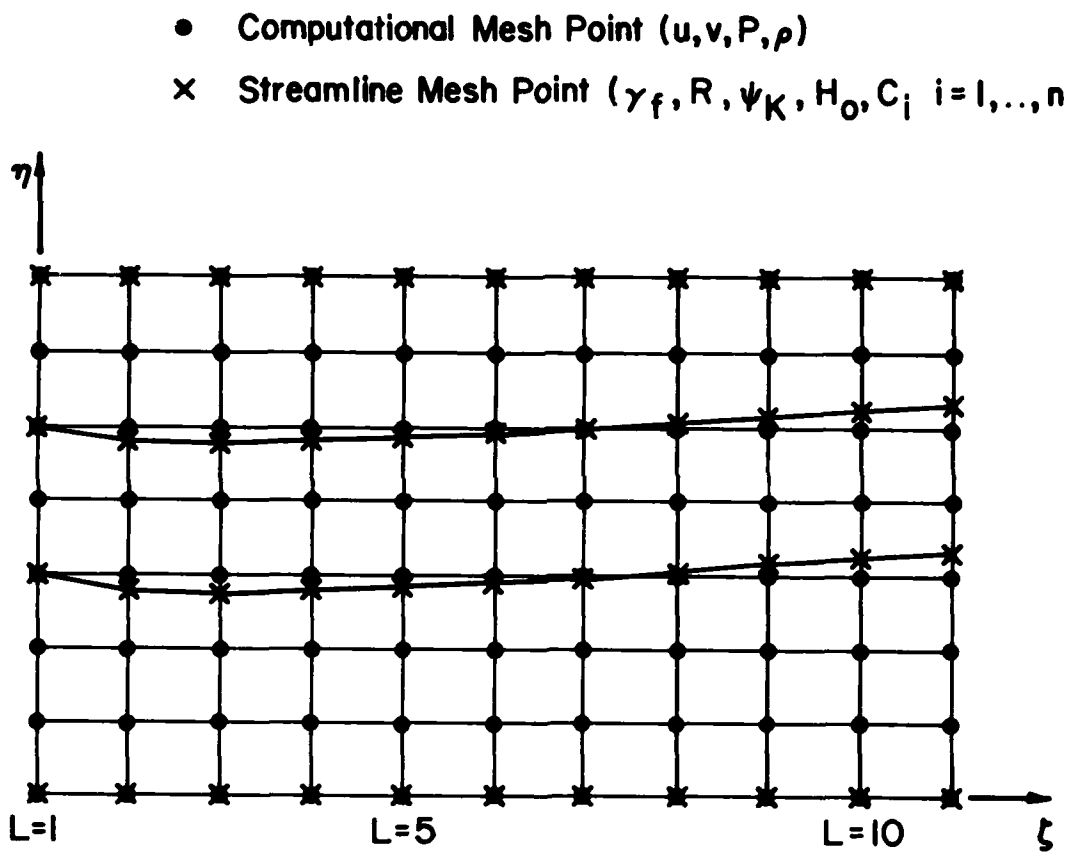

Figure 13. Variables stored at computational and streamline mesh points.

2. INITIAL-VALUE SURFACE

The initial-value surface must be a smooth distribution of the fluid dynamic variables u, v, P, and ρ throughout the computational mesh. It can be read in or computed internally within the computer program for the subject research. Three different methods have been investigated for internal generation of the initial-value surface:

1. Obtain a one-dimensional solution to the problem of interest using the program of Reference (10). Then, use the results of this analysis to provide the axial distributions of pressure, density, temperature and velocity magnitude for the initial-value surface. The local flow angle θ and velocity components at any point in the initial-value surface are estimated from the given geometry (i.e., interpolate between wall and centerbody values for θ at each L station).
2. Obtain a one-dimensional, isentropic, constant specific heats solution for pressure, density, and velocity magnitude. Values of R and γ for this analysis are representative values at the combustor exit. The local flow angle and velocity components are estimated as in method 1.
3. Using R and γ as in method 2, compute the two-dimensional, isentropic, constant specific heats solution for the subject problem and use it as the initial-value surface.

For all three methods, the distributions of species mass fractions are determined by integrating the species continuity equations through the given flow field from the known conditions at the nozzle inlet.

Method 1 requires the use of two computer programs and the transfer of data from one to the other. Also, there is no provision in the program of Reference (10) for nonuniform data at the nozzle inlet. Methods 2 and 3 can be accomplished using only the computer program of the subject research and can be used for any set of data at the nozzle inlet. Method 2 is simpler to implement than method 3 and, since there appears to be little difference in overall computational time to convergence for the two methods, method 2 is preferred. All three methods have yielded essentially the same converged solutions for the cases tested.

3. BOUNDARY CONDITIONS

The choice of steady flow boundary conditions has been discussed previously in Section IV. Recall that for subsonic flow, the flow angle θ, the total enthalpy H_0, the total pressure based on combustor exit conditions P_0, and the species mass fractions C_i are specified at the inlet; the flow angle θ is specified along the wall and centerbody; and, the exit pressure is set equal to the ambient pressure. For supersonic flow, all static conditions and species mass fractions are specified at the inlet and the flow angle is specified along the wall and centerbody.

It is essential that the data at the combustor exit be consistent with the chemical kinetics model that is employed. This fact has been noted by Cline and Hoffman (3) and has been established again in the subject research. An inconsistent set of data will yield computed values of the species source functions which can be several orders of

magnitude in error. As a result, an attempt to integrate the species continuity equations away from the combustor exit yields immediate numerical difficulty.

4. STEP SIZE AND STABILITY

No attempt has been made to perform a stability analysis for the overall numerical algorithm as applied to the governing equations for two-dimensional, unsteady, nonequilibrium, chemically reacting flow. The stability of the treatment of the equations governing the fluid dynamic variables and the stability of the species continuity equation scheme are treated separately. The stability of the overall numerical algorithm has been verified by numerical experiment.

The scheme used to advance the solutions for the fluid dynamic variables is subject to the CFL stability restriction. This requires that the finite difference domain of influence must be at least as large as the continuum domain of influence. It ensures that the speed of propogation of numerical disturbances (truncation error for example) everywhere exceeds the speed of propogation of disturbances in the flow (i.e., the speed of sound in a compressible flow). Application of the CFL criterion to two-dimensional, unsteady flow yields

$$\Delta\tau \leq \frac{1}{[(V+a)(\frac{1}{\Delta\zeta^2}+\frac{1}{\Delta\eta^2})^{\frac{1}{2}}]} \tag{50}$$

In practice, the step size is computed as

$$\Delta\tau = \frac{A}{[(V+a)(\frac{1}{\Delta\zeta^2}+\frac{1}{\Delta\eta^2})^{\frac{1}{2}}]} \tag{51}$$

where A ranges from 0.4 to 1.6 depending on the geometry of the flow [Reference (23)]. Any study of the time step multiplier A should be performed for a nonreacting flow similar to the flow with finite-rate kinetics. The proper choice of A can accelerate convergence. The author's experience indicates that the value of A used for a representative nonreacting flow will also work for the reacting flow problem.

The second-order, implicit scheme used for integration of the species continuity equations has been found to be stable for all step sizes. Note that the step size for integration of these equations is not related to $\Delta\tau$ in equation (51) since the species continuity equations are integrated along streamlines in space while the fluid dynamic equations are integrated from one time plane to the next.

5. THERMOCHEMICAL MODELS

In addition to the chemically reacting flow of a mixture of thermally perfect gases, two other thermochemical models can also be analyzed using the computer program of the subject research. These models are:

1. Isentropic flow of a thermally and calorically perfect gas (constant γ).
2. Isentropic flow of a gas whose equation of state is input in tabular form. Two-dimensional frozen and equilibrium solutions can be obtained using this model.

SECTION VII

VERIFICATION AND RESULTS

1. VERIFICATION

At the present time, there are no other methods available for the analysis of two-dimensional, nonequilibrium, chemically reacting subsonic and transonic nozzle flows. Therefore, it is not possible to make comparisons with existing results. However, a number of tests have been performed to verify the results of the subject research as discussed in the following paragraphs.

The scheme for integration of the species continuity equations must generate accurate concentration profiles for given distributions of the fluid dynamic variables along the nozzle axis. In order to test this capability in the subject computer program, one-dimensional analyses of several kinetics problems were performed using the program of Reference (10). These problems are discussed in Appendix E. Then, using the distributions of ρ, T, and V from the results, the species continuity equations were integrated through the given flow fields by the technique of the subject research. The resulting concentration profiles were compared with those computed by Reference (10). For the C-H-O-N system, an "error" of 0.35 percent in the mass fraction of monatomic hydrogen at the nozzle throat constituted the most significant deviation from the Reference (10) solution. Applying the same

procedure to the H-F system yielded "errors" at the throat which were typically less than two percent. The worst case was a 3.4 percent deviation in the mass fraction of monatomic flourine. Figure 14 illustrates the species mass fraction profiles for the H-F system as computed by the integration technique of the subject research.

There are four results which must be true of a converged solution to the subject problem and which are therefore useful in determining the validity of the computed results. First, the law of conservation of mass requires that the mass flow at each axial position along the nozzle must be constant. Values of mass flow at the nozzle inlet, throat, and exit are computed and made available as part of the program output. Second, in the steady state limit, the total enthalpy H_o must be constant along streamlines in the flow. A "total enthalpy error" has been defined so that this fact can be used as a measure of the accuracy of the solution.

$$H_o \text{ Error} \equiv \frac{H_{OL} - H_{OR}}{\frac{V_E^2 - V_I^2}{2}} \tag{52}$$

where H_{OL} is the total enthalpy at axial position L along a given streamline, H_{OR} is the total enthalpy at the combustor exit for the same streamline, and V_E and V_I are the velocity magnitudes at the nozzle exit and inlet, respectively, along the streamline. Profiles of total enthalpy error for the cases studied are presented with the discussion of results. Third, the sum of the species mass fractions must be one throughout the flow. This fact is not used explicitly

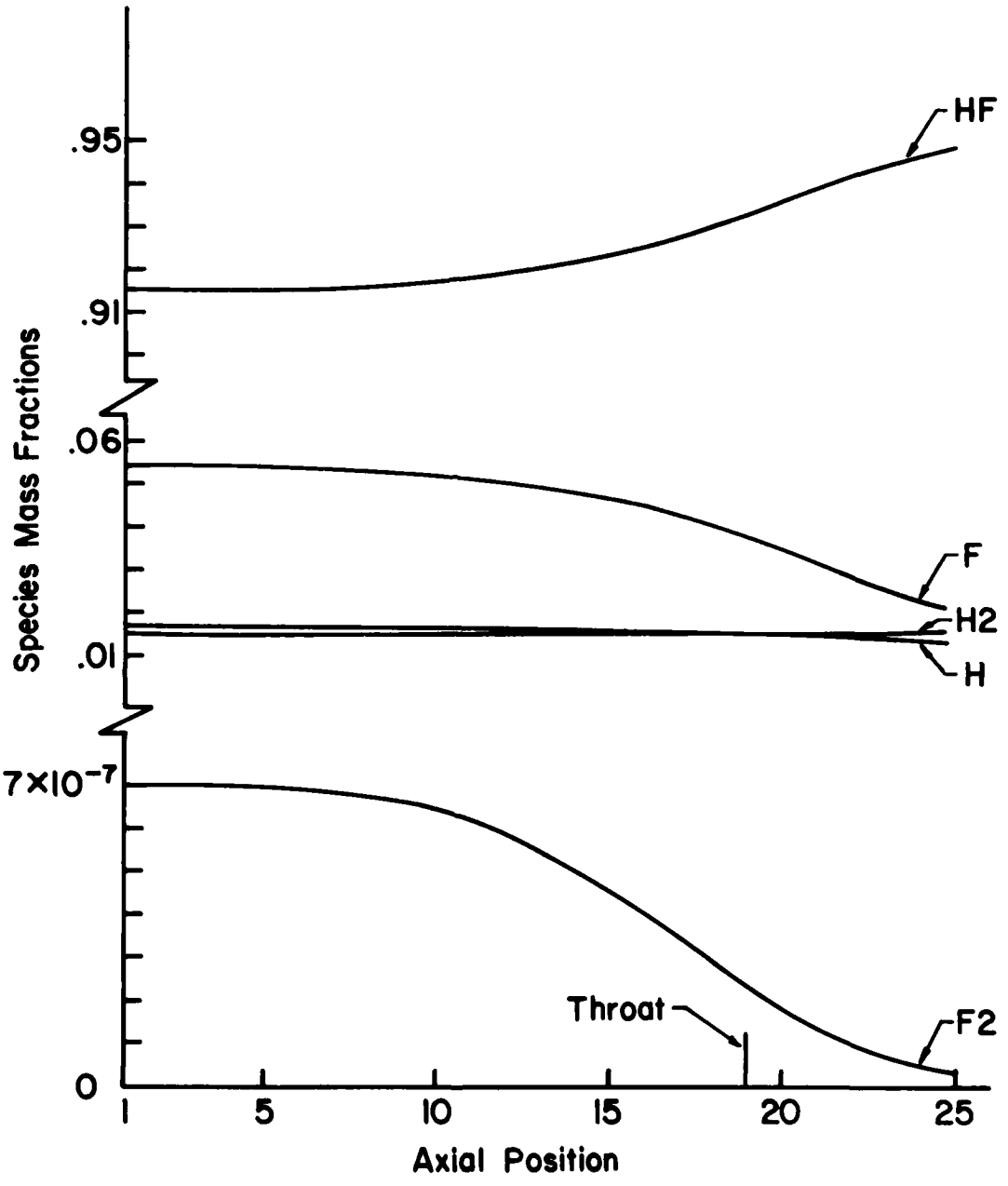

Figure 14. Concentration profiles for the H-F system.

in the problem formulation or in the numerical algorithm. However, the sum of the species mass fractions at each axial mesh point along the kinetics streamlines is computed and output. The fourth result which must be true of the converged solution is that the finite-rate kinetics results must lie between the equilibrium and frozen solutions since those cases correspond to infinite and zero reaction rates, respectively.

As a further test, the results of the subject technique have been mass-averaged (in the radial direction) and compared with an accepted one-dimensional solution [Reference (10)]. Mass-averaged temperature profiles are compared with one-dimensional temperature profiles in the discussion of results.

In the final verification step, the subject technique has been applied to a supersonic problem and the results have been compared with those from a two-dimensional method-of-characteristics solution [Reference (2)]. The results of an H-F system subsonic-transonic analysis were used to generate the initial data line for both the method-of-characteristics solution and the solution by the subject method. Eight equally spaced mesh points were used along the initial data line. A comparison of the results is presented in Figure 15 (TDK corresponds to the characteristics solution). Note the excellent agreement in the temperature and concentration profiles along the wall and the fair agreement of the centerline temperature profile.

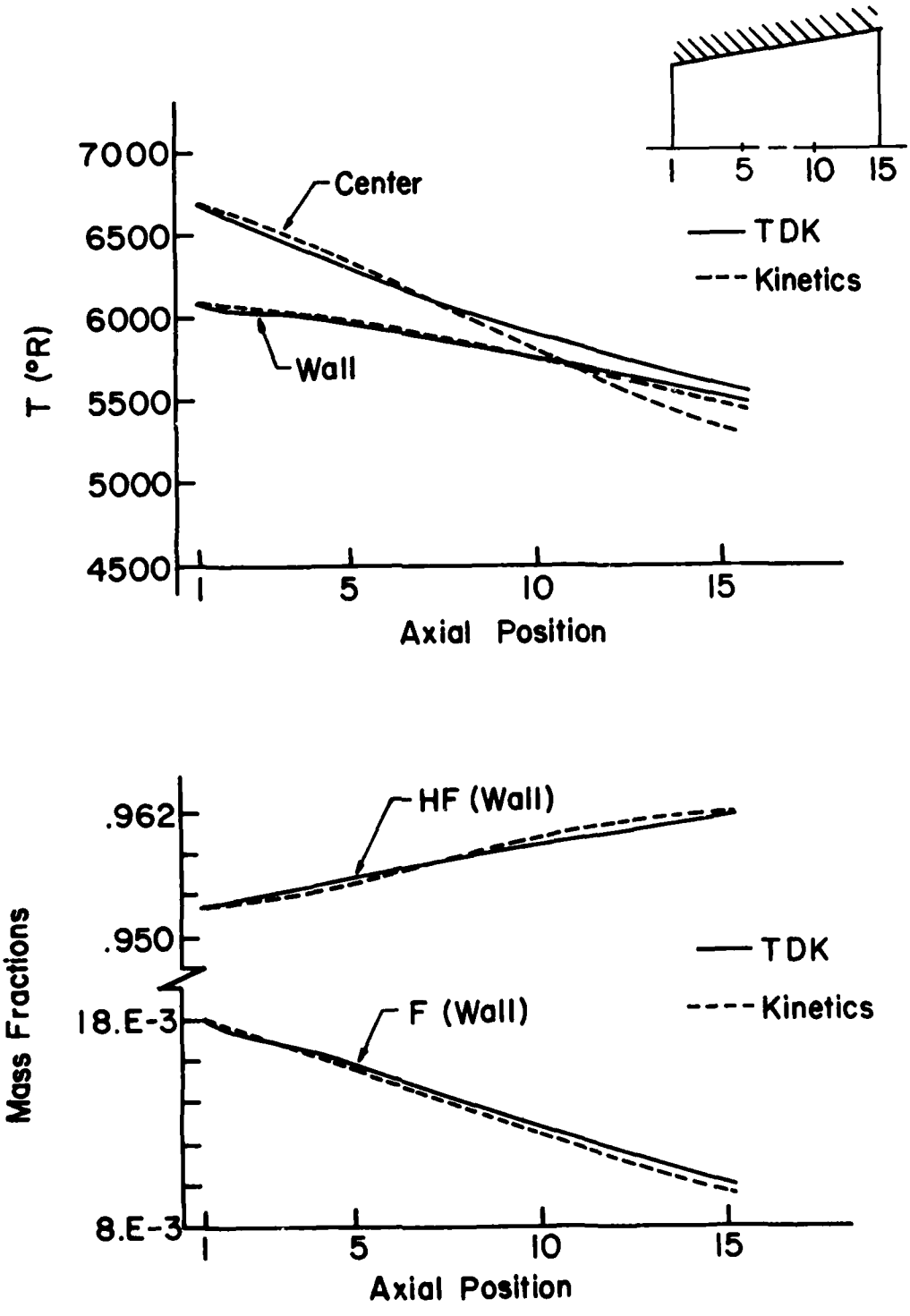

Figure 15. Verification with the TDK computer program.

2. RESULTS

Several different nozzle geometries and chemistry systems have been analyzed during this research. The details of the nozzle geometries and reaction mechanisms for the systems discussed here are presented in Appendix E.

C-H-O-N System

The C-H-O-N system corresponds to a realistic application of the subject technique to a ramjet nozzle problem. The composition of the reactive mixture of gases at the nozzle inlet results from an equilibrium calculation for the combustion of a hydrocarbon fuel in air. The nozzle size and shape is appropriate for a ramjet application. It is a circular-arc conical nozzle with a 7.5 inch inlet radius, a 4.75 inch throat radius, a 45 degree angle in the convergence, and a 15 degree angle in the divergence. There are 12 chemical species and 8 reactions in the chemistry model. Figure 16 presents the results of the analysis for this problem. Note that the mass-averaged temperature for the finite-rate kinetics solution does fall between the equilibrium and frozen solutions and that it matches the ODK solution [Reference (10)] quite well. Also note that in this case, there is only a small departure from the frozen solution. For both the isentropic (γ = constant) and kinetics solutions, a mass flow difference of 0.8 percent between the inlet and the throat values occurred in the converged results. For the kinetics solution, the sum of the species mass fractions deviated by less than 1×10^{-6} along both the center and wall streamlines. The profiles of total enthalpy error

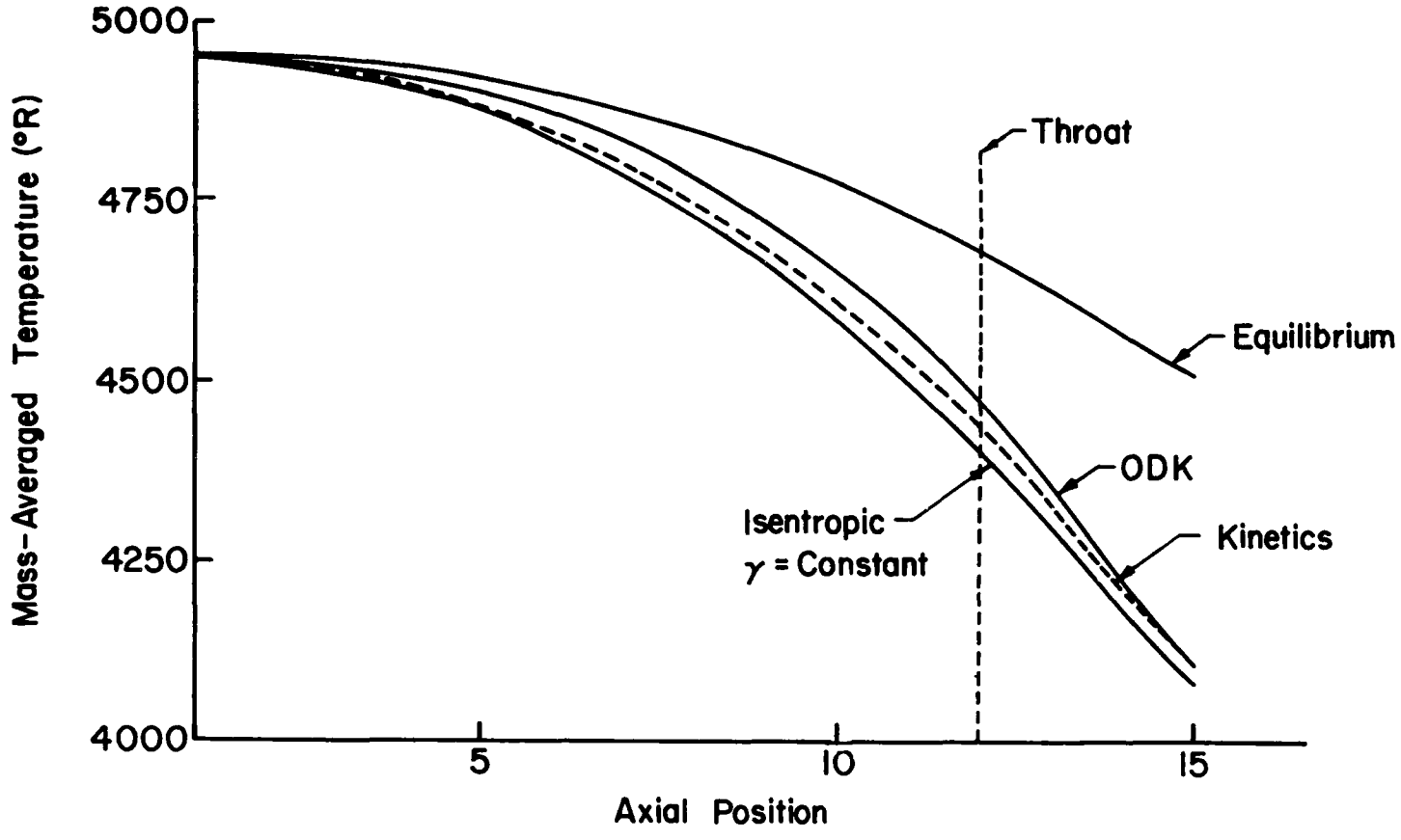

Figure 16. Temperature profiles for the C-H-O-N system.

are presented in Figure 17. Note that the error was less than one percent at all mesh points except for the isentropic solution at the last wall point. This particular point is just downstream from the junction between the circular arc in the throat region and the conical section in the nozzle divergence. The author's experience indicates that the discontinuity in the second derivative of the wall coordinates at this junction can cause distortions in the total enthalpy profile. Adding three more mesh points in the axial direction (L=16 to L=18) and recomputing the isentropic solution reduces the total enthalpy error at L=15 to one percent. Note in Figure 17 that the addition of finite-rate chemical kinetics to this problem has not significantly affected the H_0 profiles with respect to the isentropic (γ = constant) results.

With 18 mesh points along the axis, two chemical kinetics streamlines, and five intermediate points specified, each integration of the species continuity equations for the C-H-O-N system required approximately 11 seconds on the CDC 6500 computer. The addition of a third streamline increased that time to 16 seconds. Using the error control scheme with a ten percent tolerance on the truncation error yielded an integration time of 13.75 seconds (for two streamlines) while a one percent tolerance increased the integration time to 23 seconds. Integration of the species continuity equations after each time step, with two streamlines and five intermediate points, yielded an acceptable solution in an overall computational time of nearly one hour. However, for this system, it is possible to integrate the species continuity equations as infrequently as once every 30 time planes.

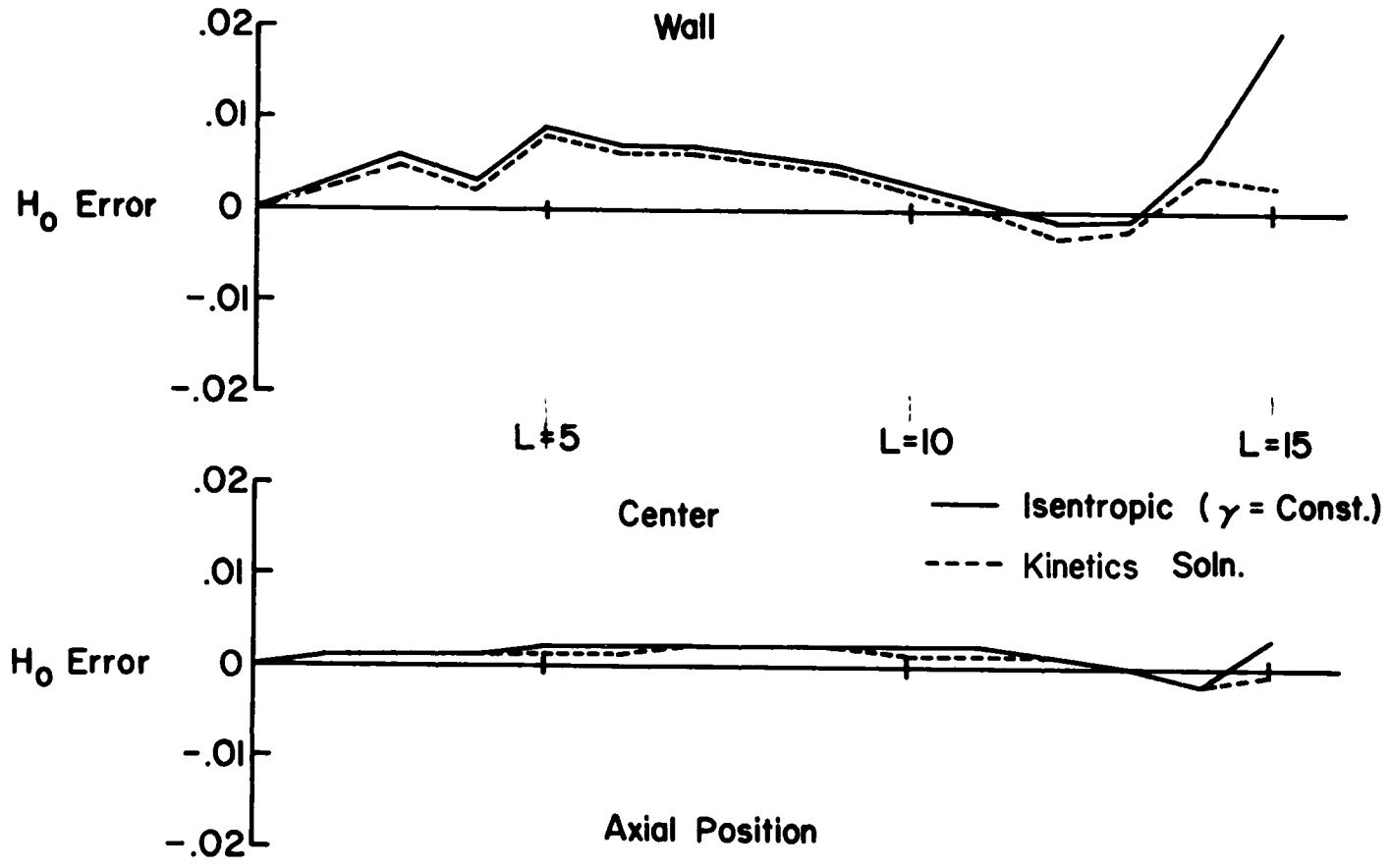

Figure 17. Total enthalpy error profiles for the C-H-O-N system.

This reduces the computational time to approximately five minutes.

C-H-O-N With C_nH_m System

It is possible that unburned fuel may be present in the reactive mixture at the nozzle inlet due to incomplete combustion in the ramjet. A five percent mass fraction of propane (C_3H_8) was added to the C-H-O-N chemistry system described above (for the same nozzle geometry) to investigate the effect of the unburned fuel and to provide initial conditions at the nozzle inlet which were not the result of an equilibrium calculation. All mass fractions of the species present in the C-H-O-N system were reduced by 5 percent to allow for the incorporation of propane. The solution with the addition of propane did not differ greatly from the C-H-O-N solution; the mass-averaged temperature at the throat increased by approximately 70°R while the mass-averaged velocity magnitude decreased by 55 ft/sec. The mass fraction of propane remained almost constant from the nozzle inlet to the exit. The addition of one chemical specie and one reaction slightly increased the computational time required for integration of the species continuity equations (about 0.5 seconds per integration).

H-F System

The H-F system was analyzed because it contains only five chemical species and six reactions; relatively short computational times per time plane can be achieved with this system. Also, since the C-H-O-N system results were near the frozen solution, the H-F system (at a high temperature) provided the opportunity to investigate a system near equilibrium. A small nozzle geometry was chosen for this

case so that some departure from equilibrium might occur before the throat. As shown in Appendix E, the nozzle is circular-arc conical with a two inch inlet radius, a one inch throat radius, a 45 degree angle in the converging section, and a 15 degree angle in the divergence. Figure 18 shows the results of the H-F system analysis. The mass-averaged temperature profile falls between the equilibrium and frozen solutions and matches the ODK [Reference (10)] solution very well. Note that this system is near equilibrium upstream of the throat but departs significantly from equilibrium downstream of the throat. A difference of approximately one percent in the inlet and throat mass flows occurred for both the isentropic (γ = constant) and kinetics solutions. The species mass fractions deviated by less than 1×10^{-10} along the center and wall streamlines. Figure 19 presents the total enthalpy profiles for the H-F system. For this particular problem, the solutions for the fluid dynamic variables along the centerline (upstream of the throat) were still oscillating slightly after more than 700 time planes for both the kinetics and isentropic solutions. This accounts for the sign difference in the total enthalpy error along the center in Figure 19. Figure 20 illustrates the two-dimensional character of the solution for the H-F system. Note the significant differences in temperatures and species mass fractions between center and wall values which develop in the solution. Also note the compression along the wall just downstream of the throat. This occurs at the junction between the circular arc of the throat region and the conical divergence. The effect is present in both the isentropic (γ = constant) and kinetics solutions.

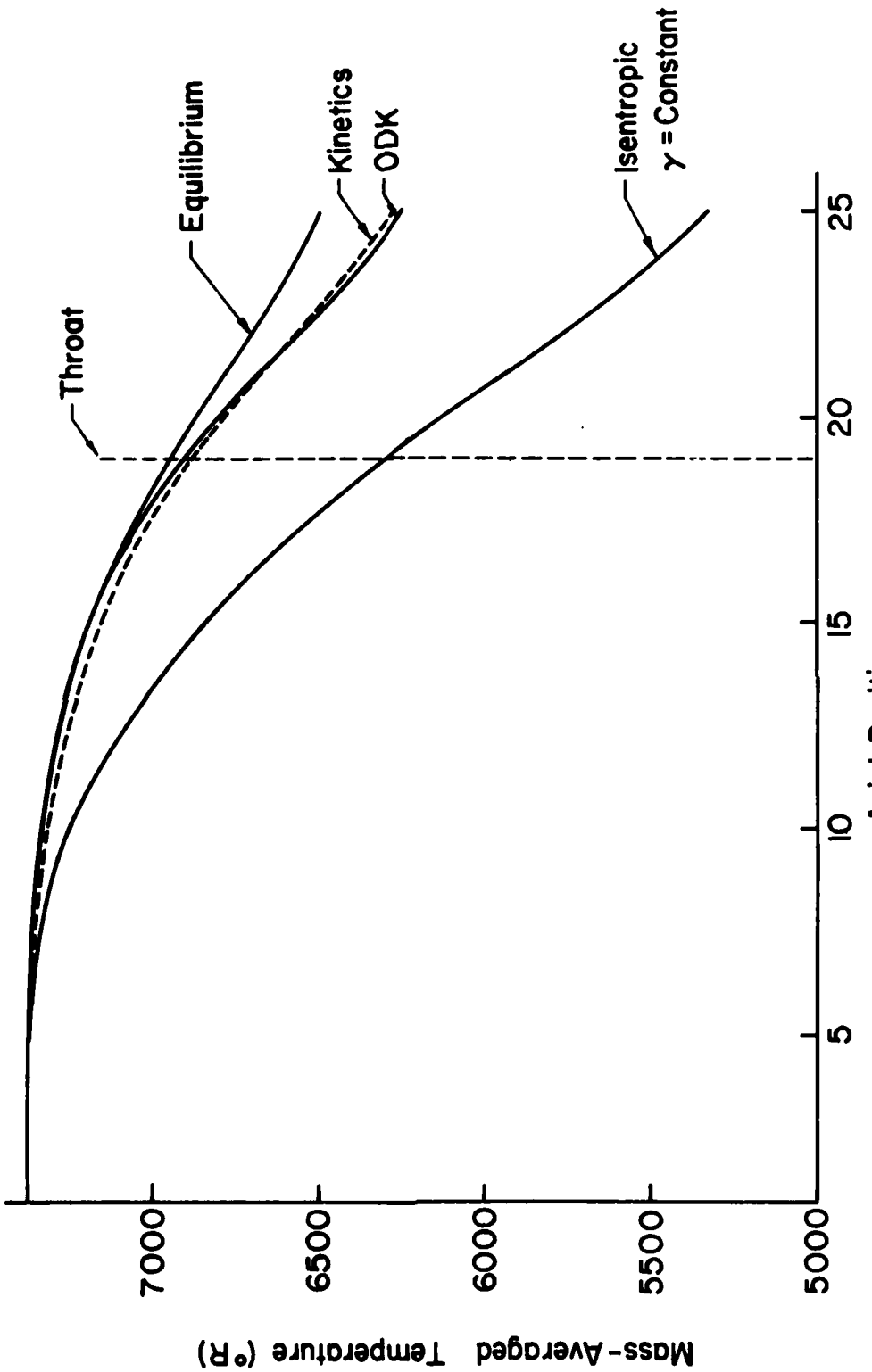

Figure 18. Temperature profiles for the H-F system.

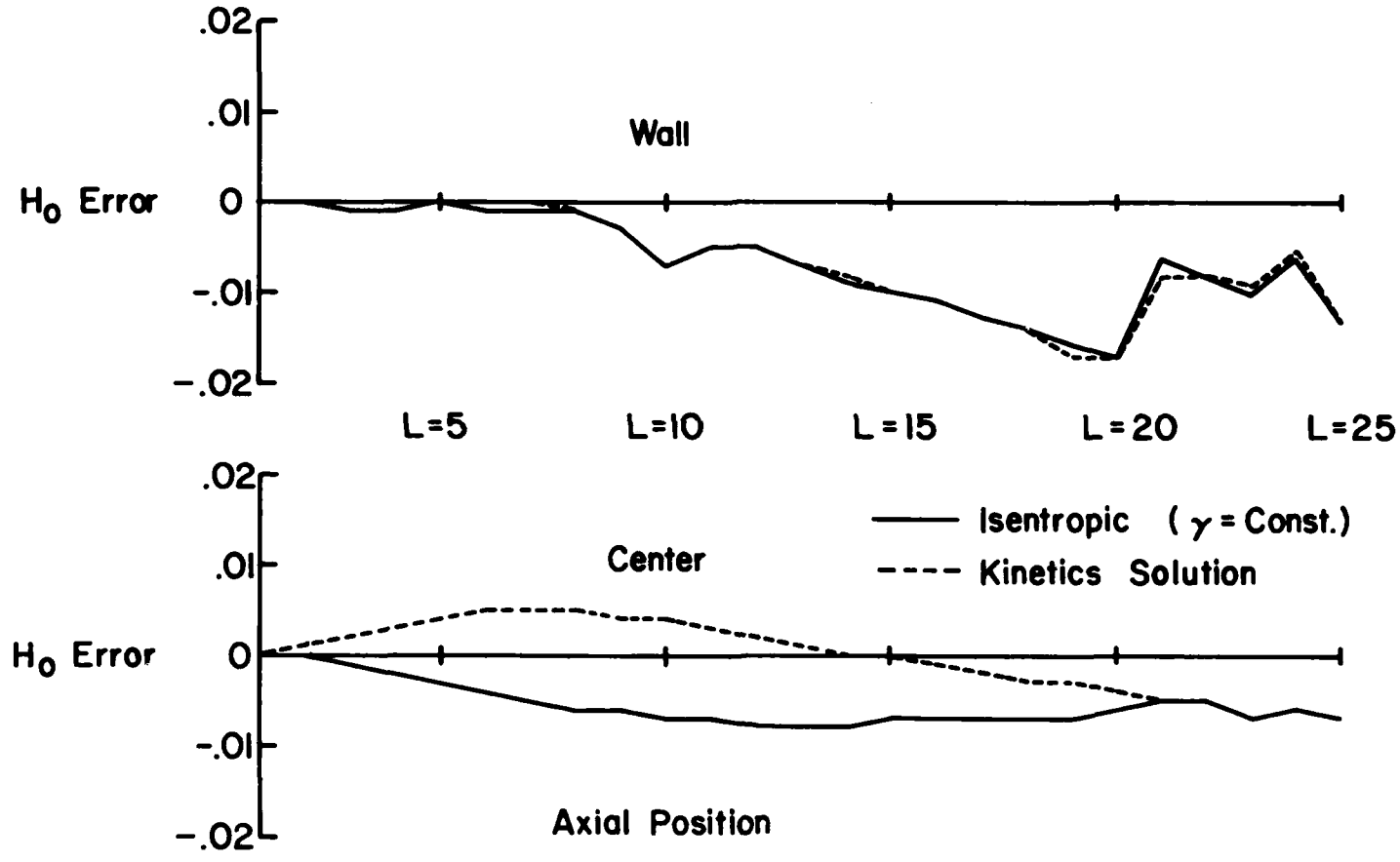

Figure 19. Total enthalpy error profiles for the H-F system.

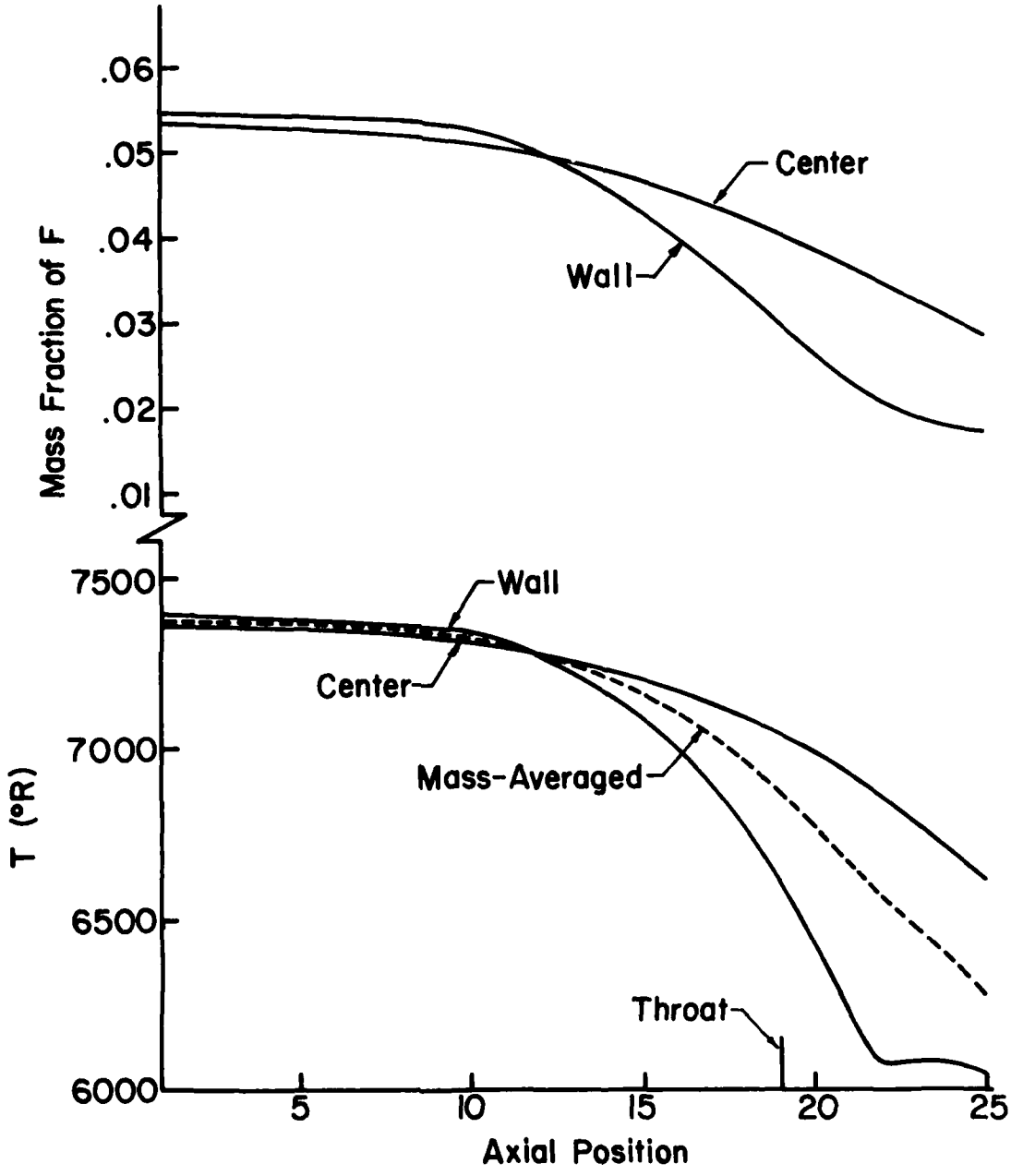

Figure 20. Wall and centerline profiles for the H-F system.

For the H-F system, with 25 mesh points along the axis, two chemical kinetics streamlines, and five intermediate points specified, each integration of the species continuity equations required five seconds on the CDC 6500 computer. The use of four streamlines increased that time to 10 seconds per integration. Using the error control scheme with a ten percent tolerance on the truncation error yielded an integration time of 5.8 seconds (two streamlines) while a one percent tolerance increased the integration time to 10.4 seconds. By adjusting the time step multiplier A [see equation (51)] it was possible to integrate the species continuity equations only every-other time plane for the H-F system. However, after more than 800 time planes, the values of the fluid dynamic variables at the centerline were still oscillating with little evidence of damping. Integrating the species continuity equations after each time step yielded an acceptable solution in a total computational time of one hour.

3. RECOMMENDATIONS CONCERNING COMPUTATIONAL TIME

Recall from the discussion of the overall numerical algorithm that the solution to the subject problem is advanced in a two-step procedure; the fluid dynamic variables are advanced, and then the species continuity equations are integrated along streamlines through the flow. The second step is much more time consuming than the first and thus, any attempt to reduce or minimize computational time should focus on the integration of the species continuity equations. The most significant factors regarding the time required for this integration are:

1) the number of chemical species and reactions in the chemical kinetics model.
2) the use of the truncation error control scheme for integration of the species continuity equations.
3) the number of chemical kinetics streamlines used.
4) the frequency of integration of the species continuity equations as the solution is marched forward in time.

Controls for these four factors are available to the program user but experience to date indicates that the proper set of controls is problem dependent. Some guidance is provided in the following discussion.

The chemical kinetics model should be as simple as possible. The technique of screening reactions for inclusion in the chemical kinetics model, as presented in Reference (38), is recommended.

The error control scheme is valuable for setting up the truncation error control parameter NINT and for refining the solution, but it is generally too costly to use throughout an entire calculation. The user should begin the analysis by computing several time planes with error control and a relatively loose tolerance (5-10%). Then, recompute the same time steps with a fixed number of intermediate points. Adjust that fixed number of points until satisfactory agreement with the solution using error control is achieved. The error control scheme should also be used to refine the solution after convergence with a fixed number of intermediate points.

For the cases studied, the addition of chemical kinetics streamlines to a two streamline solution does not make dramatic changes in

the computed results. The use of more than two streamlines significantly increases execution time and thus, should be reserved for refining the solution.

The C-H-O-N system results illustrated the dramatic computational time savings which can be realized if it is not necessary to integrate the species continuity equations after each time step. Again, some experimentation in this regard should be performed for each new problem.

SECTION VIII

CONCLUSIONS

A numerical method has been developed for solving the equations governing two-dimensional, unsteady, chemically reacting flow in propulsive nozzles. The unsteady equations are hyperbolic in subsonic, transonic, and supersonic flow regions and thus can be solved by well developed marching techniques. The steady state solution is obtained as the asymptotic solution to the unsteady equations, with steady flow boundary conditions applied, for large time. The overall numerical algorithm is inconsistent in time in the treatment of the species continuity equations but becomes consistent at the steady state limit. Interpolation for species mass fractions is not required as part of the scheme for integration of the species continuity equations.

The primary contribution of this research is the development of a production-type computer program suitable for application to a variety of nozzle problems. Verification of the results of the subject analysis for two-dimensional subsonic and transonic flows is difficult because, at present, there are no other methods available for the solution of this problem. However, for the cases studied, the solutions are quite reasonable and agree well in a mass-averaged sense with accepted one-dimensional finite-rate chemical kinetics solutions.

Also, when applied to two-dimensional supersonic flow, the results of the subject analysis compare favorably with an accepted method-of-characteristics solution.

Computational time has been found to be highly problem dependent. It is especially sensitive to the number of chemical species and reactions in the problem model, the use of the truncation error control scheme in the integration of the species continuity equations, the number of chemical kinetics streamlines used, and the frequency with which the species continuity equations are integrated through the flow field as the solution is marched forward in time. Appropriate controls for these factors are available to the program user. For the cases which have been analyzed to date, solutions have been obtained in times ranging from five minutes to one hour using a CDC 6500 computer.

The primary value of the subject technique is that it provides the analysis of the subsonic and transonic portions of the nozzle flow field, including two-dimensional and finite-rate chemical kinetics effects, and starting from nonuniform, nonequilibrium conditions at the nozzle inlet. Also, it provides consistent chemical kinetics data in the supersonic flow region which can be used to generate the initial-value line (surface) for accurate, multidimensional method-of-characteristics techniques. The method of the subject research, when coupled with a method-of-characteristics scheme for the nozzle divergence, should provide a highly accurate analysis of the entire nozzle flow field.

AD-A127 219 ANALYSIS OF STEADY TWO-DIMENSIONAL CHEMICALLY REACTING NONEQUILIBRIUM FLO..(U) PURDUE UNIV LAFAYETTE IND THERMAL SCIENCES AND PROPULSION CEN.. 2/2

UNCLASSIFIED R J STILES ET AL. SEP 82 F/G 20/4 NL

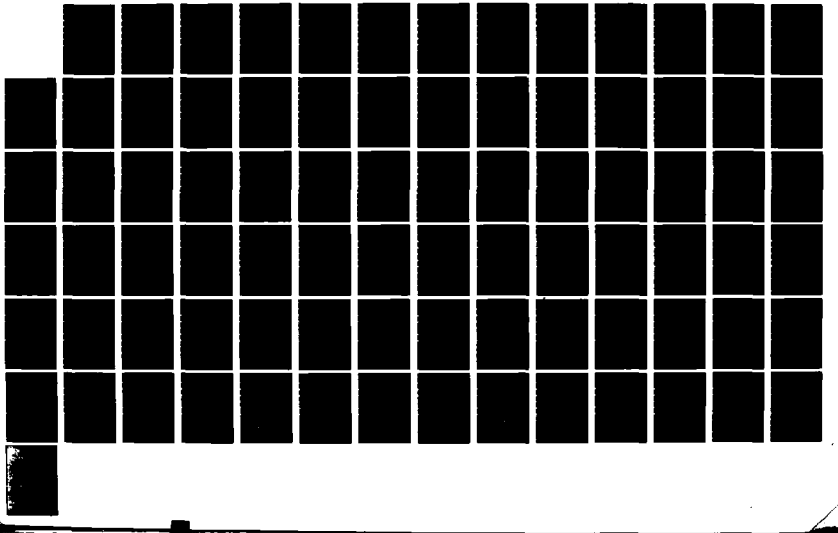

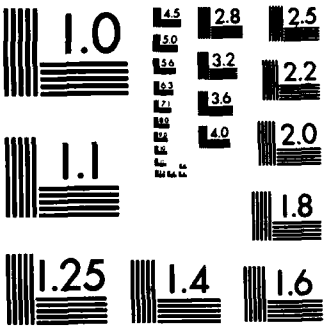

REFERENCES

1. Hoffman, J. D., Mechanical Engineering Dept., Purdue University; Hermsen, R. W., Chemical Systems Division, United Technologies; Edelman, R. B., Combustion Dynamics and Propulsion Technology Division, Science Applications, Inc.; Private Communication, July 1979.

2. Kliegel, J. R., Nickerson, G. R., Frey, H. M., Quan, V., and Melde, J. E., "ICRPG, Two-dimensional Kinetic Reference Program," Dynamic Science, Monrovia, California, July 1968.

3. Cline, M. C., and Hoffman, J. D., "The Analysis of Nonequilibrium Chemically Reacting, Supersonic Flow in Three Dimensions," Report No. AFAPL-TR-71-73, Air Force Aero Propulsion Laboratory, Wright-Patterson Air Force Base, Ohio, Aug. 1971.

4. Cline, M. C., "VNAP: A Computer Program for the Computation of Two-Dimensional, Time-Dependent Compressible, Viscous, Internal Flow," LA-7326, 1979, Los Alamos Scientific Laboratory, University of California, Los Alamos, New Mexico.

5. Bray, K. N. C., "Chemical and Vibrational Nonequilibrium in Nozzle Flows," Nonequilibrium Flows, Vol. I, Part II, ed. P. P. Weoener, Marcel Dekker, Inc., 1970.

6. Vincenti, Walter G., "Calculations of the One-Dimensional Nonequilibrium Flow of Air Through a Hypersonic Nozzle - Interim Report," SUDAER No. 101, Stanford Univ., California, Jan. 1961.

7. Emanual, George, and Vincenti, Walter G., "Method for Calculation of the One-Dimensional Nonequilibrium Flow of a General Gas Mixture Through a Hypersonic Nozzle," Rep. AEDC-TDR-62-131, Arnold Eng. Dev. Center, June 1962.

8. Sarli, V. J., "Nonequilibrium Flow Effects in High Expansion Nozzles - Final Report," Report No. B910056-12, United Aircraft Corporation, Sept. 1963.

9. Lordi, J. A., Mates, R. E., and Moselle, J. R., "Computer Program for the Numerical Solution of Nonequilibrium Expansions of Reacting Gas Mixtures," Report No. N66-26856, Cornell Aeronautical Laboratory, Inc., Buffalo, New York, May 1966.

10. Frey, H. M., Kliegel, J. R., Nickerson, G. R., and Tyson, T. J., "ICRPG, One-Dimensional Kinetic Reference Program," Dynamic Science, Monrovia, California, July 1968.

11. Widawsky, A., "Computer Program for the Determination of Chemically Reacting Flow Fields by the Method of Characteristics," RTD-TDR-63-4286, The Marquardt Corporation, Van Nuys, California, 1963.

12. Zupnik, T. F., Landis, F., Keilbach, J. R., and Ables, D., "Application of the Method of Characteristics Including Reaction Kinetics to Nozzle Flow," AIAA Paper No. 64-97, Aerospace Sciences Meeting, New York, January 1964.

13. Craig, Roger R., "Applying the Method of Characteristics to Analyze the Flow Field of a Chemically Reacting Gas in a Two-Dimensional or an Axisymmetric Nozzle," Report No. AFAPL-TR-65-20, Air Force Aero Propulsion Laboratory, Wright-Patterson Air Force Base, Ohio, April 1965.

14. Bartlma, F., "Plane Supersonic Flow with Relaxation," Applied Mechanics, Vol. 20, 1967, Proceedings of the 11th International Congress on Applied Mechanics, Springer-Verlag, Berlin, 1964.

15. Ransom, Victor H., Hoffman, Joe D., and Thompson, H. Doyle, "A Second-Order Numerical Method of Characteristics for Three-Dimensional Supersonic Flow, Volume I, Theoretical Development and Results," Report No. AFAPL-TR-69-98, Air Force Aero Propulsion Laboratory, Wright-Patterson Air Force Base, Ohio, Oct. 1969.

16. Saunders, L. M., "Numerical Solution of the Flow Field in the Throat Region of a Nozzle," Brown Engineering Co. Rept. BSVD-P-66-TN-001 (NASA CR 82601), August 1966.

17. Cuffel, R. F., Back, L. H., and Massier, P. F., "Transonic Flow-Field in a Supersonic Nozzle with Small Throat Radius of Curvature," AIAA J. 7 1364-1366, July 1969.

18. Migdal, D., Klein, K., and Moretti, G., "Time-Dependent Calculations for Transonic Nozzle Flow," AIAA J. 7, 372-374, Feb. 1969.

19. Wehofer, S., and Moger, W. C., "Transonic Flow in Conical Convergent and Convergent-Divergent Nozzles with Nonuniform Inlet Conditions," AIAA 6th Propulsion Joint Specialist Conference, June 1970, AIAA Paper No. 70-635.

20. Laval, P., "Time-Dependent Calculation Method for Transonic Nozzle Flows," Lect. Notes in Phys. 8, 187-192, Jan. 1971.

21. Serra, R. A., "The Determination of Internal Gas Flows by a Transient Numerical Technique," AIAA 9th Aerospace Sciences Meeting, Jan. 1971, AIAA Paper No. 71-45.

22. Brown, E. F., and Ozcass, H. M., "A Time-Dependent Solution of Mixed Flow Through Convergent Nozzles," AIAA 5th Fluid and Plasma Dynamics Conference, June 1972, AIAA Paper No. 72-680.

23. Cline, M. C., "NAP: A Computer Program for the Computation of Two-Dimensional, Time-Dependent, Inviscid Nozzle Flow," Los Alamos Scientific Laboratory Report LA-5984, Jan. 1977.

24. Vamos, J. S., and Anderson, J. D. Jr., "Time-Dependent Analysis of Nonequilibrium Nozzle Flows with Complex Chemistry," AIAA 5th Fluid and Plasma Dynamics Conference, June 1972, AIAA Paper No. 72-684.

25. Vincenti, W. G., and Kruger, C. H. Jr., Introduction to Physical Gas Dynamics, Chapters VII and VIII, John Wiley and Sons, Inc., New York, 1965.

26. Edelman, R. B., Fortune, O. and Weilerstein, G., "Some Observations on Flows Described by Coupled Mixing and Kinetics," Emissions From Continuous Combustion Systems, Plenum Press, 1972.

27. Edelman, R. B., and Harsha, P. T., "Laminar and Turbulent Gas Dynamics in Combustors - Current Status," Prog. Energy Combust. Sci., Vol. 4, pp. 1-62, 1978.

28. Gold, P. I., and Weekley, C. T., "Chemical Species and Chemical Reactions of Importance in Nonequilibrium Performance Calculations," Report No. 02874-6001-R000, TRW Systems, Dec. 1966.

29. MacCormack, R. W., "The Effect of Viscosity in Hypervelocity Impact Cratering," AIAA Hypervelocity Impact Conference, April 1969, AIAA Paper No. 69-354.

30. Moretti, G., "A Critical Analysis of Numerical Techniques: The Piston-Driven Inviscid Flow," PIBAL Report No. 69-25, Polytechnic Institute of Brooklyn, July 1969.

31. Zucrow, M. J., and Hoffman, J. D., Gas Dynamics, Vol. 2, Wiley, New York, 1976.

32. Curtiss, C. F., and Hirschfelder, J. O., "Integration of Stiff Equations," Proceedings National Academy of Science, Vol. 38, pp. 235-243, 1952.

33. Seinfield, J. H., Lapidus, L., and Hwang, M., "Review of Numerical Integration Techniques for Stiff Ordinary Differential Equations," Industrial Engineering Chemical Fundamentals, Vol. 9, No. 2, pp. 266-275, 1970.

34. Lomax, H., and Bailey, H. E., "A Critical Analysis of Various Numerical Integration Methods for Computing the Flows of a Gas in Chemical Nonequilibrium," NASA TN D-4109, Aug. 1967.

35. Liepman, H. W., and Roshko, A., Elements of Gas Dynamics, Wiley, 1957.

36. Cherry, S. S., "Phase II Final Report - Screening of Reaction Rates," Report No. 08832-6002-T000, TRW Systems, Redondo Beach, California, Dec. 1967.

37. Benson, S. W., and Fueno, T., "Mechanism of Atom Recombination by Consecutive Vibration Deactivations," J. Chem. Physics, Vol. 36, 1962, p. 1597.

38. Kushida, R., JANAF Performance Standardization Working Group, "Revision of CPIA 246, Section 6.2 Reaction Rate Data," Jet Propulsion Laboratory, California Institute of Technology, March 29, 1976.

39. Hoffman, J. D., "The Method of Characteristics Applied to Unsteady One-, Two-, and Three-Dimensional Flows," School of Mechanical Engineering, Purdue University, W. Lafayette, Indiana, 1978.

40. Henrici, P., Discrete Variable Methods in Ordinary Differential Equations, Wiley, New York, 1962.

41. Cline, M. C., "The Analysis of Nonequilibrium, Chemically Reacting, Supersonic Flow in Three Dimensions," Ph.D. Thesis, Purdue University, August, 1971.

42. Tyson, T. J., and Kliegel, J. R., "An Implicit Integration Procedure for Chemical Kinetics," Jan. 1968, AIAA Paper No. 68-180.

43. Roache, P. J., Computational Fluid Dynamics, Hermosa Publishers, Albuquerque, N.M., 1976.

44. Moretti, G., "Importance of Boundary Conditions in the Numerical Treatment of Hyperbolic Equations," Physics of Fluids, Supplement II, 1969, pp. 13-20.

45. Abbett, M. J., "Boundary Condition Calculation Procedures for Inviscid Supersonic Flow Fields," AIAA Computational Fluid Dynamics Conference, July 1973.

APPENDIX A

GOVERNING EQUATIONS

1. STATEMENT OF THE GOVERNING EQUATIONS

The governing equations for fluid flow within the nozzle of a propulsion system are derived from the application of the law of conservation of mass, Newton's second law of motion, and the first law of thermodynamics to an appropriate fluid model. For analyses performed for the purpose of performance prediction, the assumption of a continuous, inviscid, nondiffusing, and adiabatic fluid is generally adequate to accurately model the flow.

The macroscopic conservation equations, which can be developed from the laws stated above, are derived in detail in many basic gas dynamics texts (Ref. 35 for example). These equations are merely stated here. Applying the law of conservation of mass to the flow through a fixed volume element yields the continuity equation.

$$\frac{\partial \rho}{\partial t} + \nabla \cdot (\rho \bar{V}) = 0 \qquad \text{(A-1)}$$

where ρ is the density of the fluid and $\bar{V}$ is the velocity. When Newton's second law is applied to an element of unit mass moving with the fluid (for the fluid model described above), Euler's equations of motion are derived.

$$\rho \frac{D\bar{V}}{Dt} + \nabla P = 0 \qquad \text{(A-2)}$$

where P is the fluid pressure, and for unsteady, two-dimensional flow

$$\frac{D(\ )}{Dt} = \frac{\partial(\ )}{\partial t} + u\frac{\partial(\ )}{\partial x} + v\frac{\partial(\ )}{\partial y}$$

This vector equation provides two scalar component equations in a two-dimensional flow. Note that body forces have been assumed to be negligible in equation (A-2). Finally, the energy equation is derived from the application of the first law of thermodynamics to an adiabatic element of unit mass moving with the fluid. One possible form of this equation is as follows (Ref. 25).

$$\frac{D(h + V^2/2)}{Dt} - \frac{1}{\rho}\frac{\partial P}{\partial t} = 0 \qquad \text{(A-3)}$$

where h is the fluid enthalpy. This form of the energy equation shows that for steady flow, the total enthalpy $(h + V^2/2)$ is constant along streamlines. This fact serves as a useful check on the validity of computed results for steady flows.

In a two-dimensional flow, equations (A-1) to (A-3) provide four scalar equations in the five unknowns u, v, p, ρ, and h, where u and v are the velocity components. In equilibrium and frozen flows, an equation of state of the form $h = h(p,\rho)$ is added to provide a fifth equation and to complete the formulation of the problem. In flows with chemical nonequilibrium, equations (A-1) to (A-3) are still valid provided that the thermodynamic variables are given an "extended" definition (Ref. 25). It is assumed that the nonequilibrium system of fixed volume is in mechanical and thermal equilibrium and therefore

has a definite pressure and temperature. Also, it is assumed that the system is homogeneous in space and therefore its composition can be specified by giving the number of moles of each chemical species present. Finally, it is assumed that pressure, temperature, and the number of moles of each of the chemical species are not independent, but are related to one another through an equation of state. To insure that the equations of state for a nonequilibrium situation reduce to the equilibrium form when the equilibrium composition is substituted into those equations, the following requirement is made (Ref. 25). "The state equation for any property of a system in chemical nonequilibrium as a function of any other two properties and all the mole fractions of the constituent species is identical in form to the corresponding equation for the system in thermodynamic equilibrium." For example, it is this requirement which allows the use of the familiar thermal equation of state for a mixture of perfect gases in a flow with chemical nonequilibrium.

Consider an equation of state of the following form for the nonequilibrium flow.

$$h = h(p,\rho,C_1,\ldots,C_n)$$

where C_i $(i = 1,\ldots,n)$ are the mass fractions of each of the n chemical species in the reacting fluid. The addition of this equation of state to equations (A-1) to (A-3) provides a set of five equations in five plus n unknowns. All additional n equations are provided by the application of the law of conservation of mass to the flow of each of the chemical species through a fixed volume element. This yields the species continuity equations.

$$\frac{\partial \rho_i}{\partial t} + \nabla \cdot (\rho_i \bar{V}) = \sigma_i \quad (i = 1,\ldots,n) \tag{A-5}$$

where ρ_i is the mass density of species i and σ_i is the species source function.

As suggested above, it will be assumed in this analysis that the working fluid is a mixture of thermally perfect gases. Then the thermal equation of state is:

$$P = \rho T \sum_{i=1}^{n} C_i R_i = \rho R T \tag{A-6}$$

The caloric equation of state is:

$$h = \sum_{i=1}^{n} C_i h_i \quad \text{where } h_i = \int_{T_o}^{T} C_{pi}\, dT + h_i^o \tag{A-7}$$

In equations (A-6) and (A-7), R_i are the species gas constants, R is the gas constant for the mixture, h_i are the species enthalpies, C_{pi} are the species specific heats at constant pressure, T_o is the reference temperature, T is the fluid temperature, and h_i^o are the species energies of formation.

Summary of major assumptions and governing equations

Major assumptions:

- continuum
- inviscid
- adiabatic
- nondiffusing
- negligible body forces
- chemical nonequilibrium only
- fluid is a mixture of thermally perfect gases

Governing equations: (vector form)

Global continuity: $$\frac{\partial \rho}{\partial t} + \nabla \cdot (\rho \bar{V}) = 0 \qquad \text{(A-1)}$$

Momentum: $$\rho \frac{D\bar{V}}{Dt} + \nabla P = 0 \qquad \text{(A-2)}$$

Energy: $$\frac{D(h + V^2/2)}{Dt} - \frac{1}{\rho}\frac{\partial P}{\partial t} = 0 \qquad \text{(A-3)}$$

Species continuity: $$\frac{\partial \rho_i}{\partial t} + \nabla \cdot (\rho_i \bar{V}) = \sigma_i \quad (i = 1,\ldots,n) \qquad \text{(A-5)}$$

Thermal equation of state: $$P = \rho T \sum_{i=1}^{n} C_i R_i \qquad \text{(A-6)}$$

Caloric equation of state: $$h = \sum_{i=1}^{n} C_i h_i \quad \text{where } h_i = \int_{T_o}^{T} C_{pi}\, dT + h_i^{o} \qquad \text{(A-7)}$$

2. REARRANGEMENT OF THE SPECIES CONTINUITY EQUATIONS AND THE ENERGY EQUATION

The species continuity equations (A-5) can be simplified by expressing them in terms of species mass fractions rather than species mass densities. Substituting $C_i = \rho_i/\rho$ into equation (A-5) and using the global continuity equation (A-1) yields:

$$\frac{DC_i}{Dt} = \frac{\sigma_i}{\rho} \quad (i = 1,\ldots,n) \qquad \text{(A-8)}$$

In this characteristic form, the species continuity equations are one-dimensional equations which apply along a particle path. They are integrated in this form in the computational scheme.

The energy equation (A-3) can also be manipulated into a form which is more convenient for analysis. In this form the species source function σ_i appears directly. The species source function contains within it the set of chemical reactions and appropriate reaction rates for the assumed chemistry model (see Appendix B). By forming the dot product of the velocity vector $\overline{V}$ with equation (A-2), it is possible to develop an expression for $\frac{D(V^2/2)}{Dt}$.

$$\rho\overline{V} \cdot \frac{DV}{Dt} + V \cdot VP = \rho D(\frac{V^2}{2}) + \frac{DP}{Dt} - \frac{\partial P}{\partial t} \qquad \text{(A-9)}$$

Solving equation (A-9) for $D(V^2/2)$ and substituting into equation (A-3) yields

$$\frac{Dh}{Dt} - \frac{1}{\rho}\frac{DP}{Dt} = 0 \qquad \text{(A-10)}$$

Introducing the thermal and caloric equations of state, equations (A-6) and (A-7), respectively, and the species continuity equation (A-8), yields the desired form of the energy equation. Taking the substantial derivative of equation (A-7) gives

$$\frac{Dh}{Dt} = \sum_{i=1}^{n} C_i \frac{Dh_i}{Dt} + \sum_{i=1}^{n} h_i \frac{DC_i}{Dt} = \sum_{i=1}^{n} C_i C_{pi} \frac{DT}{Dt} + \sum_{i=1}^{n} h_i \sigma_i/\rho \qquad \text{(A-11)}$$

Logarithmic differentiation of equation (A-6) provides an expression for DT/Dt in equation (A-11). Equation (A-11) can then be used to replace Dh/Dt in equation (A-10). The result is

$$\frac{DP}{Dt} - a_f^2 \frac{D\rho}{Dt} = \psi_k \tag{A-12}$$

where $$\psi_k = \sum_{i=1}^{n} [\gamma_f R_i T - (\gamma_f - 1)h_i]\sigma_i \tag{A-13}$$

and a_f and γ_f are the frozen speed of sound and ratio of frozen specific heats, respectively.

3. THE GOVERNING EQUATIONS FOR TWO-DIMENSIONAL PLANAR OR AXISYMMETRIC FLOW

The geometries of interest in this research include two-dimensional planar and axisymmetric flows. The equations governing two-dimensional axisymmetric flow are normally expressed in cylindrical coordinates, but they can be transformed to the notation of a Cartesian coordinate system by means of the following transformation equations.

$$\begin{aligned} v_r &= v \\ v_z &= u \\ r &= y \\ z &= x \end{aligned} \tag{A-14}$$

Comparing the equations for two-dimensional planar flow with the transformed set of equations [by equations (A-14)] for a two-dimensional axisymmetric flow, it is seen that the equations are identical except for the additional term $\rho v/y$ in the global continuity equation for axisymmetric flow. Therefore, the following set of equations, in Cartesian coordinate notation, applies to both two-dimensional planar and two-dimensional axisymmetric flows.

$$\rho_t + u\rho_x + v\rho_y + \rho u_x + \rho v_y + \varepsilon(\rho v/y) = 0 \tag{A-15}$$

$$u_t + uu_x + vu_y + P_x/\rho = 0 \tag{A-16}$$

$$v_t + uv_x + vv_y + P_y/\rho = 0 \tag{A-17}$$

$$P_t + uP_x + vP_y - a_f^2(\rho_t + u\rho_x + v\rho_y) = \psi_k \tag{A-18}$$

$$C_{it} + uC_{ix} + vC_{iy} = \frac{\sigma_i}{\rho} \quad (i = 1,\ldots,n) \tag{A-19}$$

where the subscripts denote partial differentiation. In equation (A-15), ϵ is zero for planar flow and one for axisymmetric flow.

4. TRANSFORMATION OF THE GOVERNING EQUATIONS TO THE COMPUTATIONAL PLANE

Since the interior points in this analysis are to be treated by a fixed grid technique, it is convenient to transform the physical (x,y,t) plane to a rectangular (ζ,η,τ) plane in which the differencing is performed. The following coordinate transformation is used (see Figure A-1)

$$\begin{aligned} \tau &= t \\ \zeta &= x \\ \eta &= \frac{y - y_c(x)}{y_w(x) - y_c(x)} \end{aligned} \tag{A-20}$$

where $y_c(x)$ and $y_w(x)$ represent the nozzle centerbody and wall coordinates, respectively, as functions of x. Application of this transformation yields:

$$\begin{aligned} \frac{\partial(\ )}{\partial t} &= \frac{\partial(\ )}{\partial \tau} \\ \frac{\partial(\ )}{\partial x} &= \frac{\partial(\ )}{\partial \zeta} + \alpha\frac{\partial(\ )}{\partial \eta} \\ \frac{\partial(\ )}{\partial y} &= \beta\frac{\partial(\ )}{\partial \eta} \end{aligned} \tag{A-21}$$

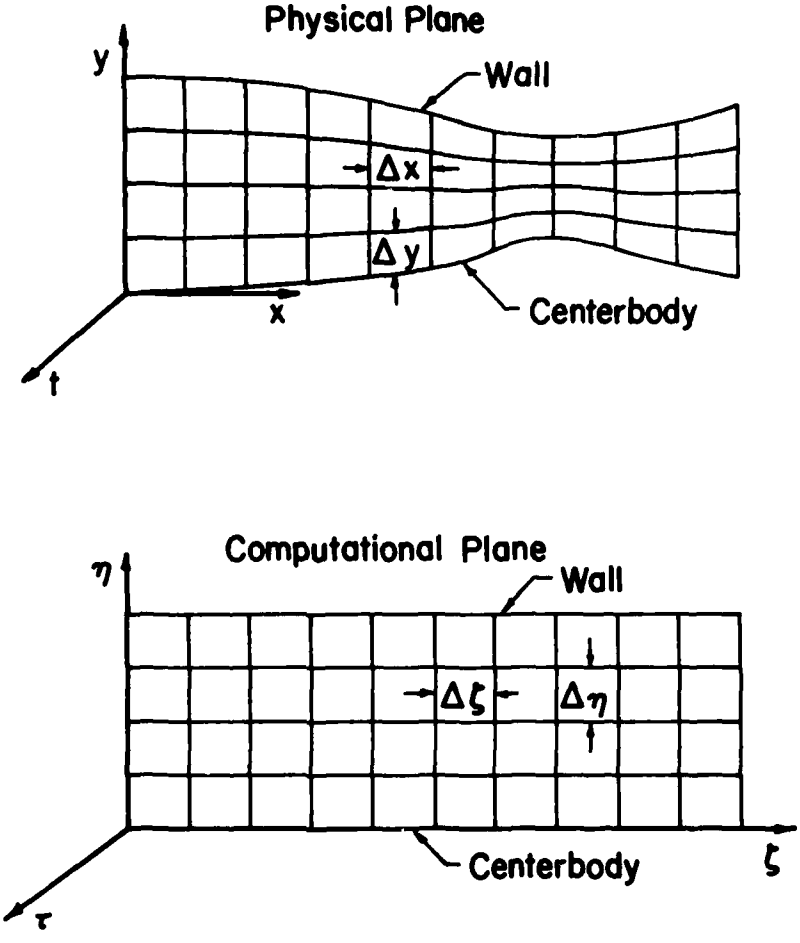

Figure A-1. Physical and computational planes.

$$\alpha = \frac{\partial \eta}{\partial x} = -\beta \frac{\partial y_c}{\partial x} - \eta\beta\left(\frac{\partial y_w}{\partial x} - \frac{\partial y_c}{\partial x}\right)$$

$$\beta = \frac{\partial \eta}{\partial y} = \frac{1}{y_w(x) - y_c(x)}$$

For convenience, the following two variables are defined:

$$\bar{v} \equiv \alpha u + \beta v \qquad \text{(A-22)}$$

$$\bar{\eta} \equiv y_c + \eta/\beta \qquad \text{(A-23)}$$

Applying the transformation in (A-21) to equations (A-15) to (A-19) and introducing the definitions given by equations (A-22) and (A-23) yields the following forms of the continuity, momentum, energy, and species continuity equations, which are used in this analysis.

Summary of the governing equations in the computational plane

$$\rho_\tau + u\rho_\zeta + \bar{v}\rho_\eta + \rho u_\zeta + \rho\alpha u_\eta + \rho\beta v_\eta + \varepsilon\rho v/\bar{\eta} = 0 \qquad \text{(A-24)}$$

$$u_\tau + uu_\zeta + \bar{v}u_\eta + P_\zeta/\rho + \alpha P_\eta/\rho = 0 \qquad \text{(A-25)}$$

$$v_\tau + uv_\zeta + \bar{v}v_\eta + \beta P_\eta/\rho = 0 \qquad \text{(A-26)}$$

$$P_\tau + uP_\zeta + \bar{v}P_\eta - a_f^2(\rho_\tau + u\rho_\zeta + \bar{v}\rho_\eta) = \psi_k \qquad \text{(A-27)}$$

$$C_{i\tau} + uC_{i\zeta} + \bar{v}C_{i\eta} = \sigma_i/\rho \qquad (i=1,\ldots,n) \qquad \text{(A-28)}$$

$$P = \rho T \sum_{i=1}^{n} C_i R_i = \rho RT \qquad \text{(A-6)}$$

$$h = \sum_{i=1}^{n} C_i h_i \quad \text{where } h_i = \int_{T_o}^{T} C_{pi}\,dT + h_i^{\,o} \qquad \text{(A-7)}$$

Note that equation (A-28) may be written as

$$\frac{DC_i}{D\tau} = \frac{\sigma_i}{\rho} \quad (i = 1,\ldots,n)$$

where $DC_i/D\tau$ is the change in C_i following a particle path in the computational plane.

APPENDIX B

THE CHEMICAL KINETICS MODEL

1. REACTION MECHANISM AND THE SPECIES SOURCE FUNCTION

In Appendix A, it was noted that for the nonequilibrium flow of a gas mixture, a third variable (the species concentrations) must be introduced into the equation of state to specify the chemical state of the reactive mixture. This, in turn, required the addition of n species continuity equations to complete the set of governing equations. In this section, an equation for the source term in the species continuity equations is presented.

Implicit within the equation for the species source function is a reaction mechanism (i.e., a set of coupled elementary reactions whose reaction rates are functions of temperature only). As an example of a reaction mechanism, consider the overall reaction between hydrogen and flourine:

$$H_2 + \phi F_2 = aH_2 + bF_2 + cHF + dH + eF \qquad \text{(B-1)}$$

where ϕ is the molar oxidizer to fuel ratio, and a through e are the moles of the various species in the completed reaction. The science of chemical kinetics is concerned with the determination of a suitable reaction mechanism for overall reactions like that specified by equation (B-1). The reaction mechanism should give an overall effect

which is in agreement with experimental observations. For the overall reaction given by equation (B-1), Cherry (36) has proposed the following reaction mechanism:

$$F_2 + M \rightleftarrows 2F + M \qquad \text{(B-2a)}$$

$$H_2 + M \rightleftarrows 2H + M \qquad \text{(B-2b)}$$

$$HF + M \rightleftarrows H + F + M \qquad \text{(B-2c)}$$

$$HF + F \rightleftarrows H + F_2 \qquad \text{(B-3a)}$$

$$HF + H \rightleftarrows H_2 + F \qquad \text{(B-3b)}$$

$$2HF \rightleftarrows H_2 + F_2 \qquad \text{(B-3c)}$$

Reactions (B-2) are called dissociation-recombination (or third body) reactions, while reactions (B-3) are known as binary exchange reactions. The symbol M in equation (B-2) represents the third body involved in the reactive collision and it can be any of the chemical species present in the reaction mechanism. A general reaction equation which will be used to represent any reaction mechanism is

$$\sum_{i=1}^{n} \nu'_{ij} X_i \underset{k_{rj}}{\overset{k_{fj}}{\rightleftarrows}} \sum_{i=1}^{n} \nu''_{ij} X_i \qquad (j=1,\ldots,m) \qquad \text{(B-4)}$$

where ν'_{ij} and ν''_{ij} are the stoichiometric coefficients of the reactants and products respectively, X_i denotes the ith chemical species, and k_{fj} and k_{rj} are the forward and reverse reaction rate coefficients, respectively, for the jth reaction of the m reactions in the reaction mechanism.

The law of mass action (Ref. 25) states that "the rate at which an elementary reaction proceeds is proportional to the product of the molar concentrations of the reactants each raised to a power equal to its stoichiometric coefficient in the reaction equation." Using this law together with equation (B-4), it is possible to develop an expression for the net production of the ith chemical species due to the jth reaction in the reaction mechanism (Ref. 31). Thus,

$$\frac{d[X_i]}{dt}_j = (\nu''_{ij} - \nu'_{ij}) \left[k_{fj} \prod_{i=1}^{n} [X_i]^{\nu'_{ij}} - k_{rj} \prod_{i=1}^{n} [X_i]^{\nu''_{ij}} \right] \qquad \text{(B-5)}$$

Converting equation (B-5) to a mass basis and summing over all m reactions in the reaction mechanism yields the equation for the species source function.

$$\sigma_i = \bar{m}_i \sum_{j=1}^{m} (\nu''_{ij} - \nu'_{ij}) \left[k_{fj} \prod_{i=1}^{n} \left(\frac{\rho C_i}{\bar{m}_i}\right)^{\nu'_{ij}} - k_{rj} \prod_{i=1}^{n} \left(\frac{\rho C_i}{\bar{m}_i}\right)^{\nu''_{ij}} \right] \qquad \text{(B-6)}$$

where $\bar{m}_i$ is the molecular weight of the ith species. Note that the species source function is the forcing term in the species continuity equations (A-8) and that σ_i is also present in the forcing term of the energy equation (A-13). Therefore, equation (B-6) provides the link between the chemical kinetics model and the governing equations for the problem of interest.

2. REACTION RATE COEFFICIENTS

Reaction rate coefficients are not readily predicted at the present time and therefore, they are generally found experimentally.

The form for the reverse reaction rate coefficient which is used in this analysis is

$$k_{rj} = a_{ij} T^{-n_j} \exp(-b_j/\bar{R}T) \qquad \text{(B-7)}$$

where a_{ij}, n_j, and b_j are empirical coefficients, $\bar{R}$ is the universal gas constant, and T is the local gas temperature. The forward and reverse reaction rate coefficients for a given reaction are not independent but are coupled through the equilibrium constant for that reaction. Using the equilibrium constant based on partial pressures ($K_{p,j}$), it is found that (Ref. 31)

$$\frac{k_{fj}}{k_{rj}} = K_{p,j} (\bar{R}T)^{-\Delta\nu_j} \qquad \text{(B-8)}$$

where

$$\Delta\nu_j \equiv \sum_{i=1}^{n} (\nu_i'' - \nu_i')j \qquad \text{(B-9)}$$

Note that the difficulties in making accurate measurements for the determination of reaction rate coefficients, the necessity of extrapolating experimental data from one situation to another, and the uncertainty as to the reaction mechanism, are all significant factors limiting the accuracy of the analysis presented in this research. However, experience with one-dimensional analyses of reacting flows indicates that the chemical kinetics model used here is adequate for performance prediction.

3. TREATMENT OF HYDROCARBONS

Unburned hydrocarbons may be present in the gas mixture at the combustor exit and therefore, provision for these species must be made in the chemical kinetics model. Edelman, et. al. (26) and Edelman and Harsha (27) have developed a kinetics model for use in combustor analyses which includes a "sub-global" partial oxidation step:

$$C_nH_m + \frac{n}{2} O_2 \rightarrow \frac{m}{2} H_2 + nCO \qquad \text{(B-10)}$$

Note that this reaction proceeds in the forward direction only. The reaction rate coefficient for equation (B-10) is determined empirically and is given by (Ref. 27):

$$a_j = 6.0 \times 10^{14} P^{0.3} c^{\frac{1}{2}}_{C_nH_m} c_{O_2} \qquad \text{(B-11)}$$

where P has units of atmospheres and c represents species concentrations in g-moles/cc.

4. THE SPECIES SOURCE FUNCTION FOR DISSOCIATION-RECOMBINATION REACTIONS AND BINARY EXCHANGE REACTIONS

Equation (B-6) for the species source function is simplified for dissociation-recombination and binary exchange reactions in the following discussion.

Dissociation-Recombination Reactions

Dissociation recombination reactions are of the form

$$A + M \rightleftarrows B + C + M \qquad \text{(B-12)}$$

From equation (B-9), $\Delta\nu_j = 1$ for all these reactions. Substituting

equation (B-8) into equation (B-6) yields

$$\sigma_{i_{D-R}} = \bar{m}_i \rho^2 \sum_{j=1}^{m} (\nu''_{ij} - \nu'_{ij}) \left[\frac{K_{p,j}}{RT} \prod_{i=1}^{n} \left(\frac{C_i}{\bar{m}_i}\right)^{\nu'_{ij}} - \rho \prod_{i=1}^{n} \left(\frac{C_i}{\bar{m}_i}\right)^{\nu''_{ij}} \right] M_j k_{rj} \qquad \text{(B-13)}$$

or

$$\sigma_{i_{D-R}} = \bar{m}_i \rho^2 \sum_{j=1}^{m} (\nu''_{ij} - \nu'_{ij}) \left[K_j \prod_{i=1}^{n} (C_i)^{\nu'_{ij}} - \rho \prod_{i=1}^{n} (C_i)^{\nu''_{ij}} \right] \frac{M_j k_{rj}}{\prod_{i=1}^{n} (\bar{m}_i)^{\nu''_{ij}}} \qquad \text{(B-14)}$$

where

$$K_{j_{D-R}} = \frac{K_{p,j}}{RT} \frac{\prod_{i=1}^{n} (\bar{m}_i)^{\nu''_{ij}}}{\prod_{i=1}^{n} (\bar{m}_i)^{\nu'_{ij}}} \qquad \text{(B-15)}$$

The effect of different third bodies is taken into account through the use of third body reaction rate ratios M_j (see section 4).

Binary Exchange Reactions

Binary exchange reactions are of the form

$$A + B \rightleftarrows C + D \qquad \text{(B-16)}$$

In this case, $\Delta\nu_j = 0$. Thus, equation (B-6) becomes

$$\sigma_{i_{B-E}} = \bar{m}_i \rho^2 \sum_{j=1}^{m} (\nu''_{ij} - \nu'_{ij}) \left[K_{p,j} \prod_{i=1}^{n} \left(\frac{C_i}{\bar{m}_i}\right)^{\nu'_{ij}} - \prod_{i=1}^{n} \left(\frac{C_i}{\bar{m}_i}\right)^{\nu''_{ij}} \right] k_{rj} \qquad \text{(B-17)}$$

or

$$\sigma_{i_{B-E}} = \bar{m}_i \rho^2 \sum_{j=1}^{m} (\nu''_{ij} - \nu'_{ij}) \left[K_j \prod_{i=1}^{n} (C_i)^{\nu'_{ij}} - \prod_{i=1}^{n} (C_i)^{\nu''_{ij}} \right] \frac{k_{rj}}{\prod_{i=1}^{n} (\bar{m}_i)^{\nu''_{ij}}} \qquad \text{(B-18)}$$

where

$$K_{j_{B-E}} = K_{p,j} \frac{\prod_{i=1}^{n} (\bar{m}_i)^{\nu''_{ij}}}{\sum_{i=1}^{n} (\bar{m}_i)^{\nu'_{ij}}} \qquad \text{(B-19)}$$

The Hydrocarbon Reaction

The hydrocarbon oxidation as shown in equation (B-10) can be treated as a special case of a binary exchange reaction. Rewriting equation (B-10) in the form of (B-16), and so that it proceeds from right to left, gives

$$\frac{m}{2} H_2 + n\ CO \overset{0}{\rightleftarrows} C_n H_m + \frac{n}{2} O_2 \qquad \text{(B-20)}$$

Since $K_{p,j}$ is equal to the ratio of the forward and reverse reaction

rates, then $K_{p,j}$ is zero for the reaction in equation (B-20). Therefore, the species source function for the special case of equation (B-10) becomes

$$\sigma_i = \bar{m}_i \rho^2 (\nu''_{ij} - \nu'_{ij}) \left[- \prod_{i=1}^{n} (C_i)^{\nu''_{ij}} \right] \frac{k_{rj}}{\prod_{i=1}^{n} (\bar{m}_i)^{\nu''_{ij}}} \qquad \text{(B-21)}$$

5. THIRD BODY REACTION RATE RATIOS

Each dissociation-recombination reaction has a different reverse reaction rate depending upon the particular third body involved in the collision. This effect is taken into account in the chemical kinetics model by the use of third body reaction rate ratios. It is assumed that the overall reverse reaction rate coefficient for the jth dissociation-recombination reaction is given by

$$M_j k_{rj} = \sum_{\ell=1}^{n} C_\ell k_{r\ell j} \qquad \text{(B-22)}$$

where the summation over ℓ represents all possible third bodies and C_ℓ is the mass fraction of the ℓth third body. Implicit in this equation is the assumption that the overall reverse reaction rate is a mass weighted average of the reverse reaction rates for each different third body. According to References (36) and (37), the temperature dependence of recombination rates can be reasonably assumed to be independent of the third body so the recombination rate associated with the ℓth species (third body) can be expressed as

$$k_{r\ell j} = a_{\ell j} T^{-n_j} \exp(-b_j/\bar{R}T) \qquad \text{(B-23)}$$

where $a_{\ell j}$ is dependent on the third body. Substituting this expression into equation (B-18) yields

$$M_j k_{rj} = \sum_{\ell=1}^{n} C_\ell \, a_{\ell j} \, T^{-n_j} \exp(-b_j/\bar{R}T) \tag{B-24}$$

$$= \sum_{\ell=1}^{n} \left(\frac{a_{\ell j}}{a_{ij}}\right) C_\ell \, a_{ij} \, T^{-n_j} \exp(-b_j/\bar{R}T) \tag{B-25}$$

or, using equation (B-7),

$$M_j k_{rj} = \sum_{\ell=1}^{n} \left(\frac{a_{\ell j}}{a_{ij}}\right) C_\ell k_{rj} \tag{B-26}$$

Therefore, M_j is defined by

$$M_j \equiv \sum_{\ell=1}^{n} \left(\frac{a_{\ell j}}{a_{ij}}\right) C_\ell \tag{B-27}$$

Physically, M_j is the mass weighted ratio of different third body reaction rate premultipliers, $a_{\ell j}$, to the known reaction rate premultiplier a_{ij}.

6. REACTION MECHANISM USED IN THIS RESEARCH

The reaction mechanism used in this research is the same as that used in Reference (3) with the addition of the hydrocarbon reaction discussed in Section 3. For a nonequilibrium, chemically reacting flow of a system of thermally perfect gases composed of the six elements carbon, hydrogen, oxygen, nitrogen, flourine, and chlorine, Gold and Weekly (28) have shown that 19 species and 48 chemical reactions should

be considered. The chemical species are shown in Table B-I and the 48 reactions are shown in Table B-II. Note that 13 reactions are shown in Table B-II. Note that 13 reactions are of the dissociation-recombination type while the remaining 35 are binary exchange reactions.

Experience with this and other reaction mechanisms has indicated there may be cases when not all of the reactions corresponding to a given set of chemical species should be included in the analysis. The number of reactions in the reaction mechanism is a significant parameter affecting execution time. Therefore, no more reactions than are necessary should be included in the analysis. Reference (38) provides a grading of the various reactions appropriate for CHON and HF propellant systems as follows:

A - Important reaction between important species with reliable rate data from a competent review

B - Energetically less significant reaction or rate data of doubtful quality

C - Reaction between minor species which may be of significance in some nozzle flows

X - Possibly significant reaction with estimated rate data (not recommended for use)

Guidelines for the selection of reactions from the overall graded set of reactions are provided in Reference (38).

TABLE B-1

CHEMICAL SPECIES CONSIDERED

Chemical Species	Chemical Species
C_nH_m	OH
CO_2	O_2
H_2O	ClF
CO	C
Cl_2	Cl
F_2	F
HCl	H
HF	N
H_2	O
N_2	
NO	

TABLE B-2

CHEMICAL REACTIONS CONSIDERED

Chemical Reaction	Chemical Reaction
$C_nH_m + \frac{n}{2} O_2 \rightarrow \frac{m}{2} H_2 + nCO$	$HCl + HCl \rightleftarrows H_2 + Cl_2$
$CO_2 + M \rightleftarrows CO + O + M$	$HCl + O \rightleftarrows OH + Cl$
$H_2O + M \rightleftarrows OH + H + M$	$HF + Cl \rightleftarrows HCl + F$
$CO + M \rightleftarrows C + O + M$	$HF + F \rightleftarrows H + F_2$
$Cl_2 + M \rightleftarrows 2Cl + M$	$HF + H \rightleftarrows H_2 + F$
$F_2 + M \rightleftarrows 2F + M$	$HF + HF \rightleftarrows H_2 + F_2$
$HCl + M \rightleftarrows H + Cl + M$	$HF + O \rightleftarrows OH + F$
$HF + M \rightleftarrows H + F + M$	$HF + OH \rightleftarrows H_2O + F$
$H_2 + M \rightleftarrows 2H + M$	$H_2 + Cl \rightleftarrows HCl + H$
$N_2 + M \rightleftarrows 2N + M$	$H_2 + O \rightleftarrows OH + H$
$NO + M \rightleftarrows N + O + M$	$H_2 + O_2 \rightleftarrows 2OH$
$OH + M \rightleftarrows O + H + M$	$N_2 + O \rightleftarrows NO + N$
$O_2 + M \rightleftarrows 2O + M$	$N_2 + O_2 \rightleftarrows 2NO$
$ClF + M \rightleftarrows Cl + F + M$	$NO + H \rightleftarrows N + OH$
$CO_2 + H \rightleftarrows CO + OH$	$NO + O \rightleftarrows N + O_2$
$CO_2 + O \rightleftarrows CO + O_2$	$O_2 + H \rightleftarrows OH + O$
$H_2O + Cl \rightleftarrows OH + HCl$	$Cl + ClF \rightleftarrows Cl_2 + F$
$H_2O + H \rightleftarrows OH + H_2$	$F + ClF \rightleftarrows Cl + F_2$
$H_2O + O \rightleftarrows 2OH$	$HF + Cl \rightleftarrows ClF + H$
$CO + CO \rightleftarrows CO_2 + C$	$HCl + F \rightleftarrows ClF + H$
$CO + H \rightleftarrows C + OH$	$HCl + HF \rightleftarrows ClF + H_2$
$CO + N \rightleftarrows C + NO$	$HF + ClF \rightleftarrows F_2 + HCl$
$CO + NO \rightleftarrows CO_2 + N$	$HF + Cl_2 \rightleftarrows ClF + HCl$
$CO + O \rightleftarrows C + O_2$	$ClF + ClF \rightleftarrows F_2 + Cl_2$
$HCl + Cl \rightleftarrows H + Cl_2$	

APPENDIX C

REFERENCE PLANE CHARACTERISTIC RELATIONS

1. GOVERNING EQUATIONS

The equations that are employed in this analysis to model unsteady, two-dimensional, chemically reacting, nonequilibrium flow are developed and transformed to the computational (ζ,η,τ) plane in Appendix A. These equations are restated here for convenience.

$$\rho_\tau + u\rho_\zeta + \bar{v}\rho_\eta + \rho u_\zeta + \rho\alpha u_\eta + \rho\beta v_\eta + \varepsilon\rho v/\bar{\eta} = 0 \qquad \text{(C-1)}$$

$$u_\tau + uu_\zeta + \bar{v}u_\eta + P_\zeta/\rho + \alpha P_\eta/\rho = 0 \qquad \text{(C-2)}$$

$$v_\tau + uv_\zeta + \bar{v}v_\eta + \beta P_\eta/\rho = 0 \qquad \text{(C-3)}$$

$$P_\tau + uP_\zeta + \bar{v}P_\eta - a_f^2(\rho_\tau + u\rho_\zeta + \bar{v}\rho_\eta) = \psi_k \qquad \text{(C-4)}$$

$$C_{i\tau} + uC_{i\zeta} + \bar{v}C_{i\eta} = \sigma_i/\rho \qquad (i=1,\ldots,n) \qquad \text{(C-5)}$$

$$h = h(P,\rho,C_i) \qquad \text{(C-6)}$$

The subscripts τ, ζ, and η in these equations denote partial differentiation and i denotes the ith chemical species. Equation (C-6) is the general form of the equation of state and since it is an algebraic equation, it is not stated again in the remainder of this appendix.

2. CONSTANT η REFERENCE PLANE

When the method of characteristics is applied to unsteady, two-dimensional flow, the characteristic surfaces and corresponding compatibility equations are determined. Hoffman (39) shows that the characteristic surfaces for this case are of two types; stream surfaces and wave surfaces. The envelope of the stream surfaces is the pseudo-pathline (the particle trajectory in $\zeta\eta\tau$ space), and the envelope of the wave surfaces is the Mach cone. The curves of tangency between the wave surfaces and the Mach cone are the bicharacteristics. One compatibility equation is valid on each wave surface, one compatibility equation is valid on each stream surface, and one compatibility equation is valid along the pseudo-pathline. Figure C-1 illustrates the Mach cone, bicharacteristics, and pseudo-pathline as discussed above. A reference-plane characteristic scheme is used in this analysis rather than a bicharacteristic scheme because the increased complexity and computational time of the bicharacteristic scheme is not warranted in view of the accuracy limitations associated with the chemical kinetics model (see Appendix B).

In reference-plane characteristic schemes, derivatives with respect to one of the independent variables are approximated and treated as forcing terms, thus reducing the number of independent variables in the problem by one. For example, in the constant η reference-plane scheme, all derivatives with respect to η are approximated (by MacCormack's method or some other suitable method) and are placed on the right-hand side of the equal sign in equations (C-1) to (C-5).

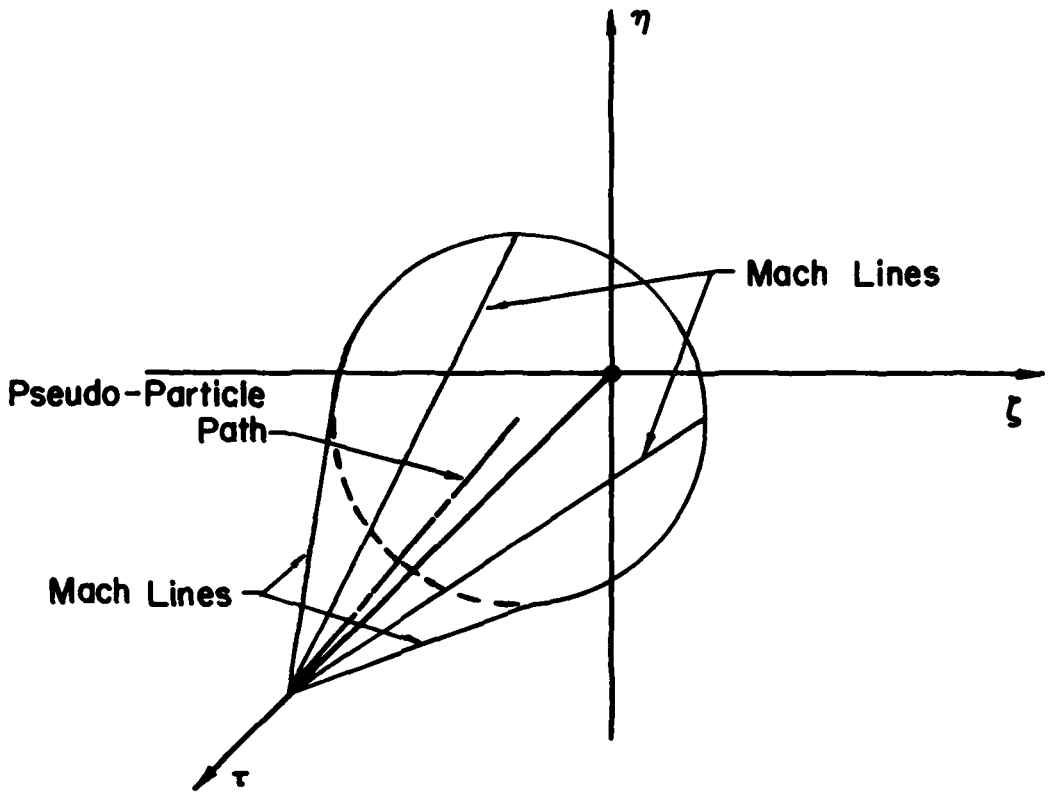

Figure C-1. Mach cone and pseudo-particle path.

This yields

$$\rho_\tau + u\rho_\zeta + \rho u_\zeta = \psi_1 \tag{C-7}$$

$$u_\tau + uu_\zeta + P_\zeta/\rho = \psi_2 \tag{C-8}$$

$$v_\tau + uv_\zeta = \psi_3 \tag{C-9}$$

$$P_\tau + uP_\zeta - a_f^2(\rho_\tau + u\rho_\zeta) = \psi_4 \tag{C-10}$$

$$C_{i\tau} + uC_{i\zeta} = \psi_{5i} \qquad (i=1,\ldots,n) \tag{C-11}$$

where

$$\psi_1 = -\bar{v}\rho_\eta - \rho\alpha u_\eta - \rho\beta v_\eta - \varepsilon\rho v/\bar{\eta}$$

$$\psi_2 = -\bar{v}u_\eta - \alpha P_\eta/\rho$$

$$\psi_3 = -\bar{v}v_\eta - \beta P_\eta/\rho$$

$$\psi_4 = -\bar{v}P_\eta + a_f^2\bar{v}\rho_\eta + \psi_k$$

$$\psi_5 = -\bar{v}C_{i\eta} + \sigma_i/\rho$$

Characteristic Curves

A linear combination of the governing equations can be formed by multiplying equations (C-7) to (C-11) by ℓ_j (j=1,2,...,4+n), respectively, and then summing them. The notation is simplified if ℓ_5 through ℓ_{4+n} are replaced by ℓ_5. The resulting linear combination is

$$\begin{aligned}&\ell_1(\rho_\tau + u\rho_\zeta + \rho u_\zeta - \psi_1) + \ell_2(u_\tau + uu_\zeta + P_\zeta/\rho - \psi_2)\\ &+\ell_3(v_\tau + uv_\zeta - \psi_3) + \ell_4[P_\tau + uP_\zeta - a_f^2(\rho_\tau + u\rho_\zeta) - \psi_4]\\ &+\ell_5(C_{i\tau} + uC_{i\zeta} - \psi_5) = 0\end{aligned} \tag{C-12}$$

Rearranging equation (C-12) yields

$$\rho_\zeta(u\ell_1 - a_f{}^2 u\ell_4) + \rho_\tau(\ell_1 - a_f{}^2\ell_4)$$

$$+ u_\zeta(\rho\ell_1 + u\ell_2) + u_\tau(\ell_2)$$

$$+ v_\zeta(u\ell_3) + v_\tau(\ell_3) \qquad \text{(C-13)}$$

$$+ P_\zeta(\ell_2/\rho + u\ell_4) + P_\tau(\ell_4)$$

$$+ C_{i\zeta}(u\ell_5) + C_{i\tau}(\ell_5) = \ell_1\psi_1 + \ell_2\psi_2 + \ell_3\psi_3 + \ell_4\psi_4 + \ell_5\psi_5$$

The following set of vectors can be defined where the components are the coefficients of the partial derivatives in equation (C-13).

$$\overline{W}_1 = (u\ell_1 - a_f{}^2 u\ell_4 \ , \ \ell_1 - a_f{}^2\ell_4) \qquad \text{(C-14)}$$

$$\overline{W}_2 = (\rho\ell_1 + u\ell_2 \ , \ \ell_2) \qquad \text{(C-15)}$$

$$\overline{W}_3 = (u\ell_3 \ , \ \ell_3) \qquad \text{(C-16)}$$

$$\overline{W}_4 = (\ell_2/\rho + u\ell_4 \ , \ \ell_4) \qquad \text{(C-17)}$$

$$\overline{W}_5 = (u\ell_5 \ , \ \ell_5) \qquad \text{(C-18)}$$

Now, introduce the notation that $d_{W1}\rho$ is the derivative of ρ in the direction of $\overline{W}_1$, $d_{W2}u$ is the derivative of u in the direction of $\overline{W}_2$, etc. Recall that the directional derivative of a function f in the direction of $\overline{W}$ is found by taking the dot product of the gradient of f with the vector $\overline{W}$. Therefore, with the notation above, and the vectors defined by equations (C-14) to (C-18), equation (C-13) can be written as

$$d_{W1}\rho + d_{W2}u + d_{W3}v + d_{W4}P + d_{W5}\,C_i = \qquad \text{(C-19)}$$

$$\ell_1\psi_1 + \ell_2\psi_2 + \ell_3\psi_3 + \ell_4\psi_4 + \ell_5\psi_5$$

If the ℓ_j (j=1,2,...,5) can be chosen so that the vectors $\overline{W}_j$ (j=1,2,...,5) are linearly dependent (lie in one direction), then the curve which contains the vectors $\overline{W}_j$ is called the "characteristic curve," its normal $\overline{N}$ is called the "characteristic normal," and equation (C-19) is called the "compatibility equation." If $\overline{N} = (N_\zeta, N_\tau)$ is the characteristic normal in the (ζ,τ) plane, then $\overline{N}$ and $\overline{W}_j$ must be related by

$$\overline{N} \cdot \overline{W}_j = 0 \qquad (j=1,2,...,5) \qquad \text{(C-20)}$$

Expanding equation (C-20) yields

$$(u\ell_1 - a_f^2 u\ell_4)N_\zeta + (\ell_1 - a_f^2\ell_4)N_\tau = 0 \qquad \text{(C-21)}$$

$$(\rho\ell_1 + u\ell_2)N_\zeta + \ell_2 N_\tau = 0 \qquad \text{(C-22)}$$

$$(u\ell_3)N_\zeta + \ell_3 N_\tau = 0 \qquad \text{(C-23)}$$

$$(\ell_2/\rho + u\ell_4)N_\zeta + \ell_4 N_\tau = 0 \qquad \text{(C-24)}$$

$$(u\ell_5)N_\zeta + \ell_5 N_\tau = 0 \qquad \text{(C-25)}$$

Note that the subscripts ζ and τ in equations (C-21) to (C-25) denote the components of the characteristic normal in directions of ζ and τ, respectively. In matrix form, equations (C-21) to (C-25) can be written as follows:

$$\begin{vmatrix} uN_\zeta+N_\tau & 0 & 0 & -a_f^2(uN_\zeta+N_\tau) & 0 \\ \rho N_\zeta & uN_\zeta+N_\tau & 0 & 0 & 0 \\ 0 & 0 & uN_\zeta+N_\tau & 0 & 0 \\ 0 & N_\zeta/\rho & 0 & uN_\zeta+N_\tau & 0 \\ 0 & 0 & 0 & 0 & uN_\zeta+N_\tau \end{vmatrix} \begin{vmatrix} \ell_1 \\ \ell_2 \\ \ell_3 \\ \ell_4 \\ \ell_5 \end{vmatrix} = 0 \qquad \text{(C-26)}$$

Equation (C-26) is a system of homogeneous equations and therefore, if it is to have a nontrivial solution, the determinant of the coefficient matrix must be zero. Setting that determinant to zero yields

$$(uN_\zeta + N_\tau)^3[(uN_\zeta + N_\tau)^2 - a_f^2 N_\zeta^2] = 0 \qquad \text{(C-27)}$$

Equation (C-27) has two possible solutions. Setting the first factor to zero yields

$$uN_\zeta + N_\tau = 0 \qquad \text{(C-28)}$$

If the term in square brackets is set to zero, the solution is

$$uN_\zeta + N_\tau = \pm a_f N_\zeta \qquad \text{(C-29)}$$

From Figure C-2 it is clear that the following relationship is true along the characteristic curves:

$$\frac{d\tau}{d\zeta} = -\frac{N_\zeta}{N_\tau} \qquad \text{(C-30)}$$

Substituting equation (C-30) into equations (C-28) and (C-29) yields the characteristic curves in the constant η reference plane.

$$\frac{d\zeta}{d\tau} = u \qquad \text{(C-31)}$$

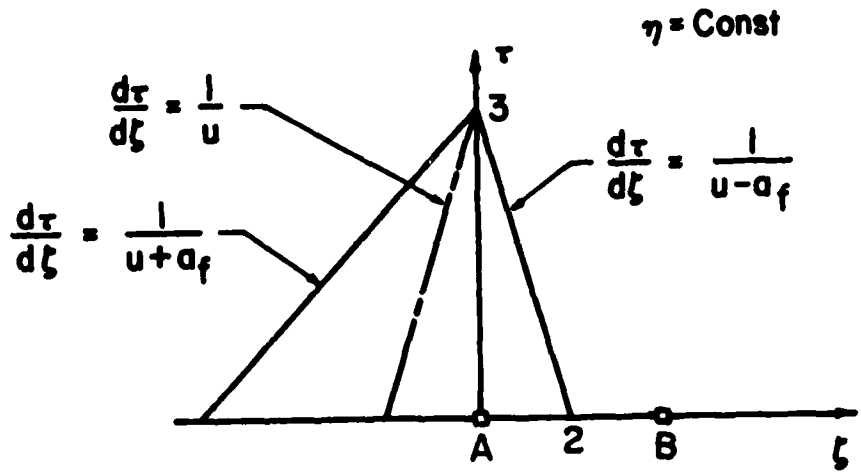

$$dv = \psi_3 \, d\tau$$

$$dP - a_f^2 \, d\rho = \psi_4 \, d\tau$$

$$dC_1 = \psi_5 \, d\tau$$

along $d\zeta = u d\tau$

$$dP + \rho a_f du = (\psi_4 + a_f^2 \psi_1 + \rho a_f \psi_2) d\tau \qquad \text{along } d\zeta = (u + a_f) d\tau$$

$$dP - \rho a_f du = (\psi_4 + a_f^2 \psi_1 - \rho a_f \psi_2) d\tau \qquad \text{along } d\zeta = (u - a_f) d\tau$$

compatibility equations — characteristic curves

Figure C-2. Constant η reference plane characteristic relations.

$$\frac{d\zeta}{d\tau} = u \mp a_f \tag{C-32}$$

Equation (C-31) corresponds to the equation (C-28). It is the projection of the two-dimensional flow pathline onto the constant η plane. Equation (C-32) corresponds to equation (C-29). It is the projection of the two-dimensional Mach cone onto the constant η plane.

Compatibility Equations

The requirement that the determinant of the coefficient matrix in equation (C-26) be identically zero has led to the determination of the characteristic curves. Now, substituting those solutions, equations (C-28) and (C-29), into equation (C-26) and solving for the ℓ_j (j=1,2,...,5) yields the compatibility equations which correspond to the characteristic directions. Specifically, substituting equation (C-28) into equation (C-26) yields the matrix equation

$$\begin{vmatrix} 0 & 0 & 0 & 0 & 0 \\ \rho N_\zeta & 0 & 0 & 0 & 0 \\ 0 & 0 & 0 & 0 & 0 \\ 0 & N_\zeta/\rho & 0 & 0 & 0 \\ 0 & 0 & 0 & 0 & 0 \end{vmatrix} \begin{vmatrix} \ell_1 \\ \ell_2 \\ \ell_3 \\ \ell_4 \\ \ell_5 \end{vmatrix} = 0 \tag{C-33}$$

Here the order of the coefficient matrix is five and its rank is two, so there are three independent solutions. Three possible solutions are

$$\ell_1 = \ell_2 = \ell_4 = \ell_5 = 0; \quad \ell_3 = 1 \tag{C-34}$$

$$\ell_1 = \ell_2 = \ell_3 = \ell_5 = 0; \quad \ell_4 = 1 \tag{C-35}$$

$$\ell_1 = \ell_2 = \ell_3 = \ell_4 = 0; \quad \ell_5 = 1 \tag{C-36}$$

Substituting equations (C-34) to (C-36) into equation (C-13) in turn yields, respectively

$$v_\tau + uv_\zeta = \psi_3 \tag{C-37}$$

$$P_\tau + uP_\zeta - a_f^2(\rho_\tau + u\rho_\zeta) = \psi_4 \tag{C-38}$$

$$C_{i\tau} + u\, C_{i\zeta} = \psi_5 \tag{C-39}$$

or

$$dv = \psi_3\, d\tau \tag{C-40}$$

$$dP - a_f^2 d\rho = \psi_4 d\tau \quad \left.\right\} \quad \text{along } d\zeta = ud\tau \tag{C-41}$$

$$dC_i = \psi_5 d\tau \tag{C-42}$$

Now consider the characteristic curve given by equation (C-29). Substituting equation (C-29) into equation (C-26) yields the matrix equation

$$\begin{vmatrix} \pm a_f N_\zeta & 0 & 0 & \mp a_f^3 N_\zeta & 0 \\ \rho N_\zeta & \pm a_f N_\zeta & 0 & 0 & 0 \\ 0 & 0 & \pm a_f N_\zeta & 0 & 0 \\ 0 & N_\zeta/\rho & 0 & \pm a_f N_\zeta & 0 \\ 0 & 0 & 0 & 0 & \pm a_f N_\zeta \end{vmatrix} \begin{vmatrix} \ell_1 \\ \ell_2 \\ \ell_3 \\ \ell_4 \\ \ell_5 \end{vmatrix} = 0 \tag{C-43}$$

The order of this coefficient matrix is five and its rank is four so there is one independent solution. Equation (C-43) yields

$$\ell_3 = \ell_5 = 0; \quad \ell_1 = a_f^2 \ell_4 = \mp a_f \ell_2/\rho; \quad \ell_2 = \mp \rho a_f \ell_4 \tag{C-44}$$

If $\ell_4 = 1$, one possible solution is

$$\ell_3 = \ell_5 = 0; \quad \ell_1 = a_f^2; \quad \ell_2 = \mp \rho a_f; \quad \ell_4 = 1 \tag{C-45}$$

Substituting equation (C-45) into equation (C-13) yields

$$\begin{aligned} &a_f^2(\rho_\tau + u\rho_\zeta + \rho u_\zeta - \psi_1) \pm \rho a_f(u_\tau + uu_\zeta + P_\zeta/\rho - \psi_2) \\ &+ P_\tau + uP_\zeta - a_f^2(\rho_\tau + u\rho_\zeta) - \psi_4 = 0 \end{aligned} \tag{C-46}$$

or

$$dP + \rho a_f du = (\psi_4 + a_f^2\psi_1 + \rho a_f \psi_2)d\tau \quad \text{along } d\zeta=(u+a_f)d\tau \tag{C-47}$$

$$dP - \rho a_f du = (\psi_4 + a_f^2\psi_1 - \rho a_f \psi_2)d\tau \quad \text{along } d\zeta=(u-a_f)d\tau \tag{C-48}$$

3. CONSTANT ζ REFERENCE PLANE

For the constant ζ reference-plane scheme, all derivatives with respect to ζ in the governing equations are approximated and treated as forcing terms. The development which follows is entirely analogous to the derivation of the constant η reference-plane relations in the previous section of this appendix. Therefore, the corresponding steps in the development of the equations will all be shown, but the arguments will be abbreviated. Moving all derivatives with respect to ζ to the right-hand side of the governing equations yields

$$\rho_\tau + \bar{v}\rho_\eta + \rho\alpha u_\eta + \rho\beta v_\eta = \psi_1 \tag{C-49}$$

$$u_\tau + \bar{v}u_\eta + \alpha P_\eta/\rho = \psi_2 \tag{C-50}$$

$$v_\tau + \bar{v}v_\eta + \beta P_\eta/\rho = \psi_3 \tag{C-51}$$

$$P_\tau + \bar{v}P_\eta - a_f^2(\rho_\tau + \bar{v}\rho_\eta) = \psi_4 \qquad \text{(C-52)}$$

$$C_{i\tau} + \bar{v}C_{i\eta} = \psi_5 \qquad \text{(C-53)}$$

where

$$\psi_1 = -u\rho_\zeta - \rho u_\zeta - \varepsilon\rho v/\bar{\eta}$$

$$\psi_2 = -uu_\zeta - P_\zeta/\rho$$

$$\psi_3 = -uv_\zeta$$

$$\psi_4 = -uP_\zeta + a_f^2 u\rho_\zeta + \psi_k$$

$$\psi_5 = -uC_{i\zeta} + \sigma_i/\rho$$

Characteristic Curves

Forming a linear combination of equations (C-49) to (C-53) yields

$$\ell_1(\rho_\tau + \bar{v}\rho_\eta + \rho\alpha u_\eta + \rho\beta v_\eta - \psi_1) + \ell_2(u_\tau + \bar{v}u_\eta + \alpha P_\eta/\rho - \psi_2)$$
$$+\ell_3(v_\tau + \bar{v}v_\eta + \beta P_\eta/\rho - \psi_3) + \ell_4[P_\tau + \bar{v}P_\eta - a_f^2(\rho_\tau + \bar{v}\rho_\eta) - \psi_4]$$
$$+\ell_5(C_{i\tau} + \bar{v}C_{i\eta} - \psi_5) = 0 \qquad \text{(C-54)}$$

Rearranging equation (C-54) gives

$$\rho_\eta(\bar{v}\ell_1 - a_f^2\bar{v}\ell_4) + \rho_\tau(\ell_1 - a_f^2\ell_4)$$
$$+ u_\eta(\rho\alpha\ell_1 + \bar{v}\ell_2) + u_\tau(\ell_2)$$
$$+ v_\eta(\rho\beta\,\ell_1 + \bar{v}\ell_3) + v_\tau(\ell_3) \qquad \text{(C-55)}$$
$$+ P_\eta(\alpha\ell_2/\rho + \beta\ell_3/\rho + \bar{v}\ell_4) + P_\tau(\ell_4)$$
$$+ C_{i\eta}(\bar{v}\ell_5) + C_{i\tau}(\ell_5) = \ell_1\psi_1 + \ell_2\psi_2 + \ell_3\psi_3 + \ell_4\psi_4 + \ell_5\psi_5$$

Define the vectors $\overline{W}_j$ (j=1,2,...,5) as follows

$$\overline{W}_1 = (\overline{v}\ell_1 - a_f^2\overline{v}\ell_4 , \ \ell_1 - a_f^2\ell_4) \tag{C-56}$$

$$\overline{W}_2 = (\rho\alpha\ell_1 + \overline{v}\ell_2 , \ \ell_2) \tag{C-57}$$

$$\overline{W}_3 = (\rho\beta\ell_1 + \overline{v}\ell_3, \ \ell_3) \tag{C-58}$$

$$\overline{W}_4 = (\alpha\ell_2/\rho + \beta\ell_3/\rho + \overline{v}\ell_4 , \ \ell_4) \tag{C-59}$$

$$\overline{W}_5 = (\overline{v}\ell_5 , \ \ell_5) \tag{C-60}$$

Then, using the directional derivative notation introduced in Section 2:

$$d_{W1}\rho + d_{W2}u + d_{W3}v + d_{W4}P + d_{W5}C_i = \ell_1\psi_1 + \ell_2\psi_2 + \ell_3\psi_3 + \ell_4\psi_4 + \ell_5\psi_5 \tag{C-61}$$

Now, determine if the ℓ_j (j=1,2,...,5) can be chosen so that the $\overline{W}_j$ are all linearly independent. If $\overline{N}$ is the characteristic normal, then $\overline{N}\cdot\overline{W}_j = 0$ (j=1,2,...,5). This gives

$$(\overline{v}\ell_1 - a_f^2\overline{v}\ell_4)N_\eta + (\ell_1 - a_f^2\ell_4)N_\tau = 0 \tag{C-62}$$

$$(\rho\alpha\ell_1 + \overline{v}\ell_2)N_\eta + \ell_2 N_\tau = 0 \tag{C-63}$$

$$(\rho\beta\ell_1 + \overline{v}\ell_3)N_\eta + \ell_3 N_\tau = 0 \tag{C-64}$$

$$(\alpha\ell_2/\rho + \beta\ell_3/\rho + \overline{v}\ell_4)N_\eta + \ell_4 N_\tau = 0 \tag{C-65}$$

$$(\overline{v}\ell_5)N_\eta + \ell_5 N_\tau = 0 \tag{C-66}$$

or, in matrix form:

$$\begin{vmatrix} \bar{v}N_\eta+N_\tau & 0 & 0 & -a_f^2(\bar{v}N_\eta+N_\tau) & 0 \\ \rho\alpha N_\eta & \bar{v}N_\eta+N_\tau & 0 & 0 & 0 \\ \rho\beta N_\eta & 0 & \bar{v}N_\eta+N_\tau & 0 & 0 \\ 0 & \alpha N_\eta/\rho & \beta N_\eta/\rho & \bar{v}N_\eta+N_\tau & 0 \\ 0 & 0 & 0 & 0 & \bar{v}N_\eta+N_\tau \end{vmatrix} \begin{vmatrix} \ell_1 \\ \ell_2 \\ \ell_3 \\ \ell_4 \\ \ell_5 \end{vmatrix} = 0 \qquad \text{(C-67)}$$

Setting the determinant of the coefficient matrix to zero yields

$$(\bar{v}N_\eta + N_\tau)^3[(\bar{v}N_\eta + N_\tau)^2 - a_f{}^2N_\eta{}^2(\alpha^2 + \beta^2)] = 0 \qquad \text{(C-68)}$$

Equation (C-68) has two possible solutions:

$$\bar{v}\, N_\eta + N_\tau = 0 \qquad \text{(C-69)}$$

$$\bar{v}\, N_\eta + N_\tau = \pm\, a_f N_\eta \alpha^* \qquad \text{(C-70)}$$

where $\alpha^* = (\alpha^2 + \beta^2)^{\frac{1}{2}}$.

Noting from Figure C-3 that $d\tau/d\eta = -N_\eta/N_\tau$, equations (C-69) and (C-70) can be rewritten as

$$\frac{d\eta}{d\tau} = \bar{v} \qquad \text{(C-71)}$$

$$\frac{d\eta}{d\tau} = \bar{v} \mp a_f\, \alpha^* \qquad \text{(C-72)}$$

respectively. Equations (C-71) and (C-72) are the characteristic curves in the constant ζ reference plane.

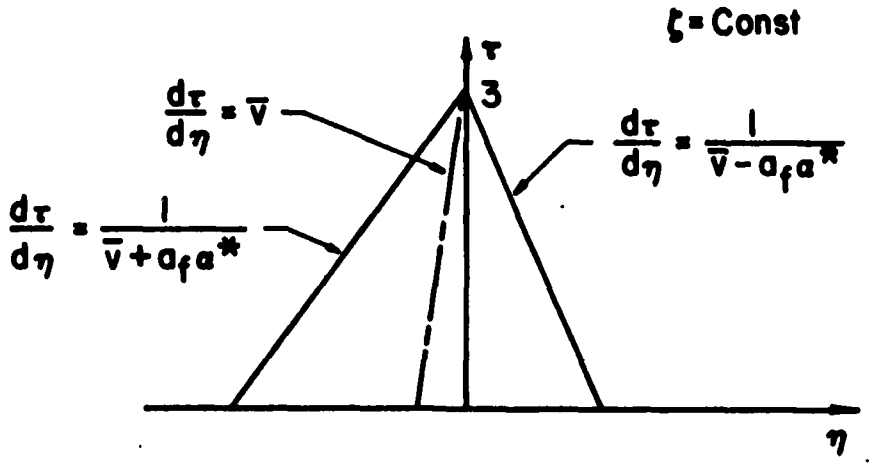

$$\beta du - \alpha dv = (\beta\psi_2 - \alpha\psi_3)d\tau$$

$$dP - a_f^2 d\rho = \psi_f d\tau$$

$$dC_i = \psi_5 d\tau$$

} along $d\eta = \bar{v}d\tau$

$$dP + \frac{\rho\alpha a_f}{\alpha^*} du + \frac{\rho\beta a_f}{\alpha^*} dv = (\psi_4 + a_f^2\psi_1 + \frac{\rho\alpha a_f}{\alpha^*}\psi_2 + \frac{\rho\beta a_f\psi_3}{\alpha^*})d\tau \quad \text{along } d\eta = (\bar{v} + a_f\alpha^*)d\tau$$

$$dP - \frac{\rho\alpha a_f}{\alpha^*} du + \frac{\rho\beta a_f}{\alpha^*} dv = (\psi_4 + a_f^2\psi_1 - \frac{\rho\alpha a_f\psi_2}{\alpha^*} - \frac{\rho\beta a_f\psi_3}{\alpha^*})d\tau \quad \text{along } d\eta = (\bar{v} - a_f\alpha^*)d\tau$$

compatibility equations — characteristic curves

Figure C-3. Constant ζ reference plane characteristic relations.

Compatibility Equations

Consider the characteristic curve given by equation (C-69). Substituting equation (C-69) into equation (C-67) yields

$$\begin{vmatrix} 0 & 0 & 0 & 0 & 0 \\ \rho\alpha N_\eta & 0 & 0 & 0 & 0 \\ \rho\beta N_\eta & 0 & 0 & 0 & 0 \\ 0 & \alpha N_\eta/\rho & \beta N_\eta/\rho & 0 & 0 \\ 0 & 0 & 0 & 0 & 0 \end{vmatrix} \begin{vmatrix} \ell_1 \\ \ell_2 \\ \ell_3 \\ \ell_4 \\ \ell_5 \end{vmatrix} = 0 \qquad \text{(C-73)}$$

Three possible solutions to equation (C-73) are

$$\ell_1 = \ell_4 = \ell_5 = 0; \quad \ell_2 = 1; \quad \ell_3 = -\alpha/\beta \qquad \text{(C-74)}$$

$$\ell_1 = \ell_2 = \ell_3 = \ell_5 = 0; \quad \ell_4 = 1 \qquad \text{(C-75)}$$

$$\ell_1 = \ell_2 = \ell_3 = \ell_4 = 0; \quad \ell_5 = 1 \qquad \text{(C-76)}$$

Substituting equations (C-74) to (C-76) in turn into equation (C-55) yields, respectively

$$\bar{v}\, u_\eta + u_\tau + \alpha P_\eta/\rho + \bar{v}(-\alpha/\beta)v_\eta - \alpha/\beta\ v_\tau + \beta/\rho(-\alpha/\beta)P_\eta = \psi_2 - (\alpha/\beta)\psi_3 \qquad \text{(C-77)}$$

$$-a_f^2\bar{v}\rho_\eta - a_f^2\rho_\tau + \bar{v}P_\eta + P_\tau = \psi_4 \qquad \text{(C-78)}$$

$$\bar{v}\, C_{i\eta} + C_{i\tau} = \psi_5 \qquad \text{(C-79)}$$

which may be written as

$$\left.\begin{aligned} \beta du - \alpha dv &= (\beta\psi_2 - \alpha\psi_3)d\tau \qquad \text{(C-80)} \\ dP - a_f^2 d\rho &= \psi_4 d\tau \qquad \text{(C-81)} \\ dC_i &= \psi_5\, d\tau \qquad \text{(C-82)} \end{aligned}\right\} \text{ along } d\eta = \bar{v}d\tau$$

Now consider the characteristic curve given by equation (C-70). Substitution of this result into equation (C-67) yields

$$\begin{vmatrix} \pm a_f N_\eta \alpha^* & 0 & 0 & -a_f^2(\pm a_f N_\eta \alpha^*) & 0 \\ \rho\alpha N_\eta & \pm a_f N_\eta \alpha^* & 0 & 0 & 0 \\ \rho\beta N_\eta & 0 & \pm a_f N_\eta \alpha^* & 0 & 0 \\ 0 & \alpha N_\eta/\rho & \beta N_\eta/\rho & \pm a_f N_\eta \alpha^* & 0 \\ 0 & 0 & 0 & 0 & \pm a_f N_\eta \alpha^* \end{vmatrix} \begin{vmatrix} \ell_1 \\ \ell_2 \\ \ell_3 \\ \ell_4 \\ \ell_5 \end{vmatrix} = 0 \qquad \text{(C-83)}$$

Equation (C-83) has one independent solution:

$$\ell_1 = a_f^2 \ell_4; \quad \ell_2 = \frac{\alpha}{\beta}\ell_3; \quad \alpha\ell_2 + \beta\ell_3 = \mp\rho a_f \alpha^* \ell_4; \quad \ell_5 = 0 \qquad \text{(C-84)}$$

If $\ell_4 = 1$ is chosen, then

$$\begin{aligned} &\ell_1 = a_f^2; \quad \ell_2 = \mp \rho\alpha a_f/\alpha^*; \quad \ell_3 = \mp \rho\beta a_f/\alpha^*; \\ &\ell_4 = 1; \quad \ell_5 = 0 \end{aligned} \qquad \text{(C-85)}$$

Substituting equation (C-85) into equation (C-55) yields the compatibility equations

$$dP + \frac{\rho\alpha a_f}{\alpha^*} du + \frac{\rho\beta a_f}{\alpha^*} dv = \left(\psi_4 + a_f^2\psi_1 + \frac{\rho\alpha a_f}{\alpha^*}\psi_2 + \frac{\rho\beta a_f}{\alpha^*}\psi_3\right)d\tau$$

$$\text{along } d\eta = (\bar{v} + a_f\alpha^*)d\tau \qquad \text{(C-86)}$$

and

$$dP - \frac{\rho\alpha a_f}{\alpha^*} du + \frac{\rho\beta a_f}{\alpha^*} dv = (\psi_4 + a_f^2\psi_1 - \frac{\rho\alpha a_f}{\alpha^*} \psi_2 - \frac{\rho\beta a_f}{\alpha^*} \psi_3)d\tau \qquad \text{along } d\eta = (\bar{v} - a_f\alpha^*)d\tau \tag{C-87}$$

APPENDIX D

THE SPECIES CONTINUITY EQUATION INTEGRATION SCHEME

1. STIFF EQUATIONS AND IMPLICIT VS. EXPLICIT INTEGRATION METHODS

It is well known that integration of the species continuity equations for nonequilibrium, chemically reacting flow, when the flow is near equilibrium, requires special treatment because the equations become quite "stiff" (Refs. 3, 5, and 31). In order to understand the concept of a stiff differential equation, consider the following general form for an ordinary differential equation.

$$\frac{dy}{dx} = f(x,y) \tag{D-1}$$

The existence of a unique solution to this equation requires that $f(x,y)$ must be continuous and that it satisfy a criterion known as the Lipschitz condition (Ref. 40). The Lipschitz condition is stated in terms of the Lipschitz constant, L, which is defined by

$$L \equiv \left| \frac{\partial f(x,y)}{\partial y} \right| \tag{D-2}$$

If the ordinary differential equation is stiff, it will have a large Lipschitz constant while its solution behaves like a polynomial (i.e., the solution has little exponential growth or decay).

The relevance of the Lipschitz constant to the species continuity equation can be understood from the following discussion. The

species continuity equation can be written in functional form as

$$\frac{DC_i}{Dt} = \frac{\sigma_i}{\rho} = f_i(\rho,T,C_i) \qquad (i=1,\ldots,n) \tag{D-3}$$

Note that $f_i(\rho,T,C_i)$ in equation (D-3) has dimensions of C_i divided by time and therefore, the partial derivative $(\partial f_i/\partial C_i)_{\rho,T}$ must have dimensions of $(\text{time})^{-1}$. Following Ref. (25), a local characteristic time for the rate process can be defined by

$$\hat{\tau} \equiv - \frac{1}{(\partial f_i/\partial C_i)_{\rho,T}} \tag{D-4}$$

Now, equation (D-3) can be written as

$$\frac{DC_i}{Dt} = \frac{\chi(\rho,T,C_i)}{\hat{\tau}(\rho,T,C_i} \qquad (i=1,\ldots,n) \tag{D-5}$$

where

$$\chi(\rho,T,C_i) \equiv \frac{f_i}{(\partial f_i/\partial C_i)_{\rho,T}} \tag{D-6}$$

Using equation (D-3) and the definition of the Lipschitz constant (D-2), the Lipschitz constant for the species continuity equation becomes

$$L = \left| \frac{\partial f_i(\rho,T,C_i)_{\rho,T}}{\partial C_i} \right| = \frac{1}{\hat{\tau}} \tag{D-7}$$

Consider the change in C_i according to equation (D-3) for an increment of time equal to the local relaxation time.

$$\frac{DC_i}{Dt} \approx \frac{C_2-C_1}{\hat{t}} \tag{D-8}$$

In equilibrium flow, the local characteristic time, $\hat{\tau}$, for the chemical reaction approaches zero and since $\frac{DC_i}{Dt}$ must remain finite for any real physical process, the change in mass fraction also approaches zero. Thus, the Lipschitz constant becomes large while the solution behaves like a polynomial and the differential equation is stiff. For the case of frozen flow, the mass fraction does not change and $\hat{\tau}$ approaches infinity, so DC_i/Dt goes to zero.

Many numerical techniques have been proposed for the solution of the species continuity equations in near equilibrium flow. Among these techniques are linearized approaches, conversion of the differential equations to integral equations, modified Range-Kutta techniques, higher-order predictor-corrector methods, and implicit methods. Curtiss and Hirshfelder (32) and Seinfield (33) provide useful reviews of the various numerical methods that have been used for stiff differential equations. Cline (41) analyzed and tested a number of proposed schemes in his analysis of three-dimensional, steady, nonequilibrium flow. It is possible to categorize the numerical methods he tested into two groups: explicit and implicit methods. In an explicit method, the solution at the unknown point is expressed entirely in terms of known points, while in an implicit method, the solution at the unknown point is expressed in terms of both the known points and the unknown point. Cline concluded that explicit schemes, and predictor-corrector methods, were stable only for very small step sizes (which would lead to excessive computational time). Tyson and Kliegel (42) show that a step size of the order of the relaxation time $\hat{\tau}$ is necessary to insure stability when the first-order Euler method (explicit) is applied to

the species continuity equations. Cline also found that only some of the implicit methods he tested gave adequate results. He concluded that a method proposed by Lomax and Bailey (34) provided the best results. It is this technique, which could be called a second-order, implicit Taylor expansion, which is used in this analysis.

2. DERIVATION OF THE SECOND-ORDER, IMPLICIT, TAYLOR EXPANSION SCHEME

To illustrate the derivation, consider the ordinary differential equation:

$$\frac{dy}{dx} = f(x,y) \tag{D-9}$$

Here, $f(x,y)$ may be nonlinear in y and $y(x)$ is assumed to be continuous and differentiable so it can be expanded in a Taylor series. Expanding through second-order terms yields

$$y_{n+1} = y_n + \frac{dy}{dx}\Big|_n (x_{n+1} - x_n) + \frac{d^2y}{dx^2}\Big|_n \frac{(x_{n+1} - x_n)^2}{2} + O(\Delta x^3) \tag{D-10}$$

where

$$\frac{dy}{dx}\Big|_n = \left(\frac{dy}{dx}\right)_{x=x_n, y=y_n}$$

and n denotes the nth mesh point. Note that

$$\frac{d^2y}{dx^2}\Big|_n = \frac{d}{dx}\left(\frac{dy}{dx}\Big|_n\right) = \frac{d}{dx}\left[f_n(x,y)\right] \tag{D-11}$$

$$\left.\frac{d^2y}{dx^2}\right|_n = \frac{\partial f_n}{\partial x} + \frac{\partial f_n}{\partial y}\frac{dy}{dx} = \frac{\partial f_n}{\partial x} + f_n\frac{\partial f_n}{\partial y} \qquad \text{(D-12)}$$

Substituting equation (D-12) into equation (D-10) yields

$$y_{n+1} = y_n + hf_n + \frac{h^2}{2}\left[\frac{\partial f_n}{\partial x} + f_n\frac{\partial f_n}{\partial y}\right] + O(h^3) \qquad \text{(D-13)}$$

where $h = x_{n+1} - x_n$. Now, f_n inside the square brackets in equation (D-13) is replaced as follows

$$f_n \cong \frac{y_{n+1} - y_n}{x_{n+1} - x_n} = \frac{y_{n+1} - y_n}{h} \qquad \text{(D-14)}$$

Substituting equation (D-14) into equation (D-13) yields the desired result.

$$y_{n+1} = y_n + hf_n + \frac{h^2}{2}\left[\frac{\partial f_n}{\partial x} + \frac{\partial f_n}{\partial y}\frac{(y_{n+1} - y_n)}{h}\right] + O(h^3) \qquad \text{(D-15)}$$

The derivation for the species continuity equations is entirely analogous to the above derivation. The species continuity equations are restated here for convenience.

$$\frac{DC_i}{Dt} = \frac{\sigma_i}{\rho} = f_i(\rho,T,C_i) \qquad (i=1,\ldots,\hat{n}) \qquad \text{(D-16)}$$

Note that equation (D-16) is a first-order, ordinary differential equation when applied along a particle path in unsteady flow or along a streamline in steady flow. Along the one-dimensional trajectory, the substantial derivative can be written as $D(\ )/Dt = Vd(\ )/ds$ where s is an elemental path length and V is the velocity magnitude. Thus,

equation (D-16) becomes

$$\frac{dC_i}{ds} = \frac{\sigma_i}{\rho V} = g_i(\rho,V,T,C_i) \qquad (i=1,\ldots,\hat{n}) \tag{D-17}$$

The i subscript is temporarily dropped in the following development for clarity. Expanding C in a Taylor series through second-order terms yields

$$C_{n+1} = C_n + \frac{dC}{ds}\Big|_n (s_{n+1} - s_n) + \frac{d^2C}{ds^2}\Big|_n \frac{(s_{n+1} - s_n)^2}{} + O(\Delta s^3) \tag{D-18}$$

But

$$\frac{d^2C}{ds^2}\Big|_n = \frac{d}{ds}\left(\frac{dC}{ds}\Big|_n\right) = \frac{d}{ds}\left[g_n(\rho,V,T,C)\right] \tag{D-19}$$

so

$$\frac{d^2C}{ds^2}\Big|_n = \frac{\partial g_n}{\partial \rho}\frac{d\rho}{ds} + \frac{\partial g_n}{\partial V}\frac{dV}{ds} + \frac{\partial g_n}{dT}\frac{dT}{ds} + \frac{\partial g_n}{\partial C}\frac{dC}{ds} \tag{D-20}$$

Note that the last term in equation (D-20) will become a summation over all species when the i subscript is re-introduced. Substituting equation (D-20) into equation (D-18) yields

$$C_{n+1} = C_n + hg_n + \left[\frac{\partial g_n}{\partial \rho}\frac{d}{ds} + \frac{\partial g_n}{\partial V}\frac{dV}{ds} + \frac{\partial g_n}{\partial T}\frac{dT}{ds} + \frac{\partial g_n}{\partial C}g_n\right]\frac{h^2}{2} + O(h^3) \tag{D-21}$$

where $h = s_{n+1} - s_n$. Now, let $ds = s_{n+1} - s_n$; $dT = T_{n+1} - T_n$, etc., and let g_n inside the square bracket be replaced by

$$g_n \cong \frac{C_{n+1} - C_n}{h} \tag{D-22}$$

Substituting into equation (D-21) yields

$$C_{n+1} = C_n + hg_n + \frac{h}{2}\left[\frac{\partial g_n}{\partial \rho}(\rho_{n+1} - \rho_n) + \frac{\partial g_n}{\partial V}(V_{n+1} - V_n)\right.$$

$$\left. + \frac{\partial g_n}{\partial T}(T_{n+1} - T_n) + \frac{\partial g_n}{\partial C}(C_{n+1} - C_n)\right] + O(h^3) \tag{D-23}$$

Re-introducing the i subscript yields

$$K_{in} = \frac{h}{2}\left[2g_{in} + \frac{\partial g_{in}}{\partial \rho}(\rho_{n+1} - \rho_n) + \frac{\partial g_{in}}{\partial V}(V_{n+1} - V_n)\right.$$

$$\left. + \frac{\partial g_{in}}{\partial T}(T_{n+1} - T_n) + \sum_{j=1}^{\hat{n}} \frac{\partial g_{in}}{\partial C_j}(K_j)\right] \tag{D-24}$$

$$+ O(h^3) \qquad (i=1,\ldots,\hat{n})$$

where

$$K_{in} = Ci_{n+1} = Ci_n.$$

The partial derivatives in equation (D-24) are determined analytically. When expanded, equation (D-24) becomes a system of $\hat{n}$ simultaneous, linear, algebraic equations which is easily solved by standard methods.

3. ERROR CONTROL

The implicit scheme derived in the previous section has been found to be stable for even large step sizes in both Cline's work (41) and in the subject research. However, the method is subject to truncation error and thus consideration of step size control must be given.

Equation (D-24) is of the form

$$K_{in} = \frac{h}{2} [\qquad\qquad] + \frac{d^3C_i}{ds^3}\Big|_n \frac{h^3}{6} + O(h^4) \qquad \text{(D-25)}$$

"computed term" "third order term"

The objective in the error control scheme is to estimate the third-order term and require that the ratio of this term to the computed term be less than a specified tolerance. The third-order term is estimated as follows.

$$\frac{dC_i}{ds}\Big|_n \cong \frac{K_{in}}{h_n} \qquad \text{(D-26)}$$

then

$$\frac{d^3C_i}{ds^3}\Big|_n = \frac{d^2}{ds^2}\left(\frac{dC_i}{ds}\right)_n = \frac{\frac{dC_i}{ds}\Big|_{n+1} - 2\frac{dC_i}{ds}\Big|_n + \frac{dC_i}{ds}\Big|_{n-1}}{(ds)^2} \qquad \text{(D-27)}$$

$$= \frac{\frac{Ki_{n+1}}{h_{n+1}} - 2\frac{K_{in}}{h_n} + \frac{Ki_{n-1}}{h_{n-1}}}{\bar{h}^2} \qquad \text{(D-28)}$$

where $\bar{h}$ is the average step size.

Assuming equal step sizes, $h_{n+1} = h_n = h_{n-1} = \bar{h}$,

$$\left.\frac{d^3 C_i}{ds^3}\right|_n = \frac{Ki_{n+1} - 2K_{in} + Ki_{n-1}}{h^3} \qquad \text{(D-29)}$$

Finally the ratio of interest is computed as

$$\text{RATIO} = \frac{\dfrac{Ki_{n+1} - 2K_{in} + Ki_{n-1}}{h^3} \cdot \dfrac{h^3}{6}}{K_{in}} \qquad \text{(D-30)}$$

$$\text{RATIO} = \frac{Ki_{n+1} - 2K_{in} + Ki_{n-1}}{6K_{in}} \qquad \text{(D-31)}$$

Note that RATIO has distinct values for each of the chemical species in the gas mixture at each step in the integration. Also, RATIO can be computed only after three integration steps have been taken. To reduce the truncation error to the desired level, intermediate points are placed between grid points along particle paths in the computational mesh.

Figure D-1 illustrates how the error control scheme is used in practice. An estimate of the number of intermediate points (NINT) required between L and L+1 is made. The values of temperature, density, and velocity at the intermediate points are determined by linear interpolation between the known corresponding values at the end points. Then the species continuity equations are integrated from L to L+1

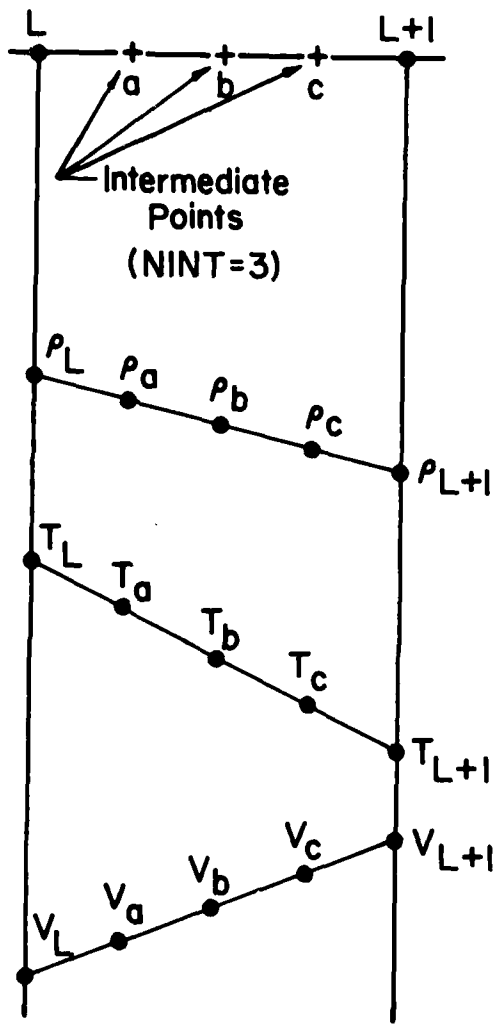

Figure D-1. The use of intermediate points.

and RATIO is computed for each of the chemical species. If, after the last intermediate integration step, the maximum value of RATIO is less than a user specified tolerance (TOL), then the integration proceeds. If the required tolerance is not achieved, then the number of intermediate points is doubled and the integration procedure is restarted from L. Also, if the maximum value of RATIO is two orders of magnitude less than TOL, then NINT is reduced by one-half before the integration from L+1 to L+2 proceeds. Figures D-2 and D-3 show the effect of NINT in integrating between given end conditions for equilibrium and nonequilibrium conditions at L. In the first two sections of the tables in those figures, NINT has been specified, while in the last section, TOL has been specified and NINT has been determined by the error control procedure described above. Note that in both figures, failure to use intermediate points yields poor results for the species mass fractions and ψ_K. However, for the cases shown here, even a small number of intermediate points improves the results significantly. Computational time for the subject problem is almost directly proportional to NINT. Experience indicates that a loose tolerance (5 to 10%) should be used until the solution is near convergence and then TOL can be reduced to the desired degree.

Figure D-4 illustrates the effect of variable property gradients between L and L+1 on the number of intermediate points required to achieve a tolerance of one percent. Part (a) of the figure corresponds to equilibrium conditions at L. Case 1 indicates that for small gradients in density and temperature, the integration from equilibrium

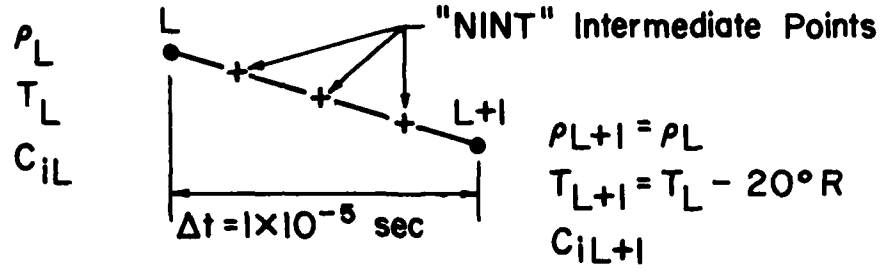

NINT		0	2	5
$C_{i_{L+1}}$	F2	6.67002079E-07	6.67088240E-07	6.67098947E-07
	HF	9.16541128E-01	9.16630067E-01	9.16633003E-01
	H2	1.44297673E-02	1.44407872E-02	1.44405314E-02
	F	5.27127187E-02	5.26282603E-02	5.26254722E-02
	H	1.63157192E-02	1.63002183E-02	1.63003262E-02
$\psi_{k_{L+1}}$		14.231 E 05	9.669 E 05	9.456 E 05

NINT		10	20.	40
$C_{i_{L+1}}$	F2	6.67113862E-07	6.67116594E-07	6.67116342E-07
	HF	9.16632195E-01	9.16632155E-01	9.16632141E-01
	H2	1.44406072E-02	1.44406089E-02	1.44406096E-02
	F	5.26262396E-02	5.26262778E-02	5.26262907E-02
	H	1.63002910E-02	1.63002915E-02	1.63002914E-02
$\psi_{k_{L+1}}$		9.515 E 05	9.518 E 05	9.519 E 05

TOL		10% (NINT=2)	5% (NINT=4)	1% (NINT=4)
$C_{i_{L+1}}$	F2	6.67088240E-07	6.67110031E-07	6.67110031E-07
	HF	9.16630067E-01	9.16631423E-01	9.16631423E-01
	H2	1.44407872E-02	1.44407117E-02	1.44407117E-02
	F	5.26282603E-02	5.26269729E-02	5.26269729E-02
	H	1.63002183E-02	1.63002255E-02	1.63002255E-02
$\psi_{k_{L+1}}$		9.669 E 05	9.575 E 05	9.575 E 05

Figure D-2. The effect of NINT intermediate points - equilibrium initial conditions (H-F system).

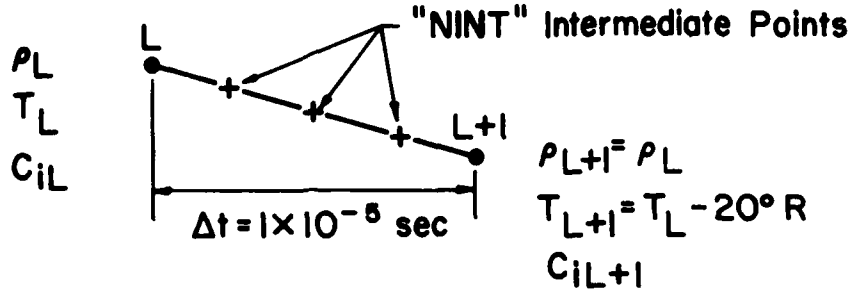

NINT		0	2	5
$C_{i_{L+1}}$	F2	9.26174224E-09	9.71138822E-09	9.74977520E-09
	HF	9.60158784E-01	9.59517223E-01	9.59466462E-01
	H2	1.71175668E-02	1.71761786E-02	1.71807494E-02
	F	1.12932851E-02	1.19025221E-02	1.19507258E-02
	H	1.14303552E-02	1.14040668E-02	1.14020535E-02
$\psi_{k_{L+1}}$		7.053 E 05	9.444 E 05	9.634 E 05

NINT		10	20	40
$C_{i_{L+1}}$	F2	9.73446971E-09	9.73981717E-09	9.74361901E-09
	HF	9.59464704E-01	9.59464162E-01	9.59464011E-01
	H2	1.71807895E-02	1.71808019E-02	1.71808054E-02
	F	1.19523952E-02	1.19529095E-02	1.19530531E-02
	H	1.14021020E-02	1.14021168E-02	1.14021210E-02
$\psi_{k_{L+1}}$		9.640 E 05	9.642 E 05	9.642 E 05

TOL		10% (NINT=4)	5% (NINT=4)	1% (NINT=64)
$C_{i_{L+1}}$	F2	9.73637961E-09	9.73637961E-09	9.74374805E-09
	HF	9.59467656E-01	9.59467656E-01	9.59463979E-01
	H2	1.71807148E-02	1.71807148E-02	1.71808061E-02
	F	1.19495923E-02	1.19495923E-02	1.19530838E-02
	H	1.14020279E-02	1.14020279E-02	1.14021219E-02
$\psi_{k_{L+1}}$		9.630 E 05	9.630 E 05	9.643 E 05

Figure D-3. The effect of NINT intermediate points - nonequilibrium initial conditions (H-F system).

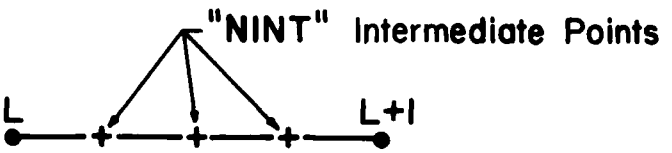

	L	L+1 Case Number				
		1	2	3	4	5
T	7377.1	7376.8	7370.8	7397.1	7376.8	7370.8
ρ	.01730	.01729	.01729	.01729	.01830	.01729
$\overline{V}$		840	840	840	340	280
NINT		129	5	5	5	9

a) Equilibrium Conditions at L.

	L	L+1 Case Number				
		1	2	3	4	5
T	6908	6812	6908	6812	6812	6812
ρ	.01079	.00983	.00983	.01079	.00983	.00983
$\overline{V}$	5373	5612	5612	5612	2806	1871
NINT		8	32	8	16	32

b) Nonequilibrium Conditions at L.

Figure D-4. The effect of property gradients on intermediate points (TOL = .01).

conditions may require a large number of intermediate points to achieve a one percent tolerance. However, cases 2 and 4 show that even modest gradients in temperature in density reduce NINT dramatically. In comparing cases 2 and 3 note that NINT is not sensitive to the sign of the temperature gradient. Case 5 corresponds to tripling the relaxation time between L and L+1.

In part (b) of figure D-4, the conditions at L are not in equilibrium. The gradients represented by case 1 are the same as those that existed between L-1 and L in the data from which this information was taken. Cases 2 and 3 show that NINT is sensitive to a change in the temperature gradient but that it is not affected by a change in the density gradient. Cases 4 and 5 illustrate the effect of the velocity gradient (or relaxation time) on NINT. In general, discontinuous gradients in temperature and velocity between the L-1 to L interval and the L to L+1 interval will require a higher value of NINT to achieve the specified tolerance than for the case of continuous gradients. NINT is also affected by the density gradient but to a lesser degree than for temperature and velocity. The significant results concerning the use of error control are summarized as follows:

1. Most of the computational time required to solve the subject problem is related to the integration of the species continuity equations. Therefore, the total execution time is nearly directly proportional to NINT.
2. Failure to use intermediate points in integrating the species continuity equations will, in general, yield poor results for species mass fractions and ψ_K.

3. Integrating from equilibrium conditions with very small gradients in temperature and density and a small value of TOL can yield very large numbers of intermediate points.
4. For equilibrium initial conditions, NINT is not particularly sensitive to the size or magnitude of temperature, density, or velocity gradients as long as the conditions in conclusion 3 do not occur.
5. For nonequilibrium initial conditions, NINT is sensitive to gradients in temperature and velocity while it is only mildly sensitive to the density gradient. If the property gradients between L and L+1 do not match corresponding gradients between L-1 and L, then more intermediate points are likely to be required.
6. Conclusions 1 to 5 appear to be valid for the several chemistry systems investigated in this research.

APPENDIX E

TREATMENT OF SUBSONIC INLET POINTS

1. IMPORTANCE OF COMPUTATIONAL BOUNDARY CONDITIONS

Roache (43) remarks that all the flow patterns of common gases and liquids are solutions to the same partial differential equations. The flows are distinguished only by boundary and initial conditions and by similarity parameters like the Reynolds number. He concludes: "It is therefore not surprising that the specification of computational boundary conditions, besides affecting numerical stability, greatly affects the accuracy of the FDE solution." Cline (23) attributes long computational times in time-dependent solutions of converging-diverging nozzle problems to poor treatment of the boundaries and inefficient schemes for the interior points. Moretti (44) and Abbett (45) have shown that reflection, extrapolation, and one-sided difference techniques give poor results when applied to solid wall boundaries. Cline (4, 23) has used a reference-plane characteristic method for boundary points in time-dependent analyses of nozzle problems. This technique is also used at all boundary points in the subject research.

2. CHOICE OF INLET BOUNDARY CONDITIONS

At the inlet, a constant n reference-plane characteristic method is used and, for subsonic flow, only one characteristic curve lies

within the flow field (see Appendix C). Since there are 4+n unknowns at the inlet (u, v, P, ρ, and C_i, i=1,...,n) and only one characteristic relation, 3+n additional conditions must be specified.

The "correct" specification of steady flow inlet boundary conditions is a difficult problem; a generally preferred set of conditions is not known at the present time. It is expected that the combustor analysis will be performed independently of the nozzle analysis. The combustor analysis may or may not include two-dimensional effects. In any case, the distributions of the fluid dynamic properties (u, v, p, and ρ) at the combustor exit may not provide an appropriate set of boundary conditions for the given nozzle problem. The total conditions at the combustor exit, however, are global properties of the flow which must be conserved between the combustor exit and the nozzle inlet. The specification of total conditions at the inlet places a constraint on the energy of the flow but still allows flexibility in the solution for the static properties at this point.

The specification of total enthalpy H_o is appropriate for the subject problem. Equation (A-3) shows that the total enthalpy $(h + V^2/2)$ must be constant along streamlines in a steady flow. Therefore, the total enthalpy distribution at the inlet is required to match that at the combustor exit. Cline (4, 23) uses the inlet flow angle θ as a boundary condition. It has also been used for the subject problem. The flow angle may be determined by experiment or from the following procedure:

1. Determine representative values of the ratio of frozen specific heats γ_f and the gas constant at the combustor exit.
2. Generate a "long inlet" geometry by adding six to ten mesh points upstream of the nozzle inlet, simulating a constant-area duct.
3. Using the program of the subject research for isentropic constant specific heat ratio flow, compute the solution to the long inlet problem described in the preceding two steps. Inlet boundary conditions for the long inlet problem are: a uniform distribution of zero flow angle θ, and total pressure P_0 and total temperature T_0 based on combustor exit conditions.
4. The flow angles at the nozzle inlet for the converged long inlet problem can be used as the inlet flow angles for the reacting flow problem.

Note that the arbitrary specification of zero flow angle at the nozzle inlet has been found to produce unreasonable velocity profiles at the nozzle inlet for some nozzle geometries.

A uniform distribution of static pressure across the combustor exit is one of the results expected from the combustor analysis. The specification of θ, H_0, C_i and a uniform static pressure distribution was tested as an inlet boundary condition set. For the cases tested, this produced a velocity distribution which had a range from very high values at the center to near zero values at the wall after only 20 to 30 time planes. The static pressure distribution at the inlet from the "long inlet" solution yielded reasonable velocity distributions.

The set of inlet boundary conditions which has been used in the subject research is the specification of θ, H_0, C_i, i=1,...,n and the

total pressure P_0 based on combustor exit conditions. Here, P_0 is the pressure that would exist as a result of an isentropic stagnation from combustor exit conditions with frozen composition.

3. RELAXATION OF THE SPECIES MASS FRACTIONS

In using total enthalpy H_0 and total pressure P_0 as inlet boundary conditions in the constant η reference-plane scheme, it is found that radial distributions of density, temperature, and velocity develop which do not necessarily match similar distributions at the combustor exit. Therefore, a hypothetical particle, upon making the transition from the combustor exit to the nozzle inlet, encounters discontinuities in the flow field. If not properly accounted for, these discontinuities provide inconsistent kinetics data at the nozzle inlet from which integration of the species continuity equations proceeds.

A series of numerical experiments was performed to study the effects of the discontinuities described above. Two different chemistry systems, in different nozzles, and in various degrees of "near equilibrium" have been subjected to discontinuities of different types and magnitudes. The geometries and chemistry systems are presented in Figure E-1.

Consider a particle at the combustor exit. Note that in functional form (see Appendix A)

$$\sigma_i = \sigma_i(\rho,T,C_i) \qquad (i=1,\ldots,n) \tag{E-1}$$

$$\psi_k = \psi_k(T,\sigma_i,C_i) = \psi_k(\rho,T,C_i, \quad i=1,\ldots,n) \tag{E-2}$$

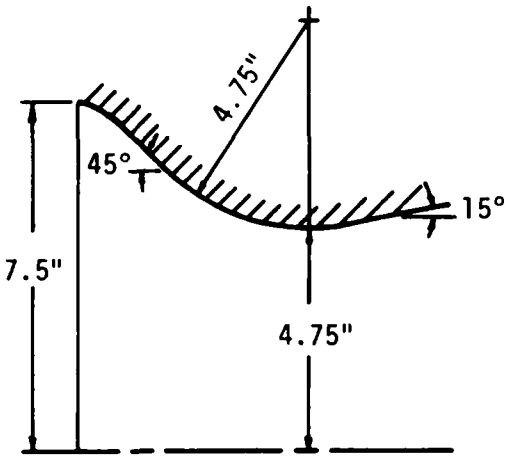

C-H-O-N GEOMETRY

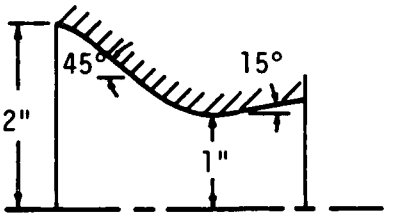

H-F GEOMETRY

$H_2O + M \rightleftarrows OH + H + M$

$H_2 + M \rightleftarrows 2H + M$

$O_2 + M \rightleftarrows 2O + M$

$CO_2 + H \rightleftarrows OH + CO$

$H_2O + H \rightleftarrows H_2 + OH$

$H_2O + O \rightleftarrows 2OH$

$OH + H \rightleftarrows H_2 + O$

$OH + O \rightleftarrows O_2 + H$

C-H-O-N REACTION MECHANISM

$F_2 + M \rightleftarrows 2F + M$

$HF + M \rightleftarrows H + F + M$

$H_2 + M \rightleftarrows 2H + M$

$HF + F \rightleftarrows F_2 + H$

$HF + H \rightleftarrows H_2 + F$

$2HF \rightleftarrows F_2 + H_2$

H-F REACTION MECHANISM

Figure E-1. C-H-O-N and H-F systems.

Since all the static properties and the species mass fractions are known at the location of the particle, the species source functions σ_i and the energy source term ψ_k can be computed at this point. In a real flow, there can be no discontinuities of the static properties and species mass fractions at the junction between the combustor exit and the nozzle inlet. Therefore, from equations (E-1) and (E-2), the distributions of σ_i and ψ_k along the flow direction must also be continuous at this junction. The discontinuities do not represent reality. They are merely the consequence of an attempt to link together separate combustor and nozzle analyses. Their effect should not be felt within the flow, but should be manifest at the inlet mesh points before the species continuity equations are integrated through the flow field. This is accomplished by allowing the species mass fractions at the combustor exit to adjust to the static conditions at the nozzle inlet. The discontinuities are replaced by ramp functions outside (just before) the inlet mesh points as shown in Figure E-2. The discontinuities in density and temperature become continuous, linear transitions from combustor to inlet conditions over the period of a variable "relaxation time." The time is chosen so that the change in the energy source term ψ_k is minimized between the combustor exit and the nozzle inlet.

Figure E-3 shows curves of ψ_k versus relaxation time for the H-F system starting from near-equilibrium conditions. The effects of temperature and density ramps are shown separately. A zero relaxation time corresponds to a discontinuity at the junction between the

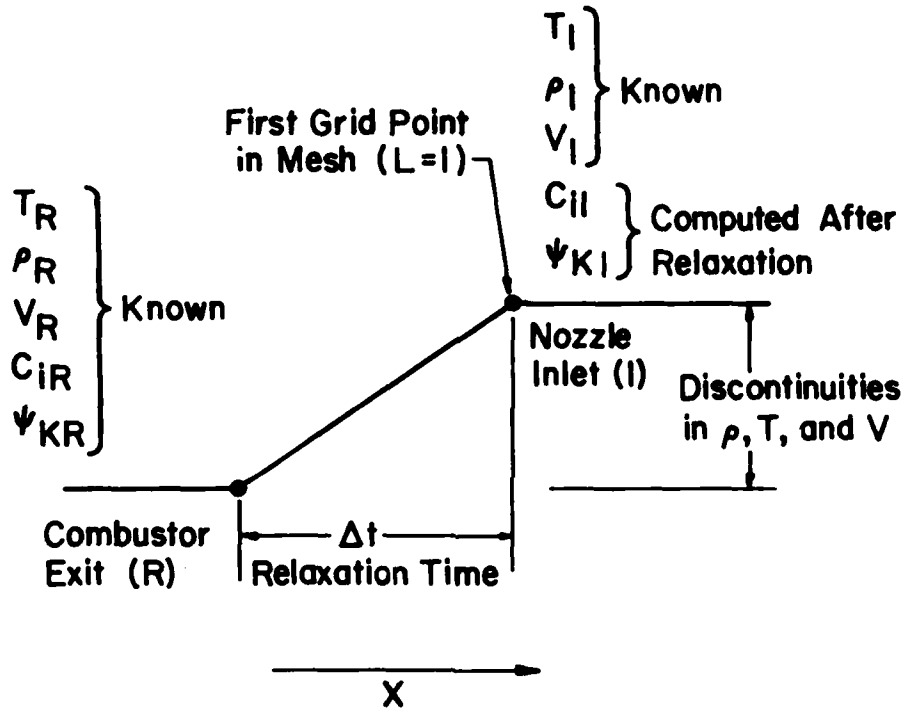

Figure E-2. Unsteady relaxation at the inlet.

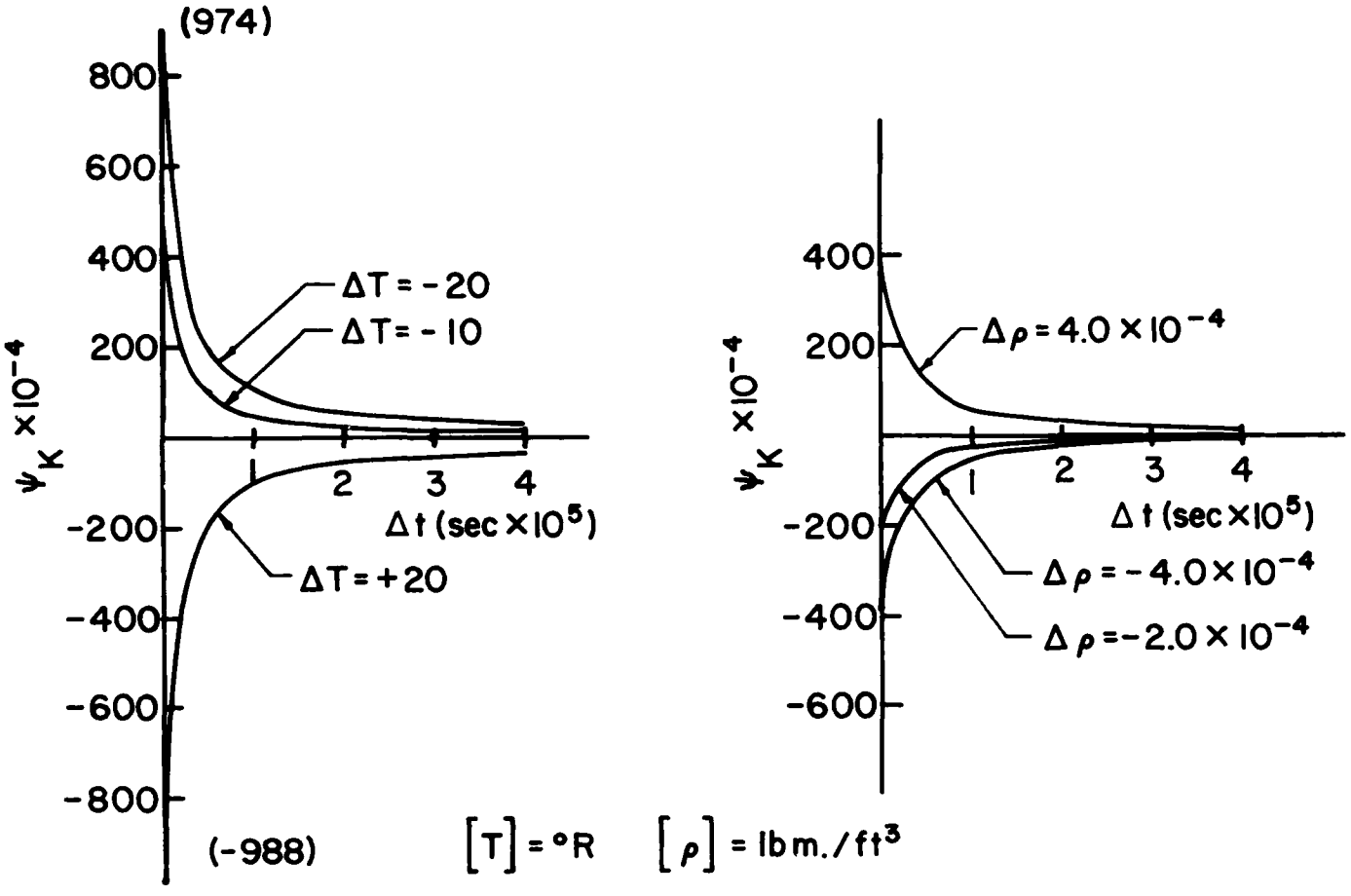

Figure E-3. ψ_K versus relaxation time - equilibrium initial conditions (H-F system).

combustor exit and the nozzle inlet. Note that a temperature discontinuity of just -20°R changes the value of ψ_k by several orders of magnitude (from 2×10^4 to 974×10^4). The size of the temperature and density discontinuities in Figure E-3 are typical for the cases studied during this research. Also, note that with increasing relaxation time, the values of ψ_k approach zero. This is because the chemical systems move toward the equilibrium condition where the species source functions (and consequently the energy source term) are zero. Table E-I shows the effect of relaxation time on the species mass fractions. Note that even relatively long relaxation times produce small changes in the species mass fractions. These changes are typically two percent or less with the exception of the change for F2 which is present in minute quantities in the reactive mixture. Figure E-4 shows ψ_k versus relaxation time curves with initial conditions corresponding to various locations in the ODK [Reference (10)] solution of the H-F problem. Note that for all sets of initial conditions (i.e., various degrees of near-equilibrium), ψ_k approaches zero for large relaxation time. Figure E-5 shows ψ_k versus relaxation time for the C-H-O-N system. Initial conditions are near equilibrium. Table E-II shows the changes in the reactive species mass fractions as a function of relaxation time.

There are several important conclusions regarding the data described above:

1. All curves of ψ_k versus relaxation time approach zero as relaxation time increases. This is because the chemical systems move

TABLE E-1

RELAXATION OF THE H-F SYSTEM

	PERCENTAGE CHANGE IN MASS FRACTION						
Dt	F_2	HF	H_2	F	H	$\Delta T(^\circ R)$	$\Delta\rho(lbm/ft^3)$
$2x10^{-6}$	4.4988	-.1093	-.3494	1.7565	.6096		
$1x10^{-5}$	4.9417	-.1707	-.7290	2.7431	1.1114	+20	-
$5x10^{-5}$	5.0561	-.1868	-.8298	3.0019	1.2442		
$2x10^{-6}$	-4.3473	.1084	.3526	-1.7419	-.6099		
$1x10^{-5}$	-4.7606	.1684	.7409	-2.7053	-1.1153	-20	-
$5x10^{-5}$	-4.8679	.1841	.8449	-2.9579	-1.2497		
$2x10^{-6}$	-2.2039	.0548	.1788	-.8810	-.3088		
$1x10^{-5}$	-2.4156	.0852	.3732	-1.3689	-.5628	-10	-
$5x10^{-5}$	-2.4706	.0932	.4248	-1.4967	-.6299		
$2x10^{-6}$	-.2075	.0425	.3630	-.6835	-.4346		
$1x10^{-5}$	-.4325	.0761	.5919	-1.2226	-.7276	-	$+4x10^{-4}$
$5x10^{-5}$	-.4908	.0847	.6504	-1.3610	-.8025		

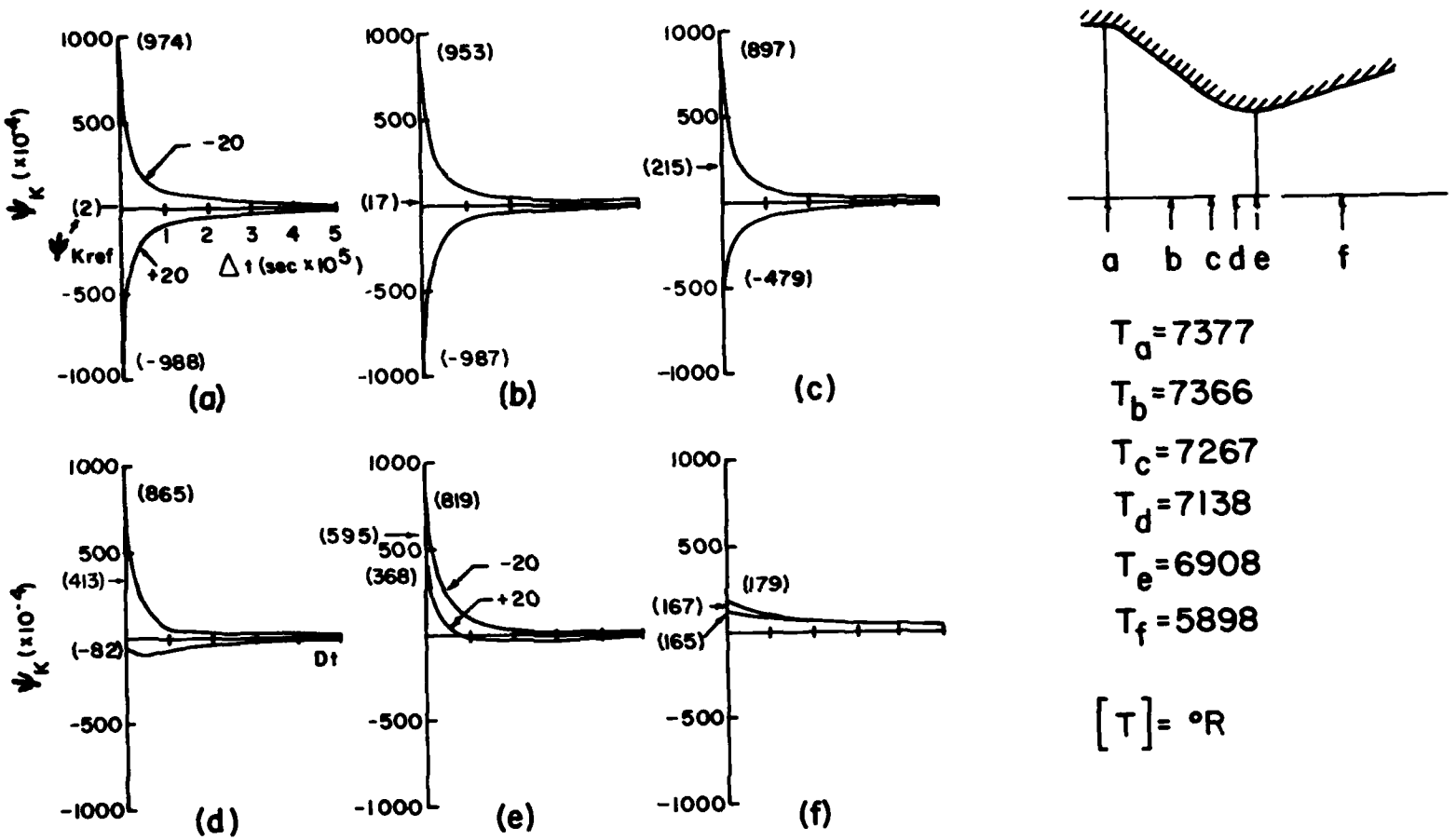

Figure E-4. ψ_K versus relaxation time - various nonequilibrium initial conditions (H-F system).

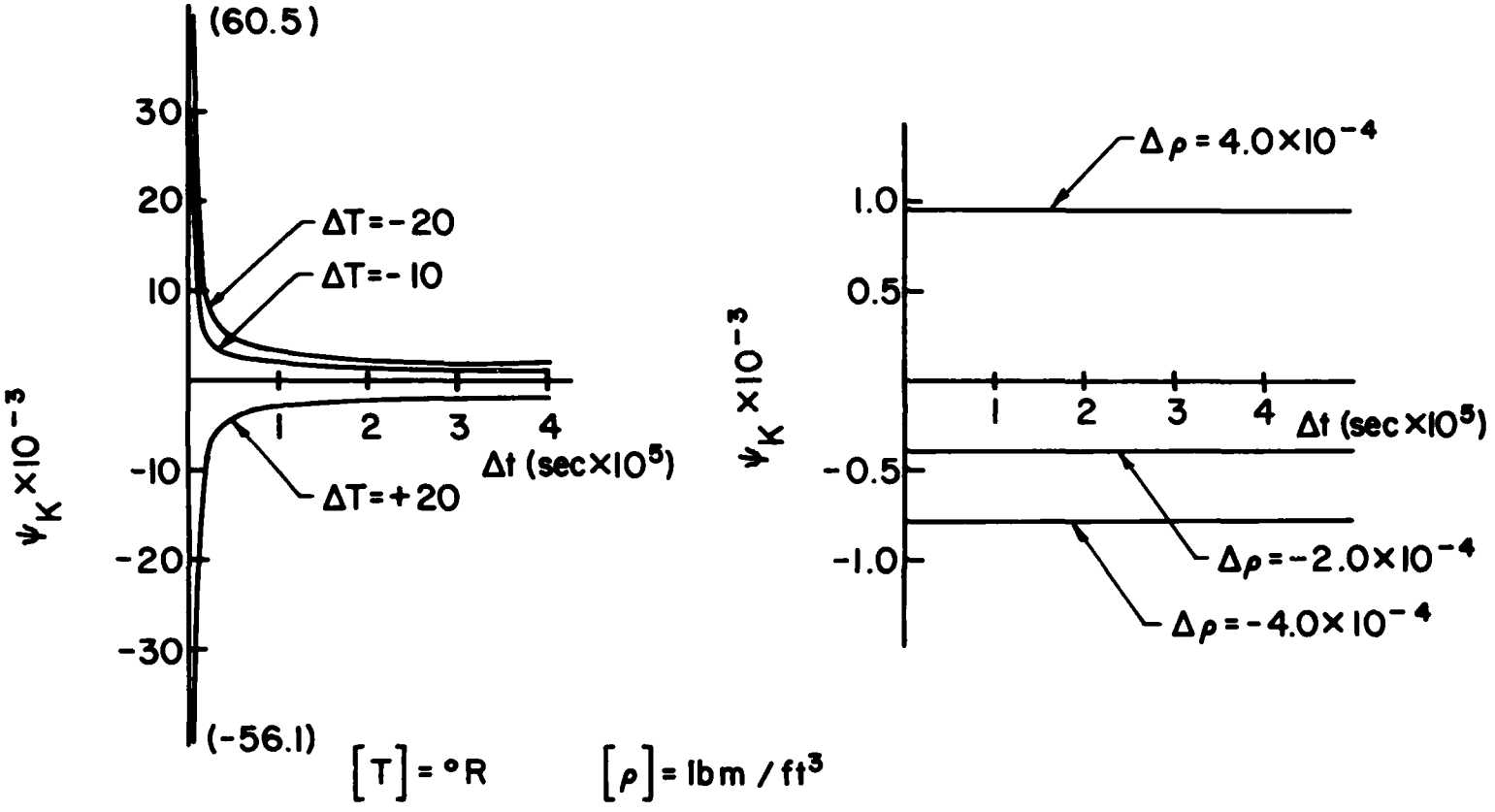

Figure E-5. ψ_K versus relaxation time - equilibrium initial conditons (C-H-O-N system).

TABLE E-2

RELAXATION OF THE C-H-O-N SYSTEM

	PERCENTAGE CHANGE IN MASS FRACTION									
Dt	CO_2	H_2O	CO	H_2	OH	O_2	H	O	$\Delta T(°R)$	$\Delta\rho(lbm/ft^3)$
$2x10^{-6}$	-.0168	-.0243	.0227	.0253	.4773	-.0813	-.4597	-.0739		
$1x10^{-5}$	-.0466	-.0195	.0630	-.0489	.5401	-.0706	-.5017	-.0553	+20	-
$5x10^{-5}$	-.1093	-.0297	.1479	-.0312	.6095	.0145	-.4019	.0772		
$2x10^{-6}$	.0183	.0267	-.0297	-.0289	-.5220	.0891	.5057	.0797		
$1x10^{-5}$	.0508	.0212	-.0687	.0520	-.5906	.0778	.5545	.0610	-20	-
$5x10^{-5}$	.1184	.0313	-.1602	.0384	-.6627	-.0135	.4535	-.0764		
$2x10^{-6}$	.0095	.0139	-.0129	-.0149	-.2717	.0463	.2628	.0416		
$1x10^{-5}$	.0265	.0111	-.0358	.0276	-.3075	.0404	.2878	.0316	-10	-
$5x10^{-5}$	.0619	.0165	-.0837	.0192	-.3456	-.0075	.2338	-.0413		
$2x10^{-6}$	-5.2E-5	-3.5E-4	7.1E-5	9.7E-4	1.6E-3	9.5E-6	3.9E-3	2.5E-3		
$1x10^{-5}$	-8.9E-4	-1.6E-3	1.2E-3	6.5E-3	5.9E-3	1.7E-3	1.5E-2	1.2E-2	-	$+4x10^{-4}$
$5x10^{-5}$	-9.0E-3	-6.3E-3	1.2E-2	2.6E-2	2.3E-2	1.5E-2	5.6E-2	5.0E-2		

toward an equilibrium condition (where the species source functions go to zero) with increasing relaxation time.

2. At high temperatures and near equilibrium conditions, ψ_k is quite sensitive to variations in temperature and density. For example, a 20°R temperature perturbation, with no relaxation, can change the computed value of ψ_k by several orders of magnitude.
3. For the chemistry systems and static property gradients studied in this research, relatively small changes in composition occur during the relaxation from combustor exit to nozzle inlet conditions. Typically, species mass fractions change by less than two percent.

Conclusion 3 is significant with respect to the use of P_o based on combustor exit conditions for the calculation of inlet points. Since the composition changes with relaxation between the combustor exit and nozzle inlet, P_o based on combustor exit conditions is only an approximation at the inlet. However, due to the very small changes in the species mass fractions between those two points, it is a reasonable approximation.

Failure to relax the species mass fractions at the inlet leads to numerical difficulties for two primary reasons. First, without relaxation, the data set (ρ,T,C_i, i=1,...,n) at the inlet is inconsistent. As noted above, discontinuities can cause the energy source term ψ_k to differ by several orders of magnitude from its value at the combustor exit. This causes a "hard start" condition in the integration of the species continuity equations away from the inlet. Second, if

the species continuity equations are not relaxed before the inlet, they will relax within the computed flow field. This can produce distributions of ψ_k within the flow with dramatic oscillations near the inlet. This ψ_k distribution, in turn, distorts the flow. Figure E-6 illustrates the difficulties described above. The "total enthalpy error" in that figure is

$$H_o \text{ Error} \equiv \frac{H_{OL} - H_{OR}}{\frac{V_E^2 - V_I^2}{2}} \qquad \text{(E-3)}$$

where H_{OL} is the total enthalpy at station L, H_{OR} is the total enthalpy at the combustor exit, and V_E and V_I are the velocity magnitudes at the nozzle exit and inlet respectively. Shown in Figure E-6 is a plot of total enthalpy error and ψ_k at each centerline L station in the H-F problem for various relaxation times at the inlet. Note that for very short relaxation times, ψ_k does not have time to adjust to conditions within the flow and, as a consequence, the rapid adjustment of ψ_k at the inlet can produce large total enthalpy errors. Once this error is established at the inlet, no recovery is made.

The proper relaxation time is determined as part of the overall numerical algorithm. The scheme is illustrated in Figure E-7 which shows a typical ψ_k versus relaxation time curve. In that figure, ψ_{kR} is computed for the conditions at the combustor exit, ψ_{k0} is computed for the species mass fractions at the combustor exit and density and temperature at the nozzle inlet with zero relaxatior time, and $\psi_{k\Delta t}$ is computed for the same conditions as ψ_{k0} but with a relaxation time

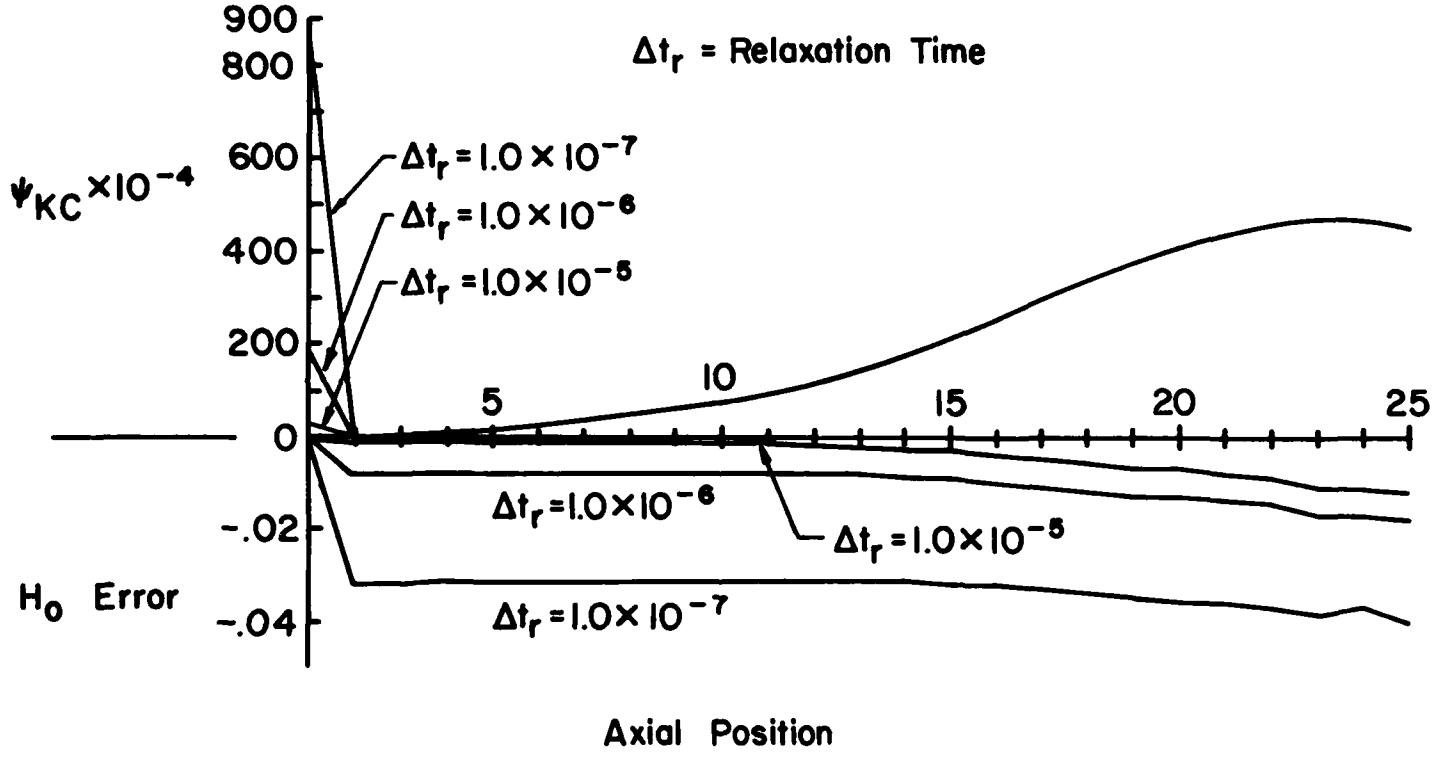

Figure E-6. Total enthalpy error and ψ_K profiles for various relaxation times.

Δt. The values of ψ_{kR} corresponding to each inlet mesh point are computed as part of the initialization procedure for the overall algorithm. They are only computed once and then are stored. Consider time level N in the solution of the subject problem. ψ_{k0} is computed at each streamline origin for the static conditions prevailing at the inlet. There is a minimum relaxation time and if $|\psi_{k0}| < |\psi_{kR}|$, then the minimum relaxation time is used. This is because ψ_k is known to approach zero with increasing relaxation time. Otherwise, the species continuity equations are relaxed through time Δt_1 (see Figure E-7) which is the relaxation time computed for a given streamline during previous time steps. Then the species continuity equations are integrated along the given streamline to the nozzle exit. Next, a check is made:

$$\frac{|\psi_{k\Delta t} - \psi_{kR}|}{|\psi_{k0} - \psi_{kR}|} \overset{?}{<} .05 \qquad (49)$$

If the check is satisfied, then Δt_1 is not changed and it is saved for use during the next time step in the overall algorithm. However, if the check is not satisfied, then a straight line is extended from ψ_{k0} through $\psi_{k\Delta t_1}$ to intersect ψ_{kR}. The relaxation time Δt_2 corresponding to that intersection is used during the next time step. The same procedure continues for subsequent time steps as shown in Figure E-7 until the check is satisfied.

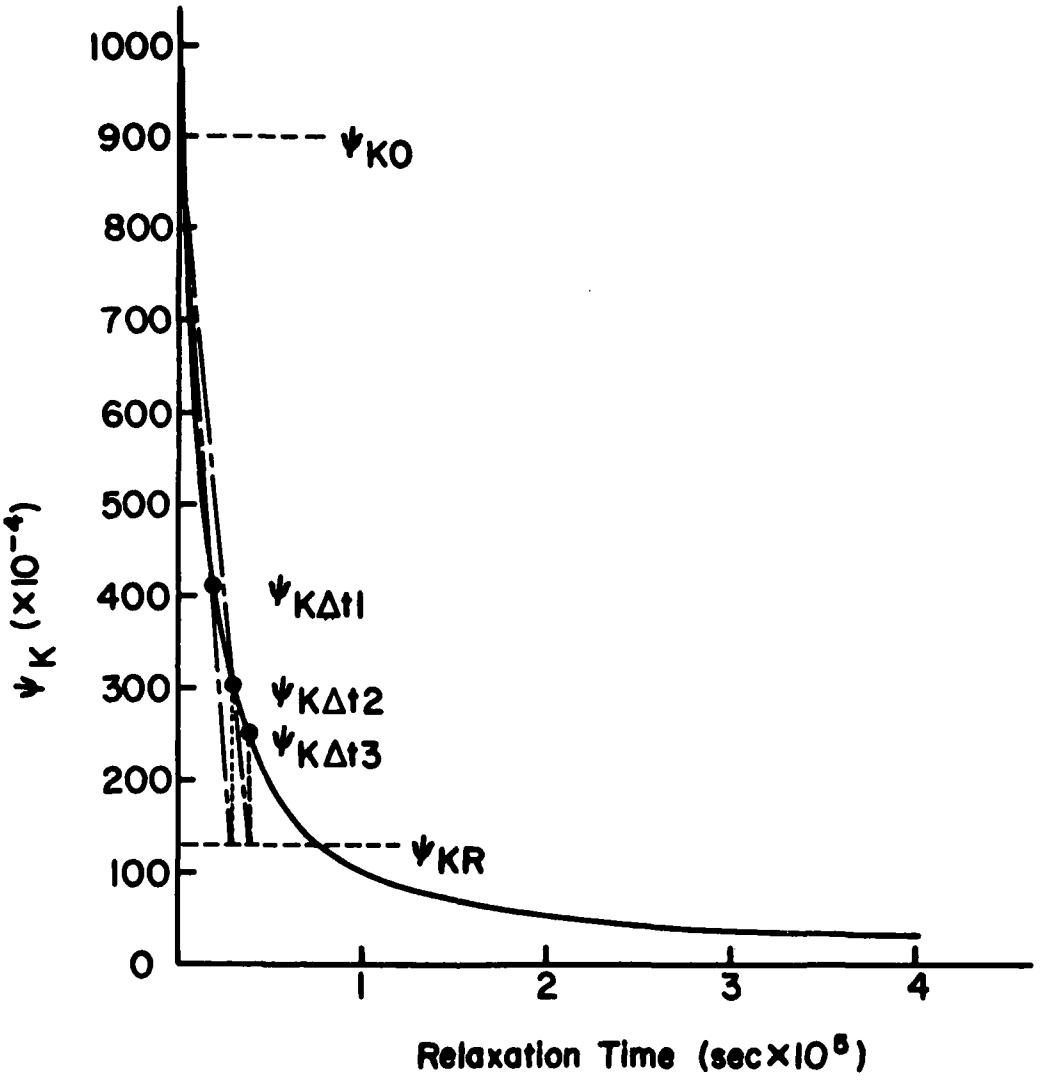

Figure E-7. Calculation of relaxation time.

AFWAL/POTX (10 cys)
Attn Maor R. J. Stiles
WPAFB, OH 45433

AFWAL/PORT (10 cys)
WPAFB, OH 45433

AFWAL/TST/PO (2 cys)
WPAFB, OH 45433

AFWAL/TST-2 (MANDATORY)
WPAFB, OH 45433

AFWAL/PS
WPAFB, OH 45433

AFWAL/XR
WPAFB, OH 45433

AFWAL/AAWP
WPAFB, OH 45433

ASD/XR
WPAFB, OH 45433

HQ Foreign Technology Division
Attn: FTD/PDTA
WPAFB, OH 45433

AUL/LSE (MANDATORY)
Maxwell AFB, AL 36112

AFRPL/MKAS
EDwards AFB, CA 93523

AFRPL/Tech Library
Edwards AFB, CA 93523

AFRPL/MKPA
Edwards AFB, CA 93523

AF Armament Laboratory
Attn: Technical Library
Eglin AFB, FL 32542

AD/DLMA
Eglin AFB, FL 32542

AD/YM
Eglin AFB, FL 32542

AD/SDES
Eglin AFB, FL 32542

AD/XR
Eglin AFB, FL 32542

AEDC/DOXP
Arnold AFS, TN 37389

HQ AFSC/DLFP
Andrews AFB
Washington, DC 20334

HQ AF/RDQA
The Pentagon
Washington, DC 20334

HQ TAC/DRAR
Langley AFB, VA 23665

HQ ADCOM/XPAW
Peterson AFB
Colorado Springs, CO 80914

HQ AFSC/XRT
Andrews AFB
Washington, DC 20334

Commander
Naval Weapons Center
Attn: Code 3245
China Lake, CA 93555

Commander
Naval Air Systems Command
Attn: Code AIR 3300
Washington, DC 20361

Commander
Naval Ordnance Station
Code 5034B
Indian Head, MD 20640

Commander
Naval Surface Weapons Center
Dahlgren Laboratory
Code F-14
Dahlgren, VA 22448

Commander
Naval Sea Systems Command
Code SEA-0231
Washington, DC 20362

U.S. Army Missile Command
DRMI-TK Bldg 7120
Redstone Arsenal, AL 35809

DISTRIBUTION LIST (CONT'D)

OUSDR&E
DD(R&AT)
3D1089 Pentagon
Washington, DC 20301

DTIC (MANDATORY) (14 cys)
Cameron Station
Alexandria, VA 22314

NASA
Lewis Research Center
Technical Library
21000 Brookpark Road
Cleveland, OH 45135

NASA
Langley Research Center
Technical Library
Hampton, VA 23365

The Johns Hopkins University/APL
Chemical Propulsion Information Agency
Johns Hopkins Road
Laurel, MD 20707

Atlantic Research Corporation
Attn: Technical Library
5390 Cherokee Avenue
Alexandria, VA 22314

Atlantic Research Corporation
Attn: Technical Library
7511 Wellington Road
Gainesville, VA 22065

The Boeing Aerospace Company
Attn: Technical Library
P.O. Box 3999
Seattle, WA 98124

Chemical Systems Division
United Technology Corporation
Attn: Technical Library
P.O. Box 358
Sunnyvale, CA 94086

General Dynamics
Pomona Division
Technical Library
P.O. Box 2507
Pomona, CA 91766

Hercules, Inc.
Allegheny Ballistics Laboratory
Technical Library
P.O. Box 210
Cumberland, MD 21502

Hercules, Inc.
Attn: Technical Library
P.O. Box 548
McGregor, TX 76657

Hughes Aircraft Company
Missile Systems Group
Bldg 262, MS B-44
8433 Fallbrook Avenue
Canoga Park, CA 91304

Hughes Aircraft Company
Missile Systems Group
Attn: Technical Library
8433 Fallbrook Avenue
Canoga Park, CA 91304

Martin Marietta Orlando Aerospace
Attn: Technical Library
P.O. Box 5837
Orlando, FL 32855

Raytheon Missile Systems Group
Attn: M26-4
Hartwell Road
Bedford, MA 01730

The Marquardt Company
Attn: Technical Library
16555 Saticoy Street
P.O. Box 2013
Van Nuys, CA 91409

McDonnell Douglas Corporation
Attn: Technical Library
P.O. Box 516
St. Louis, MO 63166

Thiokol Corporation
Huntsville Division
Attn: Technical Library
Huntsville, AL 35807

United Technologies Research Center
United Technologies Corporation
Attn: Technical Library
400 Main Street
East Hartford, CT 06108

DISTRIBUTION LIST (CONT'D)

Vought Corporation
Attn: Technical Library
9314 W. Jefferson Blvd
P.O. Box 225907
Dallas, TX 75265

Purdue Research Foundation (5 cys)
Division of Sponsored Programs
Attn: Professor J. D. Hoffman
West Lafayette, IN 47907

• U.S. GOVERNMENT PRINTING OFFICE 1989-659-062/827

END

FILMED

5-83

DTIC